THESIS FOR THE DEGREE OF DOCTOR OF PHILOSOPHY

Surface potential dynamics on insulating polymers for HVDC applications

Shahid Alam

High Voltage Engineering
Department of Material and Manufacturing Technology

CHALMERS UNIVERSITY OF TECHNOLOGY

Gothenburg, Sweden 2016

Surface potential dynamics on insulating polymers for HVDC applications

Shahid Alam

ISBN: 978-91-7597-475-0

Doktorsavhandlingar vid Chalmers tekniska högskola
Ny serie nr. 4156
ISSN 0346-718X

High Voltage Engineering
Department of Material and Manufacturing Technology
Chalmers University of Technology
SE-41296 Gothenburg
Sweden
Telephone + 46 (0)31-772 1000

Chalmers Bibliotek, Reproservice
Gothenburg, Sweden 2016

Surface potential dynamics on insulating polymers for HVDC applications

Shahid Alam

Department of Material and Manufacturing Technology
Chalmers University of Technology

Abstract

The use of high voltage direct current (HVDC) technology in power transmission systems is continuously expanding. Nowadays, HVDC transmissions operate at voltages up to 800 kV and higher levels are being developed. To secure continuous and reliable transportation of electric energy in such systems, materials used for electrical insulation should satisfy stringent requirements related to their performance under high electrical stresses. These concern, in particular, charge accumulation and its dynamics on surfaces of insulating elements which affect distributions of electric fields and may even influence flashover performance. Thus, the conducted study aimed at increasing understanding of surface charge dynamics on insulating polymers that is essential for proper design, testing and co-ordination of HVDC insulation.

The work was performed utilizing flat samples (thicknesses ~2 mm and ~300 μm) of several types of high temperature vulcanized silicon rubbers. The materials were first characterized by measuring their electrical conductivities and complex dielectric permittivities. A non-contact technique, based on application of Kelvin type electrostatic probe, was thereafter used to measure surface potentials and their decay characteristics on single- and double-layered samples of these materials. The samples were located on a grounded metallic base and their open surface was pre-charged by means of a corona source in air under atmospheric pressure. The dynamic behavior of surface potential was afterwards investigated at various air pressures (1 bar, 600 mbar and 300 mbar) and temperatures (from room temperature to 70 ^{o}C), which allowed for minimizing the influence of gas phase on the decay of the deposited charges and for examining solely the effect of solid material properties. Furthermore, a computer model describing the surface potential dynamics has been developed and utilized for analyzing the results of the experiments.

The performed study has demonstrated that deposition of charges generated by corona on the open material surface induce potential distribution decaying with time but continuously preserving its initial space distribution. The decay is found to be slower at reduced gas pressures. It also depends on material conductivity, being faster on more conductive materials as well as at increased temperatures, well responding to the thermal activation of conduction processes. These facts indicate that bulk conduction is the dominant mechanism of surface potential decay under conditions of the present study, which could also be confirmed by the computer simulations. It was in addition observed that the decay on double-layered structures could be faster as compared to that on single-layered ones, if a more conductive material was used for the base layer, which remained in contact with the grounded metallic electrode. A model of interfacial polarization was employed to analyze this effect. The analyses of surface potential decay also allowed for

independently determining bulk conductivity of the investigated materials and its variation with electric field strength, yielding results comparable with those obtained by means of the conventional method. The determination of material conductivity based on surface potential decay provides a number of advantages, in particular, a reduced measuring time and a wider range of the analyzed electric field strength.

Keywords: HVDC insulation, silicone rubber, surface potential decay, electric conductivity, intrinsic conduction, dielectric spectroscopy, activation energy.

Acknowledgments

The study of surface potential dynamics on insulating polymers for HVDC applications was carried out at the Division of High Voltage Engineering at Chalmers University of Technology. The author acknowledge the financial support provided by the Swedish R&D program ELEKTRA, project number 36132, jointly financed by ABB and the Swedish Energy Agency, as well as the support provided by Chalmers Area of Advance - Energy.

First and foremost my utmost gratitude goes to my supervisor, Prof. Yuriy Serdyuk for his valuable guidance, discussions, inspiration and most of all for his patience. I will always remember his continuous support during the development of my experimental setup. He had motivated me to do more by bringing new ideas, reading and correcting my manuscripts and finally shaping my report. I greatly acknowledge his help in finding proper literature and open discussion on experimental results throughout the course of the project. My special thanks also go to my examiner and co-supervisor Prof. Stanislaw Gubanski, Head of Division of High Voltage Engineering, for his valuable advice and support. I am extremely thankful to him for keeping an eye on the progress of the project work and critical comments on the outcomes of the conducted experiments.

I would also like to acknowledge the members of the Reference group (Lars Palmqvist, Birgitta Källstrand, Olof Hjortstam) for providing material samples for conducting experiments related to surface charging and potential decay measurements. Furthermore, I appreciate valuable discussions we had during Reference group meetings, which resulted in new ideas and suggestions for better continuation of the project work. My thanks also go to Carolina Osterberg and Dr. Henrik Hillborg from ABB Corporate research for preparing samples of several types of soft HTV silicone rubbers.

At last, but not least, I would like to thank my wife, my parents, my family members, my friends and my colleagues here in the department as well as in the Electrical Power Engineering groups for their invaluable support and inspiration to continue this study abroad.

Shahid Alam
Gothenburg, Sweden
November, 2016

List of abbreviations

HVDC	High voltage direct current
SPD	Surface potential decay
SM	Standard measurements
HTV	High temperature vulcanized
ATH	Aluminumtrihydrate
XLPE	Cross-linked polyethylene
MW	Maxwell-Wagner
PF	Poole-Frenkel

List of symbols

Symbols without asterisk (e.g. A, B, C, etc.) indicate studied materials of thickness in the range of ~300 µm.

Symbols with asterisk (e.g. A*, B*, C*, etc.) indicate ~2 mm thick silicone rubbers.

Table of Contents

1. Introduction

1.1 Background

HVDC, regarded as a key technology for future power transmission systems, is continuously impacting the industrial world as well traditional systems since it has been introduced. The predictions and ambitions made in the last couple of decades about huge HVDC networks and grids are gradually converting into reality and large scale projects are running all over the globe [1, 2]. Efficient transportation of electricity from remotely located renewable energy sources (solar, wind and hydro), reduced losses, cost effectiveness, fewer numbers of conductors, etc. have given a further boost to the demand of this technology. The ongoing research and industrial developments of different components of electrical power systems has made it possible to reach operating voltages even higher than 800 kV. With the emergence of polymers and later on with the use of advanced technology (e.g. adding fillers of micro- and nano-scales to base insulating materials for enhancing their properties), it has become possible to provide better insulation systems for such ultra-high voltages and thus secure reliable production and transportation of electrical energy. In spite of all the inherent advantages that this technology has and further improvements offered by the modern industry, there is still a lack of clear understanding of certain basic physical phenomena induced by strong electric fields in dielectric materials, which has put constraints on the manufacturing of various devices and equipment. Thus, charge accumulation on solid dielectrics, which is inherent phenomenon in HVDC systems, affect distribution of electrical fields and may even influence flashover performance of insulators [3]. Equally, the increasing penetration of solid insulating polymers in various HVDC applications [4 – 6] demands reconsideration of design principles of the electrical equipment. Thus, operating constraints are getting rigid and, therefore, knowledge about physical processes associated with charge dynamics on polymeric surfaces become essential for proper insulation design, testing and co-ordination.

1.2 Objectives

The work presented in the thesis was conducted aiming at increasing understanding of physical processes associated with accumulation and dynamics of charges on surfaces of high voltage polymeric insulating materials. For this, several types of high temperature vulcanized (HTV) silicon rubbers and cross-linked polyethylene were considered. Firstly, the experiments related to electrical characterization of the studied materials were conducted using various measuring and diagnostic techniques. Dielectric spectroscopy measurements on single and double layered materials of silicone rubbers were conducted for the purpose of examining the role of interfaces

in composite insulators. Further, surface charging of material samples with different electrical properties and effects of various parameters on surface potential distributions were analyzed. Surface potential decay (SPD) measurements were performed at different pressures of ambient air to study the relative contribution of gas neutralization to the total charge decay as well as to analyze solely the influence of solid material properties on surface charge dynamics. Thermal effects and influences of macroscopic interfaces between the layers on SPD were investigated by conducting measurements at elevated temperatures and on sandwich structures, respectively. In addition to that, SPD based technique was thoroughly examined as an alternative tool to standard method for determining bulk conductivities of insulating polymers at room as well as at elevated temperatures. Finally, surface potential decay characteristics obtained from experimental studies and simulation model were analyzed in order to explore information about the fundamental mechanisms of charge transport.

1.3 Outline of the thesis

Chapter 2 presents background information on polymeric based insulating systems as well as charging of polymeric surface through corona discharges in air. Effects of various parameters on surface charge accumulation and physical mechanisms responsible for potential decay are elaborated in the light of previously performed experimental and simulation studies. Also, it includes a review of surface potential/charge measuring techniques and an outline of a mathematical model of potential decay taking into account charge leakage through material bulk and along gas-solid interface.

Chapter 3 focuses on results of electrical characterization of several types of silicone rubber based insulating materials at room as well as at elevated temperatures utilizing standard methods. Time dependencies and steady-states of volume and surface currents are elaborated as well as the role of materials compositions and thicknesses on magnitudes of electrical conductivities are examined. Current densities are plotted against applied electrical fields and reciprocal absolute temperatures for analyzing possible effects of space charge accumulation and activation energies, respectively. In addition, measurements related to dielectric spectroscopy are presented for the studied silicone rubbers.

Chapter 4 elucidates corona charging of the studied materials and analyses effects of charging voltage magnitude, polarity and materials properties on resulting surface potential distributions. Experimental setup and procedure used for conducting measurements of potential decay and background ion densities in air at different ambient pressures are discussed. Results of SPD measurements on relatively conductive silicone rubber samples and highly resistive materials (XLPE) are demonstrated and the effects of pressure level and solid material properties on the obtained characteristics are analyzed.

Chapter 5 focuses on measurements on double layered samples of silicone rubbers. Experimental results related to surface potential decay and dielectric spectroscopy of sandwich structures are presented and compared to those for individual materials. In addition, layered structures are modelled using Maxwell-Wagner capacitor theory and the influence of material properties and that of externally introduced charge densities on numerical outputs are analyzed.

Chapter 6 focuses on surface potential decay at elevated temperatures. Necessary requirements for the experimental setup for conducting the measurements at higher temperatures are highlighted. Charge decay characteristics recorded for silicone rubbers samples of various thicknesses and compositions are presented.

Chapter 7 presents a detail discussion on surface potential decay as a complementary technique for electrical characterization of insulation materials. Field dependent bulk conductivities obtained from SPD based method are compared with the results of standard measurements at room and elevated temperatures. Further, activations energies estimated from fittings of temperature dependences of the conductivities are compared to known values. A comparative study has been carried out to elaborate the strengths and weaknesses of both the methods. Results of exponential fittings of bulk conductivities are demonstrated for examining the applicability of Poole-Frenkel model.

Chapter 8 focuses on simulations of surface potential decay accounting for charge leakage through material bulk and along gas-solid interface. A comparison is made between the experimental results and output from the performed simulations. Further, results of a parametric study aiming at identifying the influences of the volume and surface conductivities as well as that of dielectric permittivities of the materials on surface potential decay are examined.

Chapter 9 presents conclusions drawn from the experimental and simulation results.

Chapter 10 includes suggestions to continuation of the work.

1.4 List of publications

The performed studies are summarized in the following scientific publications.

- S. Alam, Y. V. Serdyuk and S. M. Gubanski, "Surface potential decay on silicon rubber samples at reduced gas pressure", Proceedings of 23rd Nordic Insulation Symposium, Trondheim, Norway, pp. 19-22, 2013.

- S. Alam, Y. V. Serdyuk and S. M. Gubanski, "Potential decay on silicone rubber surfaces affected by bulk and surface conductivities", IEEE Transaction on Dielectrics and Electrical Insulation, Vol. 22, No. 2, pp. 970-978, 2015.

- S. Alam, Y. V. Serdyuk and S. M. Gubanski, "Contribution of gas neutralization to the potential decay on silicon rubber surfaces at different ambient pressures", International Conference on High Voltage Engineering and Applications (ICHVE 2014), September 8-11, 2014, Poznan, Poland, pp. 1-4, paper B-2-4, 2014.

- S. Alam, Y. V. Serdyuk and S. M. Gubanski, "Effect of interfaces on surface potential decay on double layered HTV silicone rubber samples", Proceedings of International Conference on Dielectrics (ICD), July 3-7, 2016, Montpellier, France, paper 85828.

- S. Alam, Y. V. Serdyuk and S. M. Gubanski, "Surface potential decay as a complementary technique for determining electric conductivity of insulating polymers", Measurement, Elsevier, 2016, under reviewing.

Publications not included in the thesis

- S. Kumara, S. Alam, I. R. Hoque, Y. V. Serdyuk and S. M. Gubanski, "DC flashover characteristics of a cylindrical insulator model in presence of surface charges", IEEE Transactions on Dielectrics and Electrical Insulation, Vol. 19, No. 3, pp. 1084-1090, 2012.

- S. Kumara, I. R. Hoque, S. Alam, Y. V. Serdyuk and S. M. Gubanski, "Surface charges on cylindrical polymeric insulators", IEEE Transactions on Dielectrics and Electrical Insulation, Vol. 19, No. 3, pp. 1076-1083, 2012.

2. Literature review

This chapter summarizes literature analyses on subjects related to the use of polymeric materials in HVDC applications and surface charging of polymeric insulators with emphasis on corona discharges in air. Physical mechanisms responsible for charge/potential decay on pre-charged insulating materials are highlighted based on previously performed experimental and simulation studies. Various study methods including measuring techniques as well as computational models are briefly discussed. Further, a mathematical model of potential decay taking into account charge leakage through material bulk and along gas-solid interface is introduced.

2.1 Polymeric based high voltage insulating systems

To meet increasing demands in electric energy, it is essential to enhance production of electricity from renewable energy sources (solar, wind and hydro). Such generation sites, however, are usually separated from consumption sites by long distances. An efficient transportation of energy requires implementations of transmission systems based on high voltage direct current (HVDC), which are the most suitable technology providing low energy losses. HVDC transmissions operate today at rated voltages up to 800 kV and even higher voltage levels are considered. To provide electric insulation for such voltages, polymeric insulators are preferable due to a number of advantages over traditionally used ones made of glass or porcelain [7].

Natural properties of insulating polymers (light weight, elasticity, toughness, ease of manufacturing and feasibility for various shapes, recycling, processability, high insulation strength) combined with the capability of accommodating other materials for forming composites (adding fillers of micro- and nano-scales to the base materials for enhancing their properties) have given them a unique position in a sustainable 21st century society. Such materials are of great technical importance and find use in a large number of electrical and electronic applications. They provide numerous functions e.g. mechanically supporting conductors, separating or shielding different parts of electrical systems, isolating live wires from ground potential, operational safety, etc. In addition to that, they are used for a variety of other purposes such as making handles for different tools, coatings for wires, casing for electrical equipment etc. During last decades, the use of polymers in HV insulation systems, where requirements for reliability are extremely high, has increased drastically. This concerns, in particular, outdoor application (line- and post-insulators, bushings, surge arresters, cable terminations etc.) where materials like silicone rubbers provide also high hydrophobicity that is important for suppressing leakage currents and thus for improving the withstand capability against surface flashovers [8]. Different types of fillers such as fumed silica, quartz and alumina try-hydrate (ATH) are usually

added to silicone rubbers to further enhance mechanical and electrical properties to achieve various requirements in outdoor applications [9, 10].

Long term performance of polymer-based insulation systems has become more demanded with the passage of time as their failure can lead to interruptions of power supply. Various factors may act as potential ageing threats such as space charge accumulation, increased dielectric losses, water and electrical treeing, etc., and may result in intensification of undesirable conduction processes in the material [11, 12]. In addition, local field enhancement may appear due to defects (e.g. voids, irregularities, cavities, protrusions, conducting particles, non-homogeneous dielectric properties etc.). All these may lead to phenomena like partial discharges, unexpected flashovers and even breakdowns of insulators [12]. Additional factors may affect performance of outdoor polymeric insulators in transmission and distributions systems, such as corona, leakage current due to dust accumulation, corrosion at metal-material contacts, environmental stresses (high temperatures, ultraviolet radiations, direct sunlight, high humidity) and may inevitably cause degradation of materials in a relatively short time [8, 13, 14].

2.2 Charging polymeric surfaces

High voltage polymeric insulators operating under dc voltages are normally exposed to electric stresses which provide conditions for deposition and accumulation of charged species (ions) on gas-solid interfaces. The accumulated surface charges may become strong enough to alter field distribution around an insulator, which in turn may affect its flashover performance [3, 15]. In addition, it may activate field assisted mechanisms inside the material bulk (e.g. field induced conduction) that influence the isolation between different parts of electrical systems. For a proper design of insulation, it is therefore important to understand processes associated with charge dynamics on polymeric surfaces.

Surface charging of polymeric materials have been studied extensively especially during last decades due to the development of new HVDC systems for ultra-high voltage levels. Effects of various parameters like voltage amplitude, polarity, time duration, geometry of an insulating system as well as environmental factors on surface charge accumulation and its distribution along the surface have been elucidated [5, 16, 17]. It has been shown that deposition and relaxation of surface charges are affected by properties of both phases, i.e., solid material (such as transverse (surface) and longitudinal (bulk) electrical conductivities, dielectric permittivities) and parameters related to surrounding gas medium (e.g., conduction due to free ions, rate of ions generation by natural radiation and electric field distribution within the gas phase) [18 - 20]. Further, it was demonstrated that in most of practical cases surface charging cannot be explained by considering only one mechanism and it is a result of competitive action of several processes activated during high voltage application [16].

Despite of the core information on surface charge accumulation and relaxation in HV systems obtained in previous studies, newly emerging applications require more detailed knowledge and more complete understanding of associated physical processes. A number of unclear questions arising from practical use of polymeric insulators related to the surface charge deposition, charge behavior with respect to time, dynamic changes of electric fileds due to charge deposition on various HVDC equipment [21], different factors influencing surface charge accumulation etc. are still required to be properly addressed. In the literature, it is commonly accepted that phenomena associated with surface charge accumulation involve several physical mechanisms (polarization and conduction, external discharges, etc.) and each of them may become dominant under certain conditions [17, 22, 23].

Corona charging

Surface charging of insulation materials may be achieved in different ways, e.g. by corona charging, contact charging, use of an electron beam, polarization, exposing an insulator to high static voltages (that provides conditions for accumulation of free ions present in air), by nearby partial discharges in the surrounding gas, etc. [17, 24, 25]. For research purposes, corona charging has appeared to be most popular due to its simplicity and high repeatability of results. It is also utilized in the present study.

Corona is a self-sustainable, non-disruptive localized electrical discharge in gas that can be initiated by connecting electrodes with small surface curvature (e.g. sharp edges) to a high voltage source. Needle-plane or wire-plane are typical examples of electrodes configurations providing highly non-uniform electric filed distributions and, thus, giving rise to localized electrical discharges [17]. If material samples are placed in the vicinity of such electrode system, deposition of generated charged species may take place on its surface. One should note that using simple point (needle) - plane electrode arrangements as a way of charging solid material surfaces provides uneven distribution of charges on gas-solid interfaces that, in general, is typical for practical situations. If a uniform surface charging is required, a more advanced approach based on the use of a corona triode (where a metallic grid is inserted in the gap between the corona electrode tip and the material surface) is usually utilized [17].

The localized discharges in the vicinity of sharp points in air appear due to high electric field stresses stimulating electron impact ionization of molecules of surrounding gas and, as a result, leading to an increased amount of charged species (ions) of both the polarities. The threshold voltage for corona discharge inception depends on the availability of free electrons produced due to background gas ionization, which can trigger an electron avalanche. The charged species generated in the ionization zone move towards counter electrodes in the applied electric filed provided by the electrodes and eventually enter into a low filed region (so-called drift region), where further ionization is suppressed. Under certain conditions, e.g. at voltages of sufficiently highly amplitudes, electron avalanches in the ionization volume may surpasses a critical length X_c and produce space charge strong enough for development of a plasma channel (streamer),

which can extend in both directions (towards anode and cathode). From measurements [26], it has been found that such transformation occurs when the number of charge carriers within the electron avalanche head reaches a critical value $n = \exp(\alpha X_c) = 10^8$, here α is the ionization coefficient. Under such conditions a complete breakdown in homogeneous fields usually occurs. For the purposes of solid material surface charging, such situation must be avoided.

The type of ions generated in positive and negative coronas in gas depends on its nature [17]. To identify their types in air, spectrometric studies for both positive and negative coronas have been performed [27, 28]. It has been found that chemical composition of produced charges is quite complex and strongly depends on the amount of moisture (H_2O molecules) in gas. Thus, dominant species produced in positive corona in air are clusters of type $(H_2O)_n\,H+$, where the integer *n* increases with relative humidity. At low humidity, other species such as $(H_2O)_n\,NO+$ and $(H_2O)_n\,(NO_2)+$ are found to be dominant. In case of negative corona in air, the dominating species are CO_3^- ions, although other ionic species such as O^-, O_3^- and NO_2^- are also found and their relative fractions are highly dependent on air pressure. Moreover, at atmospheric pressure and 50% of relative humidity, about 10% of the ions are in the hydrated form $(H_2O)_n\,CO_3^-$. Thus, effects of the environmental factors such as humidity, temperature and pressure on the nature of generated ions in the vicinity of the corona treated materials are important to investigate, so that to identify correctly ion species deposited on polymeric surfaces.

If polymeric material is placed in the vicinity of a corona source, ionic species and free charge carriers present in the atmosphere (e.g. dust micro-particles) may experience forces driving them towards solid surfaces where they may be partially trapped and/or injected into the bulk, thus charging the material surface. From the previous works of several authors [29, 30] related to charge trapping, it has been made possible to show that polymeric surfaces are associated with both deep and shallow surface traps (note that the depth characterizes energy level). The authors suggested that ions generated e.g. in a corona discharge, once come to the surface of polymeric materials, can either stay as stable entities on the surface or can be distributed according to the energy states of the ions and surface thus forming surface charge layers. It is claimed also that transfer of electrons might occur to neutralize the ions, thus charging the surface state of the polymer to the same charge as the incident ions.

2.3 Surface charge/potential decay

Surface potential decay (SPD) on pre-charged insulating materials has been studied extensively in relation to various applications, in particular, to gas-insulated (GIS) equipment. During the last couple of decades, the interest to this subject has gained substantial attention in connection with ongoing development of HVDC power transmission technology. The conducted research focused at evaluations of effects of material properties (their volume and surface conductivities, presence of fillers in base polymers, thicknesses, etc.), surrounding gasses and environmental factors, charging voltage levels, etc. [4, 25, 31 - 36]. Based on results of the performed studies, different mechanisms and theories have been proposed to describe SPD, e.g. in terms of bulk processes

(charge trapping/detrapping, intrinsic conduction, slow polarization, etc.), charge spreading along the material surface, etc. [31, 37 - 41]. The potential decay characteristics have been treated in different formats, e.g. utilizing so-called "V vs. time" and "log(V) vs. log(time)" dependencies in order to elucidate quantitative interpretation of the initial stages of the decay as well as to discuss cross-over phenomenon of SPD curves [24, 38, 41]. In addition, different hypothesis and various models have been suggested to describe surface charge dynamics [3, 24, 38, 40]. Despite of all the efforts made, there is still a lack of knowledge in the subject due to continuous development of hybrid gas-solid insulation systems for various HVDC applications and extensive use of new materials [4 - 6]. Therefore, further investigations are required to explore the research area and to contribute to the available knowledge.

2.3.1 Charge/potential decay mechanisms

Electric charges deposited on surfaces of insulating materials, e.g. by utilizing corona charging techniques, induce a potential on the surface that changes with time. The charge can either flow out in the longitudinal or transverse directions to the surface and also can be compensated by the appearance of charges of opposite polarity (bonded or free) at gas-solid interface due to the electric field setup by the surface potential. From the documented literature on the charge decay, it is commonly accepted that the amount of charges on a polymeric surface under normal conditions can diminish due to several processes, namely, bulk [5, 39, 41] and surface [42, 43] conduction in the solid material and due to arrival of free counter ions present in the gas phase [3, 44 - 46]. The latter mechanism is usually referred to as gas neutralization in the literature. It is dependent on many factors like the amount of free ions in the gas, conditions of their drift and diffusion, extension of the so-called capturing volume, etc. [44]. It has been shown [3, 47] that contribution of gas neutralization to charge decay may become significant (and even deterministic) especially for highly resistive materials at high magnitudes of the potentials induced by deposited surface charges. Similarly, the role of surface conduction in the potential decay can be enhanced due to material aging [48] and high humidity [32, 43, 49]. Under normal conditions, all three decay mechanisms act simultaneously and it is hard to distinguish between their relative contributions to the total effect that is highly desirable for understanding of the phenomenon. Though it is not clear which mechanism is dominant under certain conditions, it is worth to explore the relative importance of each of them.

Bulk neutralization

Bulk neutralization of surface charges may occur due to the intrinsic conduction, polarization processes, charge injection and trapping/detrapping of charges in the bulk of the solid material [24]. Most of theories of surface charge decay assume that during and immediately after surface charge deposition it is injected into the material and transported through its bulk that is accompanied by slower processes of volume polarization [39, 50]. Similarly, in addition to the sequential dominance of these two mechanisms, intrinsic conduction was claimed to be responsible for potential decay at the very late stages of the measurements (typically at ~10^5 sec

after charge deposition) [51]. However, it is worth mentioning that surface charges may be neutralized under the influence of a single process depending on various factors, in particularly, the strengths of induced electrical fields and properties of solid materials. Thus, polarization processes are found to be adequate for explaining charge decay on 7 mm thick epoxy resin, which is considered as one of the highly resistive insulating polymers [25]. Similarly, it has been demonstrated that SPD on ~2 mm thick and relatively more conductive ~(10^{-15} - 10^{-14}) S/m HTV silicone rubbers may be well described taking into account field dependent intrinsic conductivities of the materials [47].

Intrinsic conduction may play significant role due to its dependence on the amount of transported charges defined by the rate of charge carriers generation, intensities of charge trapping, de-trapping, recombination as well as mobilities of the carriers within the material bulk [30, 52]. In this context, it is worth noting that intrinsic conduction is in general field dependent and is often considered as negligible under low fields and moderate temperatures [40].

The relative contribution of the physical processes inside the material bulk to the total charge decay has been also evaluated with the help of various mathematical representations. Thus, it has been shown in [25, 38] that exponential decay characteristics are typically associated with intrinsic conduction process while other mechanisms (charge injection, slow polarization, etc.) result in power law type of surface potential – time dependences.

Surface conduction

Surface conduction refers to the charge leakage along the insulator surface. It is highly field dependent (surface current is usually negligible at low fields) [40]. The leakage current is induced by a tangential component of the electric field activated due to a potential gradient along the material surface, and is quantified by a magnitude of surface conductivity [43]. This mechanism dominates mostly under initial stage of surface charge decay [40]. The surface leakage strongly depends on the material ageing and air humidity. This process may only cause a lateral spread of the charge leading to a more uniform potential distribution while not changing the total amount of charge on the surface [44].

Gas neutralization

The term “gas neutralization” refers to the compensation or neutralization of surface charges due to arrival of free counter ions present in gaseous medium [44, 53]. Normally, free ions of both polarities exist in air due to various background ionization processes caused by terrestrial radiation, cosmic rays, etc. Electric field set up by the surface charges within the surrounding gas volume can lead to electrostatic forces attracting the ions to the surface. The arrival and accumulation of such free ions results in a reduction of a surface potential. Concentration of free ions and strength of electric field in the vicinity of a charged sample are critical factors which determine the efficiency of surface charge/potential decay due to gas neutralization [3, 44].

2.3.2 Methods of surface charge measurements

Measurements of SPD on corona charged polymeric materials is a powerful tool to electrically characterize highly resistive (insulating) materials and can be used e.g. as a complementary method to traditional techniques. It also allows evaluating various electrical processes associated with charge/potential decay such as charge transport, trapping/detrapping, etc.

Presence of electrostatic charges on surfaces of polymeric materials can be detected using different techniques which can be split into qualitative and quantitative methods. Thus qualitatively, the polarity and relative magnitude of surface charges can be detected by using an electrostatic powder which is typically a mixture of two different types of particles e.g. talc and jewelers' rough [54]. The powder, when put on a surface that is charged positively, attracts talc particles while rough particles are attracted to surfaces with opposite polarity. An increased amount of the attracted particles indicate locations on the surface with enhanced charging. Due to its nature, this method may provide qualitative information on charge polarity and surface charge distribution but other parameters, e.g. related to a decay of surface charges can't be obtained [55]. Quantitative evaluations can be based on measurements of induced electric fields or electrostatic potentials and there is a variety of instruments developed for this purpose. Potential probes and electrostatic fieldmeters [56] are among such devices, utilizing contactless methods. Moreover, the former type of devices is the most attractive for research purposes and widely used nowadays due to its simplicity.

Most of the potential probes are of capacitive type. Their working principle is to detect charge quantity electrostatically induced on the detecting electrode of the probe. When brought closer to surface under test, as show in Figure 2.1, the charged sample induces a floating potential on the plate depending on the capacitive coupling between the surface and the probe. Thus, the potential on the probe is a ratio of induced charges to the capacitance between the probe and surface. Therefore, any changes in the distance may cause a flow of current in either direction in order to

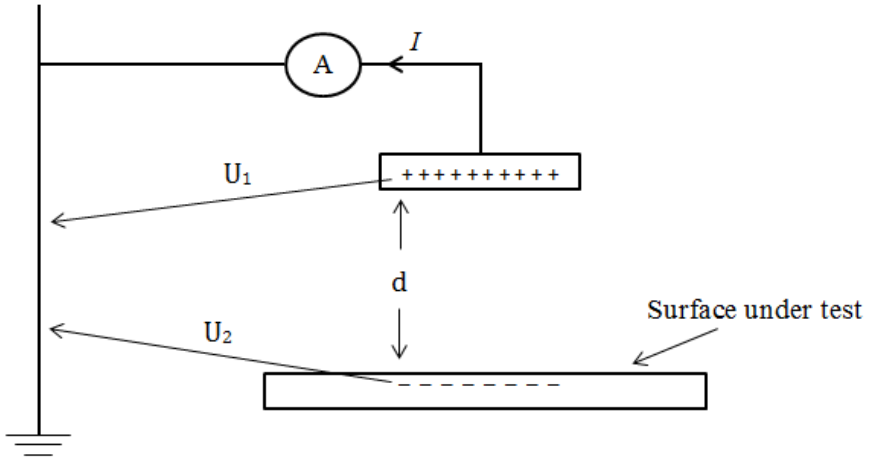

Figure 2.1. Schematic view of a capacitive probe.

adjust the potential on the probe. By measuring the current *I* and distance *d*, the actual charge density on the analyzed surface can be determined [56]. The sensitivity of such devices should be high enough to detect small changes in the current amplitudes due to its strong dependence on the probe-to-surface distance. A schematic diagram of a capacitive probe is shown in Figure 2.1.

Another method called "field-nullifying technique" has been developed, which is mostly used for flat charged samples. Kelvin's type electrostatic probes are based on such techniques. In this method, a variable voltage source is connected to a vibrating sensor through a feedback loop. Vibrations of the sensor (in the electrical field induced by deposited surface charges in the surrounding volume) result in a certain current that can flow in or out from the probe. When the probe is brought in the close vicinity of the analyzed surface, the potential on the sensor is adjusted through the feedback loop in such a way that the current approaches zero indicating that the probe potential is the same as that of the charged sample. Since the gradient of the potential defines electric field, zero voltage between the probe body and the charged surface leads to zero electric field between them. Therefore, this method is called "filed nullifying technique". Major advantages of using Kelvin's probe are: (1) physical state of the object under test does not change and also modifications of charges on the surface are minimized due to its non-contact nature; (2) unlike the capacitive probe, surface to probe distances, if changed within a few mm, don't have a significant effect on the measurements of actual surface potential and a good resolution can be maintained. A schematic diagram of the probe utilizing filed-nulling technique and its equivalent capacitances are shown in Figure 2.2.

Although surface potential measurements are easy and fast to perform using electrostatic voltmeters, the quantification of the measured results is not always simple. In order to extract

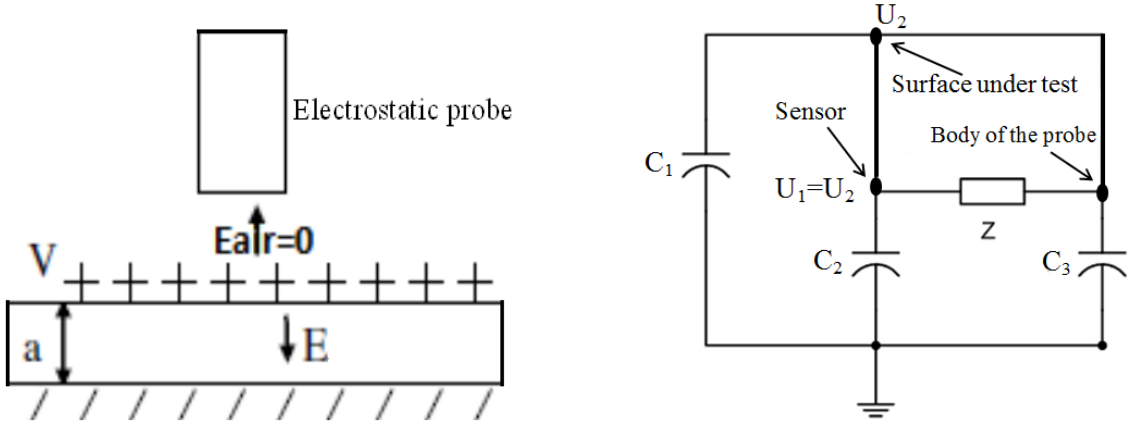

(a) Electrostatic potential measurement by means of a Kelvin probe

(b) Capacitive coupling

Figuere 2.2. Kelvin probe placed above a charged surface. Capacitances C_1, C_2 and C_3 represent the surface to ground, sensor to ground and body of the probe to ground respectively.

surface charge densities from measured potential magnitudes, analytical and numerical relations should be sometimes carefully considered in order to obtain meaningful values. Thus for flat material samples, as shown in Figure 2.2, the situation during the potential measurement corresponds to open circuit configuration, where the electric field between the probe and the surface is zero. Therefore, surface charges can be coupled only to the grounded electrode [38, 57]. Assuming steady state conditions when initial polarization is stabilized (thus a material can be modelled by a constant permittivity) and neglecting space charge effect, a surface potential V_s due to uniform surface charge density σ_s can be presented as

$$V_s = \frac{L}{\varepsilon}\sigma_s \qquad (2.1)$$

Here, L is the thickness and ε is the permittivity of the material sample. Potential to charge conversion for cylindrical and other geometries involve complex numerical calculations for determining probe response functions [58].

2.3.3 Governing equations

Potential decay mechanisms, described in section 2.3.1, are not the only physical processes inside the material bulk and on the gas-solid interface that cause decay of charges deposited on surfaces of insulating materials. Charge decay may be affected by other processes e.g. dielectric relaxation of insulating materials and space charge accumulation in the material bulk. Taking into account all the possible decay mechanisms, the general equation can be derived as described below.

Consider a plane insulator of thickness L placed on a grounded electrode on one side, the other surface is free and is large enough as compared to the thickness so that the side effects can be neglected. Under such conditions, surface charge densities, field and potential are functions of the distance to ground only [38]. Assuming that the surface is charged instantly at time t = 0 (by e.g. corona) to an initial voltage V_s and afterwards is kept in open circuit configuration (E=0 outside the sample that is satisfied during measurements using Kelvin probe). For this situation, a continuity equation for a current density can be written for any point of the insulation [24]

$$\frac{\partial D}{\partial t} + K_v E + \sum_i \mu_i \rho_i E = 0 \qquad (2.2)$$

Here, the first term is the time derivative of the electric displacement $D = \varepsilon_0 E + P$ defining the displacement current density (ε_0 is the permittivity of vacuum, E is the electric filed and P is the polarization vector). The second term represents the current density due to intrinsic conductivity K_v of the dielectric material. The third term describes the current density due to additionally injected charge carriers into the material bulk, μ_i and ρ_i being the mobility and charge density of the particular injected charge carrier respectively. It can be noticed that equation (2.2) is valid

only in case of zero gas neutralization. Further, contribution from the surface conduction should be taken into account in order to a get a more insight into equation (2.2). The influence of each term in equation (2.2) on surface potential decay is separately discussed in the following sections.

In the present study, a mathematical model of the potential decay neglecting gas naturalization and taking into account the charge leakage through material bulk and along gas-solid interface is adopted as presented in the section (2.4).

Potential decay due to dielectric polarization

When a solid dielectric is subjected to an external electric field, the material's molecules may start to acquire a dipole moment depending on the direction and frequency of applied stress indicating that the dielectric is polarized. The dipole moment in an electro-neutral material is usually comprised of both permanent micro-dipoles (e.g. coupled pairs of opposite charges) as well as non-coupled dipoles of micro-charges. A characteristic feature of almost all insulating materials including polymers is that they can be considered either as polar (e.g. polymethylmethacralate, epoxy resin, PET, etc.) or non-polar (polyethylene, silicones, polyfluoroethylene, etc.) dielectrics. The latter type constitutes most of the polymers.

Dielectric relaxation of insulating polymers induced by the field of deposited surface charges, being considered as a slowly varying dc field, can be linked to a very low frequency polarization mechanisms comprising alignment of dipoles existing in the polymer as well as interfacial polarization in the material. Activation of such mechanisms can create an additional electric field that, when interacting with the external field (due to deposited surface charges), may cause a decay of surface potential. The physics behind such field interactions is still required to be further investigated. However, conditions that needed to be satisfied to consider surface potential decay solely due to polarization processes are that intrinsic conductivity (K_v) and space charge (ρ) effects in the material should be equal to zero. The consideration of such assumptions transforms equation (2.2) into a form $\frac{\partial D}{\partial t} = 0$ that implicates that the free charge density on the surface remains constant and, thus, potential on the surface can decay under the influence of polarization processes. In this regard, there is a lack of extensive literature which can be attributed to e.g. difficulties in quantitative discrimination of the physical processes that results in similar decay characteristics. Another reason may be due to the performed analysis on finer samples (thickness in the range of μm) where the possibility of charge injection into solid dielectrics at interfaces followed by their drift/diffusion in the bulk can be no longer underestimated, especially at higher induced electric fields or at higher energies of deposited surface charges. Despite of the difficulties in physical interpretation, mathematical expressions have been derived to describe the role of dipolar polarization for highly resistive insulating polymers (e.g. polypropylene and epoxy) by Molinie and coworkers [24, 25]. According to the performed work, the response of these materials to applied electric fields (in polarization current measurements) can be modelled by a dielectric response function that can be further correlated to surface potential decay rate.

In addition, it has been reported in [59] that for a charging period up to 10^5 seconds, the polarization and depolarization currents can be described by a time power law similar to known Curie-von Schweidler absorption currents

$$i_{pol}(t) \approx i_{depol}(t) \propto t^{-n} \tag{2.3}$$

Here, exponential factor *n* is found less than 1, affected by temperature and field stress and *t* stands for time. Thus the polarization current in epoxy resin materials for constant electric field is noticed to be of absorption type [60], attributed to dipolar processes.

Similarly in [25], it has been shown that the dependence of the surface potential decay rate vs. time in a log-log coordinate system can be represented by straight lines which can be mathematically expressed by time power law as

$$\frac{dV_s}{dt} \propto t^{-n} \tag{2.4}$$

The typical exponent *n* for epoxy resin materials is found to be ~0.85 [25].

The similarity of equations (2.3) and (2.4) suggests that the quantities on the left hand sides of the two expressions may be governed by similar physical processes, thus supporting the linkage between surface potential decay and dipolar polarization in the materials. Further, taking into account the fact that dielectric response function of materials is usually composed of time power laws as studied by Jonscher [61], (2.4) in a piecewise form can be written as

$$-\frac{dV_s}{dt} = \begin{cases} M_1 t^{-(1-\alpha_1)} & t < t_T \\ M_2 t^{-(1+\alpha_2)} & t > t_T \end{cases} \tag{2.5}$$

where M_1 and M_2 represent constant numbers, α_1 and α_2 are power factors and t_T denote the characteristics time corresponding to the intersection point of the two power laws used to fit the decay characteristics.

With regards to (2.5), it has been observed that three different physical processes (dipolar relaxation, charge injections and detrapping) may result in similar characteristics of the decay rates [38]. In the present work, effects of interfaces have been revealed using dielectric spectroscopy measurements performed for sandwich structures (section 5.3). Therefore, based on the fact that contributions of interfacial polarization may no longer be discarded, the right hand side of equation (2.5) is numerically calculated from the measured decay characteristics on double layered HTV silicone rubbers and the obtained results are elaborated in section 5.4.

Potential decay due to intrinsic bulk conduction

The negligible effects of space charge accumulation and stabilized polarization in the solid dielectrics allows for considering only intrinsic conduction within the material bulk and transforms the potential decay equation (2.2) into a very simple form that is given as

$$\frac{\partial V_s}{V_s \partial t} = -\frac{K_v}{\varepsilon_0 \varepsilon_r} \tag{2.6}$$

Solution of equation (2.6) with a constant intrinsic conductivity yields an exponential shape of the potential decay with a time constant equal to the ratio between the intrinsic conductivity and permittivity (K_v/ε). The conductivity $K_v = q\sum \mu n$ is proportional to the product of the charge carriers density *n* and their mobility μ (q is the elementary charge and the summation is to be done for all types of carriers in the material). The latter quantities may change depending upon the internal filed strength in the material that makes it necessary to consider certain hypotheses on the processes leading to such variations in order to rely on the solution of equation (2.6) [38].

As shown in previous works [55, 62], surface potential decay on highly resistive materials can be associated with bulk conduction. In these studies, the intrinsic conductivity of the materials is assumed to be field-dependent and is represented utilizing Poole-Frenkel model. According to this approach, charges being deposited on material surface stimulate an electric field and thus a current inside the material bulk that varies exponentially with the square root of surface potential for high electric fields [63]. This kind of behavior can be described mathematically as

$$K_v(V_S) = K_{v0}\, e^{\beta\sqrt{V_s}} \tag{2.7}$$

Here, $K_v(V_{s)}$ is the field (or potential) dependent bulk conductivity and K_{v0} is its zero-field limit value; and β is the Poole-Frenkel factor. The parameters in equation (2.7) can be obtained by plotting $K_v(V_{s)}$ as a function of square root of surface potential and fitting the variations of the field dependent bulk conductivity with exponential function. A theoretical value of β can be estimated from equation (2.7) and is given as

$$\beta = \frac{q}{kT}\sqrt{\frac{q}{\pi\varepsilon L}} \tag{2.8}$$

Here, *k* is Boltzmann's constant, and *T* stands for temperature. As seen, the theoretical value of β is dependent on the material thickness and permittivity. In [55], a fairly good agreement was found between the theoretical and experimental values of β except for materials with high amount of additional fillers. Concerning the quantitative contribution of bulk conduction, it has been

shown in the previous studies that intrinsic conductivity of the insulating material, naturally enhanced at higher magnitudes of surface potential, can be employed to describe the charge decay and surface potential kinetics observed experimentally [62].

Potential decay due to charge injection and transport

As follows from (2.2), the injection of charge carriers deposited on gas solid interfaces into solid material and its transport through its bulk may be another process influencing charge/potential dynamics on material surfaces. This hypothesis has been introduced in order to provide an explanation for the cross-over phenomena of SPD curves in [24, 64]. Many SPD models are based on this charge injection assumption [38, 39]. Evidences of both types (unipolar and bipolar) of charge injections have been observed and bulk transport of charge carriers has been considered to support the measured and computed studies of SPD in [33, 39, 65, 66]. However, detailed description of the physical mechanisms of injection is still lacking and various assumptions and simplifications are usually introduced to support such models and theories [33, 38]. Thus in [33], possible mechanisms of charge injection have been related to possible presence of deep traps on materials´ surfaces and shallow traps in the bulk. Deposited charges associated with high electric fields (and thus higher energies) may overcome the potential barrier at the interface and migrate into the material bulk. Field dependent bipolar charge injections at electrical strengths of 25 kV/mm have been reported in [33]. On the other hand, surface charging at low corona voltages may result in deposition of stable entities on the gas-solid interfaces. Apart from injections due to strong corona discharges, charge may directly be injected into the bulk of solid insulation materials using electron beams with typical energies in tens of keV [38].

Injection at interfaces may leads to existence of space charges in polymeric materials which may also appear due to, bulk processes (e.g. due to dissociation of impurities). This injected species or migrated charge is then transported through the bulk depending on the energies of charge carriers, depth of trapping sites and conduction properties of the dielectric materials. Space charge limited current (SCLC), trapping/detrapping processes, hoping conduction etc. may be considered as possible mechanisms that control such charge transport. These processes are normally induced by strong electric fields, associated with higher surface potentials. SCLC can be mathematically described as [67]

$$J_{SCLC} = \frac{9}{8}\mu\varepsilon_0\varepsilon_r\theta\frac{V_s^2}{L^3} \tag{2.9}$$

where factor θ is defined as

$$\theta = \frac{N_c}{N_t}exp\left(-\frac{(E_c-E_t)-\beta\sqrt{E}}{kT}\right) \tag{2.10}$$

Here, N_c and N_t are the density of states and ($E_C - E_t$) is the energy gap between the conduction and trap states, $\beta\sqrt{E}$ accounts for Poole-Frenkel effect.

To evaluate the SCLC, information about densities of traps and their energy distributions is needed. In this regard, approximations are usually introduced to make the quantitative analysis simpler [67]. By considering equation (2.10), one may notice that the SCLC in the material is strongly field-dependent. The electric filed induced by deposited surface charges can lower the electrostatic barrier of the trapped carriers [68] causing de-trapping. This leads to an increase in the SCLC (due to increased θ) and, as a consequence, enhances the surface potential decay according to (2.2). Also, the fact that SCLC is proportional to L^{-3} (L is the thickness of the sample) makes this mechanism more efficient at higher field strengths which is achieved at higher surface potentials and smaller thickness of material samples [68, 69]. Thus in [69], the SCLC regimes have been reported at ~950 V and material thickness of 27 µm. Hence, the results of theoretical and computed models based on charge injection and transport is mostly documented for very thin samples in tens of µm range. Therefore, for thick material samples of couple of hundreds of µm or even more, charge injections and associated transport mechanisms may be of secondary importance and the applicability of such models needs to be examined.

2.4 Computational model of surface potential decay

A relationship between the rates of variations of surface charge density σ_s(C/m^2) and induced surface potential V_s (V) for flat material samples and zero field induced in air (provided by the measuring probe) can be derived from Gauss law and can be written as [70]

$$\frac{d\sigma_s(t)}{dt} = \frac{\varepsilon_r \varepsilon_0}{L}\frac{dV_s}{dt} \qquad (2.11)$$

Here, ε_0 is permittivity of vacuum, ε_r is the relative permittivity of the material. At the same time, the rate of change of the surface charge density can be linked to charge sources and sinks by utilizing current conservation conditions. Thus assuming leakage of deposited charges along gas-solid interface and through the solid material bulk as well as their neutralization by gas ions, one may write

$$\frac{d\sigma_s(t)}{dt} = -j_s(t) - j_b(t) - j_g(t) \qquad (2.12)$$

Here, j_s is the current density due to surface conduction, j_b is the current density due to bulk conduction and j_g is the current density caused by gas ions arriving to gas-solid interface and neutralizing surface charges. The latter term can be ignored in the present study due to the especially designed experimental setup, where the involvement of the gas phase is minimized by reducing air pressure (see sections 4.3 below). The reduced ambient pressure inside the test

vessel causes weaker background ionization, which yields lower amount of free ions in air making gas neutralization negligible.

The bulk current density in (2.12) can be expressed as

$$J_b = \frac{K_v V_s}{L} \tag{2.13}$$

For non-uniform potential distributions, a potential gradient exist along the surface that may stimulate a lateral spread of the charges. Mathematically, the corresponding surface current density can be represented as [43, 70]

$$J_s = -K_s \frac{d^2 V_s}{ds^2} \tag{2.14}$$

Here, K_s is the surface conductivity. Note that in (2.14), the derivative of the potential along the gas-solid interface (s) is to be considered.

Inserting (2.13) and (2.14) into (2.12) and accounting for (2.11) yields the equation for the potential decay

$$\frac{\partial V_s(t)}{\partial t} = \frac{L \cdot K_s \cdot d^2 V_s(t)/ds^2}{\varepsilon_0 \varepsilon_r} - \frac{K_v V_s(t)}{\varepsilon_0 \cdot \varepsilon_r} \tag{2.15}$$

which is one of the possible ways of implementing SPD mechanisms accounting for charge leakage through material bulk and along gas-solid interface.

The use of (2.15) for interpretation of the results of the present study is discussed in chapter 8.

3. Electrical characterization of studied materials

This chapter focuses on electrical characterization of soft HTV silicon rubber materials utilizing various measuring instruments and diagnostic techniques. Details about studied materials (compositions, samples types, etc.) as well as experimental setup used for measurement of surface and bulk conductivities at ambient and elevated temperatures are described. Results of the measurements, in particular, current densities vs. applied electric fields characteristics and data from dielectric spectroscopy measurements, are presented and discussed.

3.1 Factors influencing electrical conductivity of insulating polymers

Electrical conductivity is one of the main characteristics of an insulation material defining its applicability and performance in high voltage (HV) insulation systems. Proper selection of materials based on their conductive properties is the key for developing HV insulation for ac and dc applications. Accurate determination of material's conductivity is therefore important from the point of view of insulation design as well as from the perspective of controlling charge accumulation and distribution on/in solid materials [18, 71]. The latter is unavoidable feature which affects operating conditions of the insulation and may even influence flashover performance. It may be stronger or weaker depending upon material nature and external factors, in particular, type of the applied electric stress. Thus under HVDC conditions, insulation is exposed to long-lasting unipolar electric fields providing conditions for accumulation of both surface (interfacial) and volume charges on/in solid insulating elements. These types of charges are tightly coupled due to electrostatic interactions making, for instance, relaxation and decay of surface charges being strongly influenced by bulk conduction processes. To be able to account for such effects, reliable and consistent data about materials´ conductivities (and possibly on their field and temperature dependences) are required.

Measurements of volumetric conductivity are standardized and applied in practice [72, 73]. Despite of this, the measurements on highly resistive materials are not straightforward. Usually, a material sample of certain thickness is placed between metallic electrodes (two or three electrode configurations) with known dimensions which are energized by applying a sufficiently high stabilized dc test voltage and a current through the sample is measured (may be as low as few pico-amperes). Further, the conductivity value is deduced knowing the applied field and the current density provided that a contribution of the surface current to the total one is minimized (e.g., by using measuring system with a guard electrode). To obtain actual dc conductivity, a steady state magnitude of the current should be utilized achieving of which may be very time consuming [74] or may even appear to be not achievable [47]. Results of the measurements may

be affected by a number of factors both external, e.g., the strength of the applied field (dependent on the magnitude of the test voltage and sample thickness) and temperature, as well as specific to the tested material such as composition, morphology, presence of filler and its content, etc. [75-79]. In addition, the contact nature of the standard method makes the impact of electrodes of a test cell on measured electrical conductivity unavoidable [80, 81]. Under certain field and temperature conditions, external charge injections may become significant especially in presence of oxide layers on metallic electrodes as has been highlighted in [81]. Hence, the effects of electrodes introduce uncertainties in the results of conductivity measurements of insulating materials which are hardly predictable and may change with time, e.g., due to progressive oxidation of the electrodes at elevated temperatures.

The influence of electrodes can be in principle avoided by using some non-contact technique. An attempt to realize such method is presented in [82] where the volume resistivity of epoxy resin based materials was deduced from surface potential decay (SPD) characteristics. These were obtained by charging the open surface of a flat material sample resting on a grounded metallic plate by corona discharge and recording time variations of the induced potential after switching off the corona source. The measurements of the surface potentials were realized utilizing non-contact method [56]. The main distinction of such procedure from the tradition technique is that one on the metal-material interfaces is replaced by a virtual electrode created by charges deposited on open surface of the sample. Also, the voltage applied across the sample (and thus the electric field strength) decreases due to SPD that is in contrast to the standard method where the voltage is fixed during the test. Due to the latter, the traditional technique yields a single value of conductivity from each measurement while the SPD method may bring information about field dependence of the conductivity from a single characteristic.

In the performed work, the approach proposed in [82] is developed further and its applicability is verified by comparing conductivities of materials obtained at room and elevated temperatures by using standard and SPD techniques (will be discussed in chapter 7). Results from both the methods are compared for a certain range of electric fields (constituting more than a single data point) that allows for verifying the feasibility of such complementary technique in a broader extent. Further, activations energies estimated from fittings of temperature dependences of the conductivities obtained by both techniques are analyzed.

3.2 Materials types

In the present study, flat samples $100\times100\times L$ mm^3 (L stands for the thickness) of four types of high temperature vulcanized (HTV) silicon rubbers (SIR) are used. All the materials were based on poly-di-methyl-siloxane (PDMS) and reinforced with silica fillers. Further, some of the materials were doped with additives and fillers that are usually introduced to meet requirements in diverse high-voltage applications. The first type of the silicone rubber, commercially known as Elastosil R401/50 and represented by symbols A and A* in Table 3.1, was cured with

Table 3.1. Specification of the material samples used within the performed study.

Material	Commercial name	Curing agent	Additional filler
A, A*	Elastosil R401/50	peroxide	-
B, B*	Elastosil R401/50	peroxide	50 wt. % ATH
C, C*	Elastosil R4001/50	Pt catalyst	-
D, D*	Elastosil R4001/50	Pt catalyst	50 wt. % ATH
E*	Elastosil R401/60	peroxide	-
F*	Elastosil R401/40	peroxide	58 wt. % ATH

dicumylperoxide and then degassed for 17h at 70 ^{o}C. The second type (referred to as B and B*), based on the same specifications as material A, was additionally filled with 50% aluminumtrihydrate (ATH). The third type, commercially known as Elastosil R4001/50, was cured with platinum (Pt) catalyst and degassed under the same conditions as mentioned above. The fourth type, similarly as material B, was additionally filled with 50% ATH, however, it has been manufactured using curing agent of Pt catalyst. The last two materials are correspondingly referred to as C and C* and D and D* in Table 3. 1. The type of ATH filler used is OL-104 ZO. It is a vinyl-silane treated, finely precipitated aluminium hydroxide. Specifications of all the materials are summarized in Table 3. 1. As seen, silicone rubbers in the top four rows are represented by two different symbols which are merely used to indicate different thicknesses, given in Table 3.2, of the same materials and these notations are used throughout the text and in the figures in this report. For thinner materials, the listed thicknesses (Table 3.2) are mean values, obtained by averaging four different readings recorded at various distances from the edge of the samples. In addition to the materials described above, two other types of thick silicone rubbers E* and F* (Table 3.1) were used in the present study, details of which can be found in [3].

3.3 Setup and procedure for conductivity measurements

The experimental setup for conductivity measurement consisted of a Keithley 6517A electrometer with an inbuilt ± 1 kV test voltage source and an ammeter that can measure currents in the range from 1 fA to 20 mA. The electrometer is equipped with a resistivity test fixture Keithley 8009. The test fixture has a pair of top and bottom electrodes between which a material sample is placed to be electrically characterized. It also includes a concentric ring electrode (guard) that can be electrically configured differently to measure either surface or volume current. Guarding is used to increase the accuracy of the measurements by providing a ground

path to the leakage currents. The electrodes are made of stainless steel and are enclosed inside a shielded box to minimize measurement errors and external disturbances. In addition to that, the electrodes are covered with conductive rubber in order to maintain good contact with a sample with uniform pressure (from 6.894×10^3 Pa to 6.894×10^4 Pa depending on thicknesses of materials) on smooth parallel samples and even on hard material surfaces such as glass, epoxy, polyethylene, ceramic etc. The dimensions of resistivity test box (108 mm high × 165 mm wide × 140 mm deep) allow for accommodating samples from 64 mm to 102 mm in diameter and up to 3.2 mm in thickness. Concerning the operating limits under cool and warm conditions, the test fixture is capable of smoothly running at ambient temperature variations from -30 °C to 85 °C.

The bulk and surface conductivities of the studied materials were measured according to ASTM standard D257. The different arrangements of the internal circuit of test fixture used during surface and volume current measurements are shown in Figure 3.1. In case of volume conductivity, the electrodes are configured in such a way that the current is measured across the

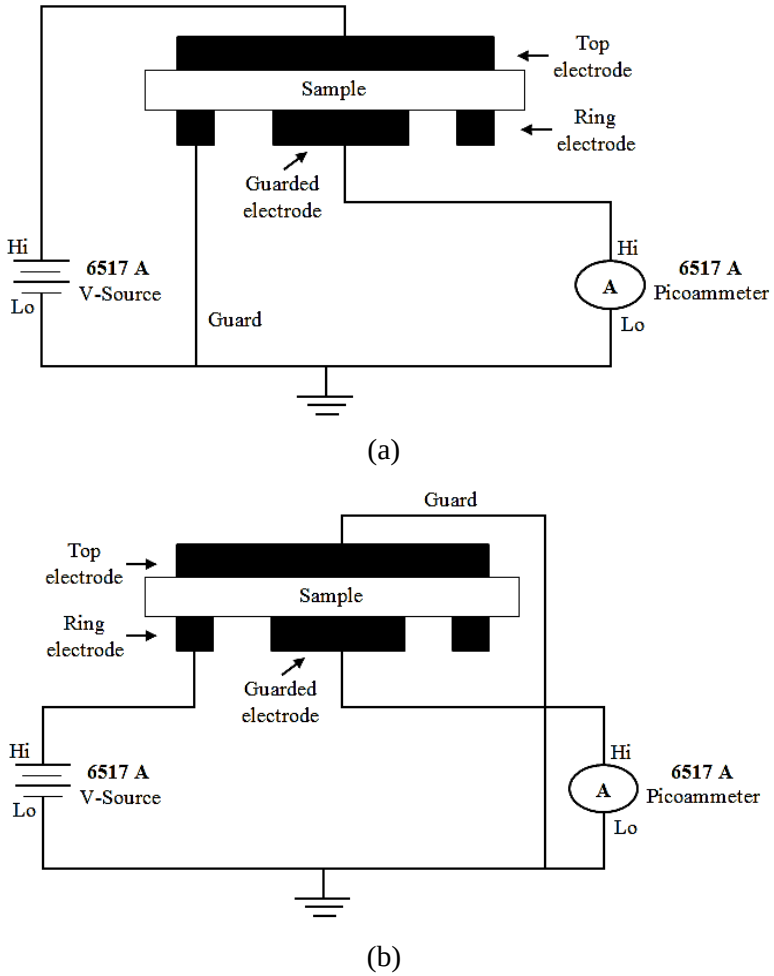

Figure 3.1. Different configurations of the electrodes during bulk conductivity (a) and surface conductivity (b) measurements.

material sample. The top electrode is connected to the voltage source while the bottom electrode is connected to the picoammeter. For surface conductivity measurements, the voltage is applied to the ring electrode and the current is allowed to flow along the material surface and is recorded by the electrometer. Information on the magnitude of the current was communicated to a computer through a GPIB card.

Measurements were performed both under normal laboratory ambient conditions (temperature 22 ^{o}C and relative humidity 50-60%) and at elevated temperatures. Further, procedures followed were slightly different depending on the thicknesses of materials (Table 3.2). For thick silicone rubbers, currents (volume and surface) were recorded only at a single value of the applied test voltage of 1 kV. However, the relatively thin samples of the same materials allowed conducting experiments at different test voltages. The measurements were performed as follows. A dc test voltage of 300V was initially applied and the resultant current was measured. Immediately after voltage application, a spike of a capacitive current was observed followed by decaying polarization current. The current was allowed to relax and after achieving a (quasi) steady-state, the test voltage was increased to 600V and the procedure was repeated. Following this way, the measurements were performed for test voltages of 800V, 900V and 1kV. The conductivities of the materials were deduced from respective steady state currents. The experiment was repeated for all materials at least three times in order to check the repeatability of the results. Between the consecutive measurements, the samples were short circuited and grounded for sufficiently long time to discharge the material.

For current (volume and surface) measurements at elevated temperatures, the resistivity test fixture was placed inside an oven (Memmert Universal oven UN 55) that provided controlled isothermal conditions. Currents were recorded at various temperatures on materials samples of different thicknesses following the same procedures as mentioned above for normal ambient room conditions.

3.4 Volume conductivity measurements at ambient temperature

Measurements on thick silicone rubbers

Measured volume currents for thick samples of HTV silicon rubbers at the applied voltage of 1 kV (the electric field strength is in the range of 0.4-0.5 kV/mm depending on the thickness of materials) and ambient room conditions are shown in Figure 3.2. As can be seen, the decay of the current in different materials is dependent on their compositions (curing agent and additional filler). Maximum variations are obtained for materials B* and D* while minimum ones can be observed for silicone rubber A*. Since the former types are heavily doped with additional ATH filler, volume polarization may be much higher and, therefore, a much higher initial capacitive current is observed. This is confirmed by permittivity measurements discussed below (see Figure 3.15a). The relaxation of volume polarization is a time consuming process. In the present case, even after a time period of 10^5 sec (~28 h), the measured currents were still not purely conductive

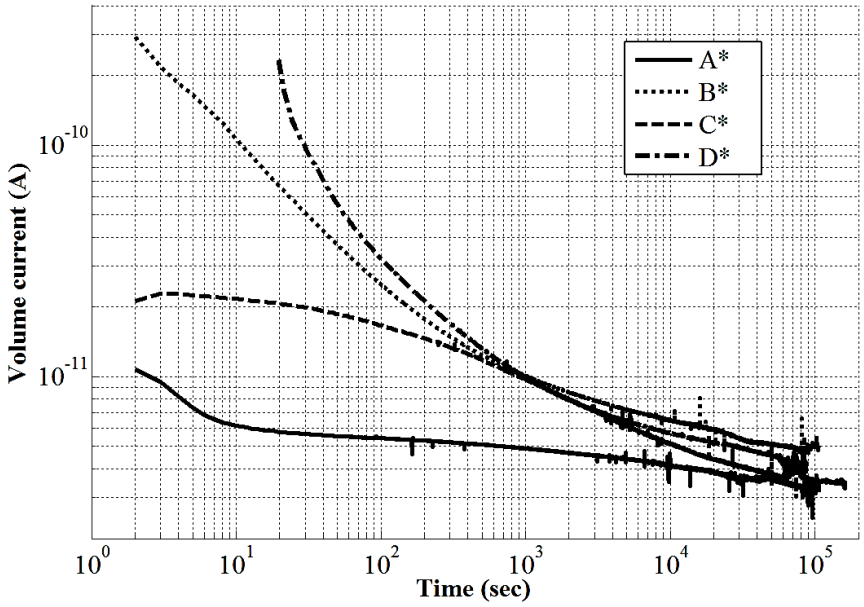

Figure 3.2. Volume currents measured for thick samples of silicon rubber materials.

(note that the time span is shorter for silicone rubbers without additional ATH filler). Nevertheless, the measurements were stopped in all the cases after reaching quasi steady state values that took nearly 28 h. At that time, as can be seen in Figure 3.2, the profiles of the currents for all the silicone rubbers merged into a narrow region of the same decade indicating insignificant influence of curing agents and presence of additional ATH fillers on current magnitudes. The corresponding current magnitudes were used to obtain bulk conductivities as

$$K_v = \frac{L}{A} * \frac{I}{V} \qquad (3.1)$$

Here L is the thickness of the material sample, A is the area (2290 mm^2) of the measuring electrode, I is the steady state value of the bulk current and V is the applied test voltage. Volume conductivities of materials A – D obtained using equation (3.1) are given in Table 3.2 while the properties of materials E* and F* are provided in Table 3.3.

Measurements on thin samples

The recorded currents at room temperature and different strengths of applied electrical fields are shown in Figure 3.3. As mentioned above, the spikes appearing immediately after application of the test voltage are attributed to the capacitive current component and the following relaxation stage depends on the nature of the bulk polarization processes and may be quite time consuming. Times required for the volume currents to reach steady state values are different for the studied HTV silicone rubbers and are strongly influenced by material composition and electric field strength. Thus times to steady state are ~14 h and ~28 h after applying the first voltage step for

Table 3.2. Applied electric fields (kV/mm), volume (K_V) conductivities, dielectric constants ε_r (at 50Hz) and thickness of samples of the studied materials.

Material	Applied field, kV/mm	K_v , S/m	ϵ_r	L, mm
A	3.91	1.4×10^{-15}	2.4	0.256
A*	0.44	3.7×10^{-15}		2.282
B	2.77	6.6×10^{-15}	3.5	0.360
B*	0.44	5.4×10^{-15}		2.293
C	3.17	5.0×10^{-15}	3.0	0.315
C*	0.44	3.5×10^{-15}		2.254
D	2.98	1.5×10^{-14}	3.2	0.335
D*	0.48	3.8×10^{-15}		2.072

ATH filled rubbers B and D, respectively, while they are ~22 h and ~50 h for corresponding counterparts A and C without additional filler. Hence, doping with ATH leads to faster relaxation of the volume current that may be attributed to relatively conductive paths formed along interfacial layers between filler particles and base material [75]. This would also explain higher magnitudes of the currents for ATH filled materials as compared with those measured for unfilled ones observed in Figure 3.3. It is important to mention here that the currents at the instants mentioned above are essentially at quasi steady state and still slowly vary reflecting processes of slow polarization in the bulk. To determine actual conduction current, much longer time span is required. The longest measuring time ~116 h (~5 days) was applied for material C in one of the experiments. Such long-lasting measurements clearly suggest that it is very difficult to completely mitigate polarization currents and, hence, it is not trivial to obtain actual dc bulk conductivities of highly resistive materials.

Table 3.3. Volume (K_v) and surface (K_s) conductivities, dielectric constants ε_r (at 50Hz) and thickness of studied silicone rubber materials.

Material	K_v, S/m	K_s , S	ϵ_r	L, mm
E*	1×10^{-15}	5×10^{-19}	2.7	2.0
F*	8.5×10^{-14}	3.2×10^{-17}	3.3	2.1

Comparing the current-time profiles recorded for thin materials with those shown in Figure 3.2, one can see that the characteristics are dissimilar. Thus, differences in the times to steady states and current magnitudes are more visible (Figure 3.3). Further, the time span after the application of the first voltage step is shorter for filled materials compared to the unfilled materials, which is opposite to the findings for thick materials (Figure 3.2). These may be attributed to the effects of relatively stronger electrical fields causing more intensive polarization in thin materials. In addition to that, the higher volume fractions of interfacial regions, achieved due to lower

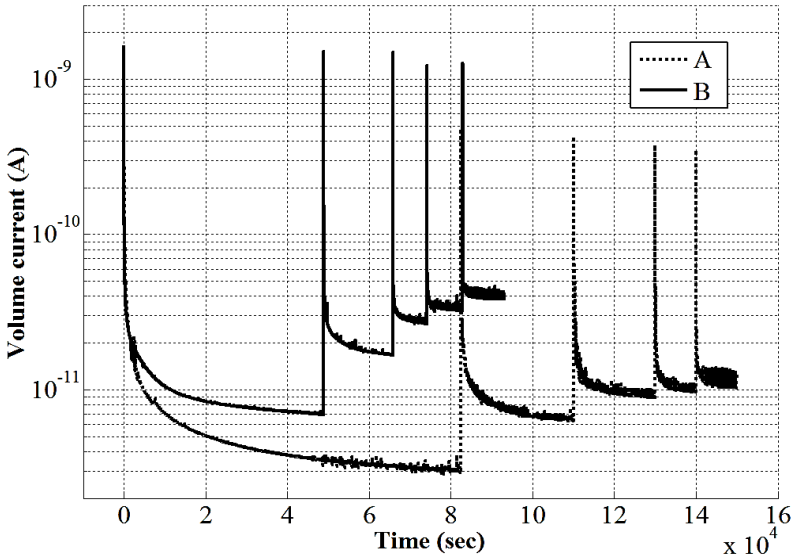

(a)

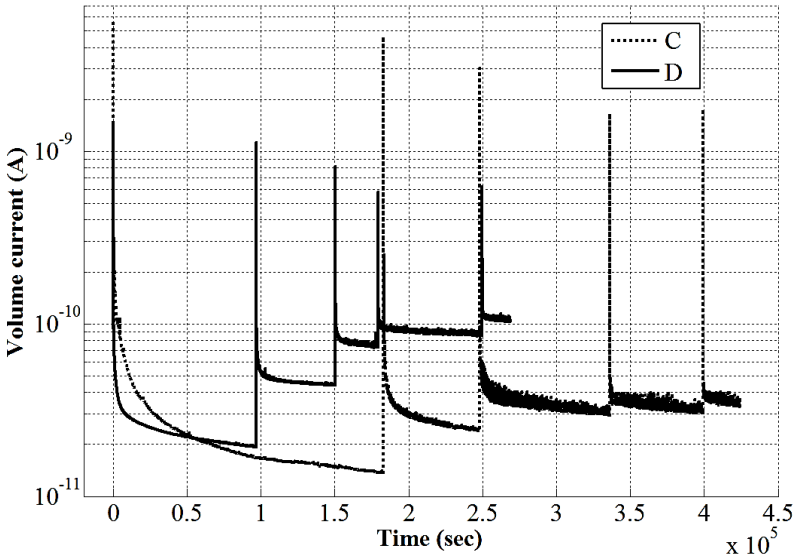

(b)

Figure 3.3. Measured volume currents for materials A, B (a) and C, D (b) at different test voltages. The first spike in both the figures corresponds to the application of 300V, followed by 600, 800, 900 and 1kV.

thicknesses of materials since the ATH contents are 50% by weight (Table 3.1), make the role of filler more important and efficient in the studied silicone rubbers.

The experimental procedure described in section 3.3 may cause space charge accumulation in the material due to the sequential application of increasing test voltages. Charges may be injected from the metallic electrodes into the dielectrics by various field assisted mechanisms such as field emission, field assisted thermionic (Schottky) emission, etc. [52, 83]. To identify existence of space charges in the material, measured dependencies of the current density J on the applied field E can be plotted in log-log coordinates and fitted by a straight line. According to the theory of space charge limited current, any increase of the slope of the line above unity (this corresponds to pure Ohmic conduction) reflects space charge accumulation in the material [67, 84]. A typical example of this behavior is shown in Figure 3.4 (which is a reproduction of the plot presented in [84]). As seen, the data points follow Ohms law (dotted line) at low field strengths, however, above a certain threshold, presence of space charge accumulation can be observed. The latter is characterized by the solid line having a slope lager than one and the estimated thresholds for the two different materials are indicated by the arrows. The existence of such physical processes will distort the applied test fields under analysis and as a consequence the evaluated macroscopic conductivities will no more remain intrinsic in nature that is a more natural parameter of the materials. Following the demonstrated approach, the J(E) characteristics obtained in the present work utilizing the quasi-steady state currents from Figure 3.3 are plotted in Figure 3.5. As can be seen, data for materials A and C are best fitted by lines with slopes nearly equal to 1. However

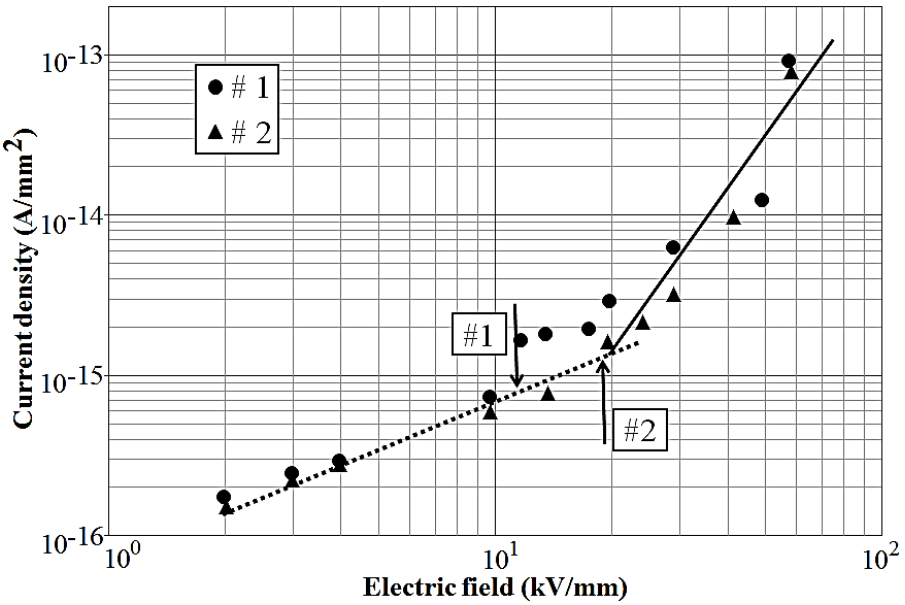

Figure 3.4. Current density (J) vs. applied electric field (E) characteristics for samples of PE based materials marked as #1 and #2. The dotted line represents pure Ohmic conduction while the solid line indicates presence of space charge accumulation. The estimated threshold electrical fields for both the materials are shown by the arrows [84].

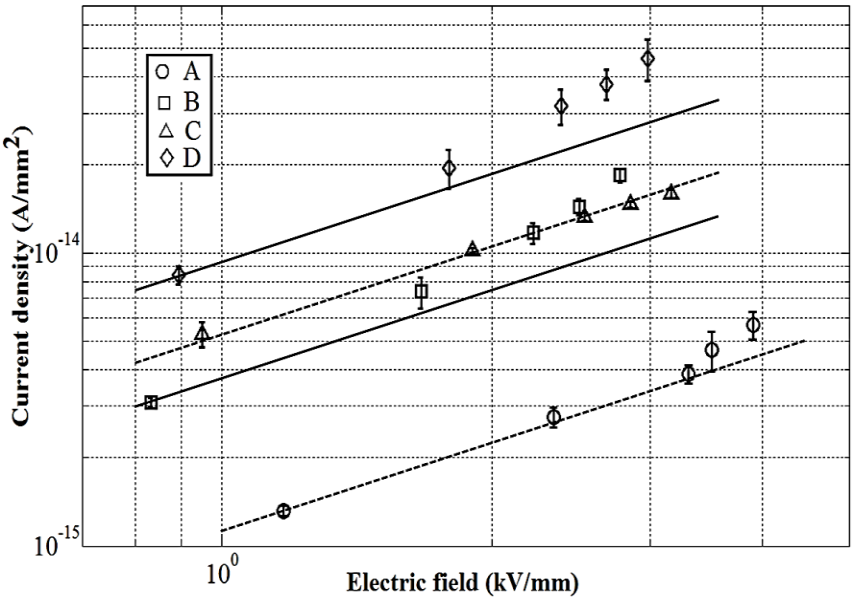

Figure 3.5. Current density J vs. applied electric field E characteristics for studied materials. The solid and broken lines indicate the slopes equal to 1, the error bars show the standard deviations.

for ATH filled materials B and D, the data points deviate from the linear fit at higher fields indicating certain threshold above which a possibility of charge injection and accumulation may rise. At the highest field level, the current magnitudes exceed those expected from Ohmic conduction in approximately two times. Hence, one may suggest that space charge is negligible in the unfilled materials as well as in the materials doped with ATH at low fields and thus Ohm's law is obeyed under these conditions.

Volume conductivity values K_v calculated from (3.1) using the quasi-steady state currents in Figure 3.3 are given in Table 3.4 for different magnitudes of the test voltages. As can be seen,

Table 3.4. Bulk conductivities of the studied materials deduced from the measured volume currents at different amplitudes of dc test voltages.

Material	K_v, fS/m				
	300V	600V	800V	900V	1kV
A	1.13	1.17	1.24	1.33	1.45
B	3.71	4.43	5.27	5.75	6.63
C	5.55	5.32	5.24	5.10	5.03
D	9.42	10.9	13.3	14.1	15.5

conductivities of silicone rubbers A and C are pretty constant while the values of K_v increase with the field (i.e. test voltage magnitude) for ATH doped materials and material D appeared to be most conductive. However in general, the field dependences are rather weak and the obtained values of K_v change in less than two times.

As for the effect of sample thickness on measured conductivity, one may notice that the magnitudes of K_v for all the materials are in general within one order of magnitude and the obtained weak influence can be related to the magnitude of the applied electric fields. Thus for thick materials, the obtained values of K_v are quite close indicating negligible influence of curing agent and presence of additional ATH filler. On the other hand for thinner samples, the applied fields are stronger and the values of the conductivities differ more significantly. Moreover, for all the silicone rubbers, magnitudes of K_v are higher for thin samples as compared to thick ones except for material A. This fact can be attributed to possible intrinsic morphological and structural differences in the same material, possibly introduced during the manufacturing and processing of the thin samples (recall that studied materials are soft and there are known difficulties in producing thin layers of them). Nevertheless, the discrepancies are rather typical for this kind of measurements and the obtained values of conductivities are acceptable.

3.5 Bulk current measurements at elevated temperatures

The recorded volume currents for silicone rubber A and ATH doped material B at different controlled isothermal conditions inside the oven are shown in Figure 3.6 (a) and Figure 3.6 (b), respectively. As can be seen, the amplitudes of the current spikes are getting higher for each step in ambient temperature regardless of materials compositions. This can be related to increased dielectric permittivities although their dependence on temperature is found to be rather weak [85, 86]. The decay of the current for both the materials is strongly dependent on ambient temperature. In general, the polarization processes are mitigated much faster at elevated temperatures and the steady state currents are shifted to the higher magnitudes for each rise in temperature level. For silicone rubber A, a weak decay of polarization current can be observed even at maximum studied temperature of 70 ^{o}C while for ATH filled material B, the phenomenon under the same conditions is nearly obsolete. The demonstrated influence of elevated temperatures on current-time characteristics can further be described mathematically by the ratio of dielectric permittivity and bulk conductivity termed as time constant of an insulation system. A decreasing value of the mentioned parameter can be found for each rise in ambient temperatures indicating the dominant influence of conduction over polarization.

In order to examine possible space charge effects on current magnitudes that may be induced due to temperature assisted mechanisms, the J(E) characteristics are plotted in Figure 3.7. As can be seen, the data points can be fitted quite well by the solid lines characterized by the slope equal to unity at all the studied temperatures indicating the dominant influence of intrinsic conduction. It is worth mentioning that the threshold electrical fields above which space charges may

accumulate in the materials are found with lower magnitudes at elevated temperatures [74]. Nevertheless, the range of the applied field strengths are well below the threshold values as indicated by the fitting characteristics and, therefore, such possibilities can be ignored. Regarding the scattering of the measurements, the maximum deviations from the mean values, obtained from three different experiments, were close to 10% and thus ensuring good repeatability of the results.

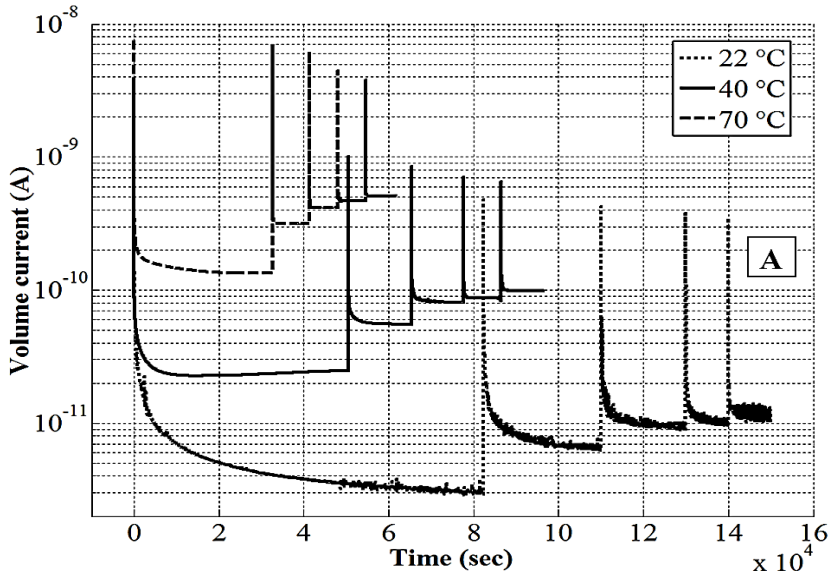

(a)

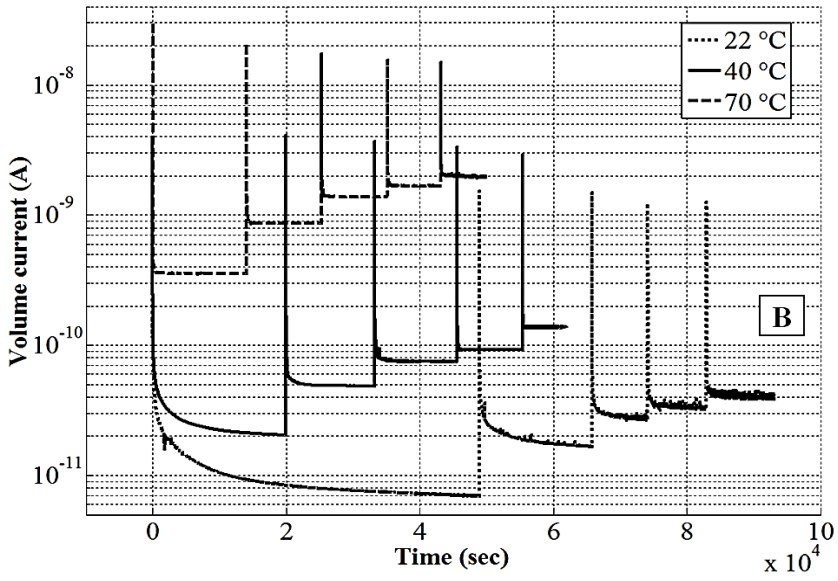

(b)

Figure 3.6. Measured volume currents for silicone rubber A (a) and ATH doped material (b) at different test voltages and ambient temperatures.

The variations in the current densities brought about by each increase in ambient temperatures are found to be dissimilar for the materials. Thus for silicone rubber A, the first increment is nearly one order of magnitude which is even more than the one observed for ATH filled material B under the same experimental conditions. However, the following increase associated with the temperature variation from 40 ^{o}C to 70 ^{o}C is even less than it is for the first rise. On the other hand for material B, the increments along the y-axis are quite regular for the studied range of temperatures that may be attributed to the presence of additional fillers.

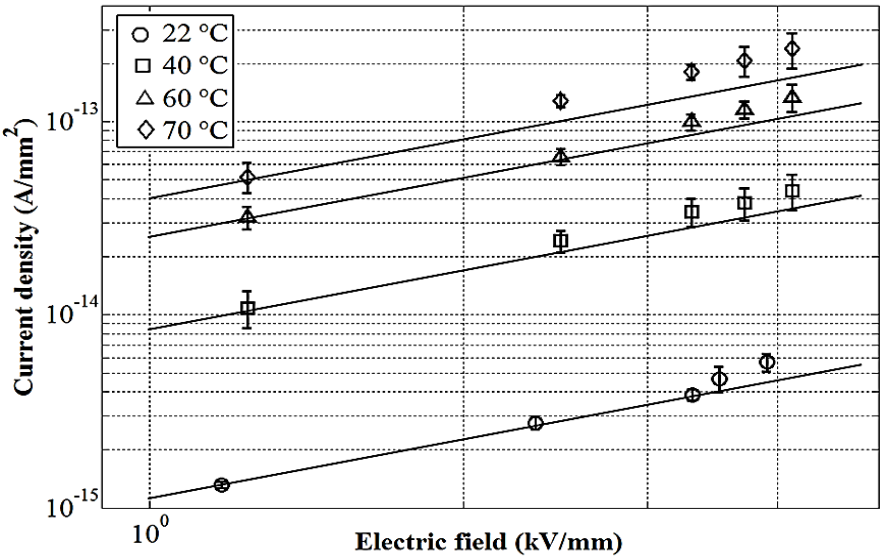

(a)

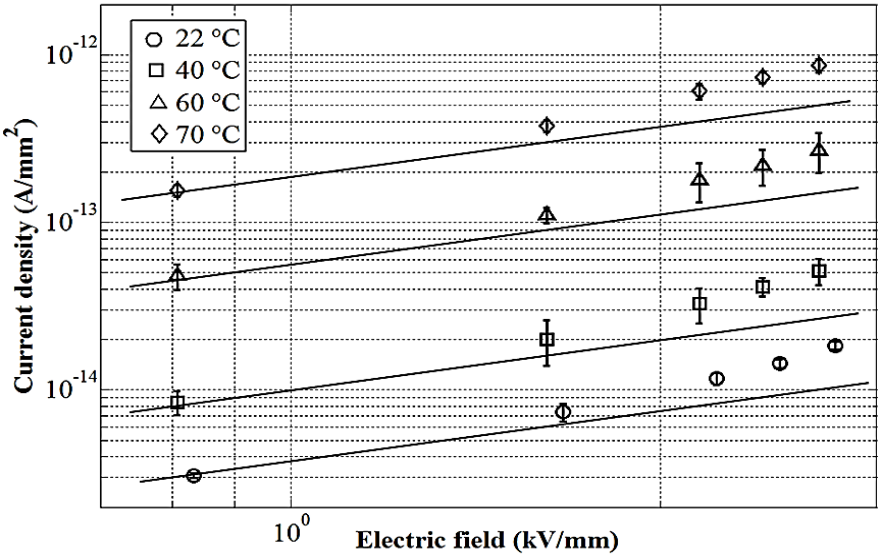

(b)

Figure 3.7. Current density (J) vs. applied electric field (E) characteristics for materials A (a) and B (b) at different ambient temperatures. The solid lines indicate the slopes equal to 1, the error bars show the standard deviations.

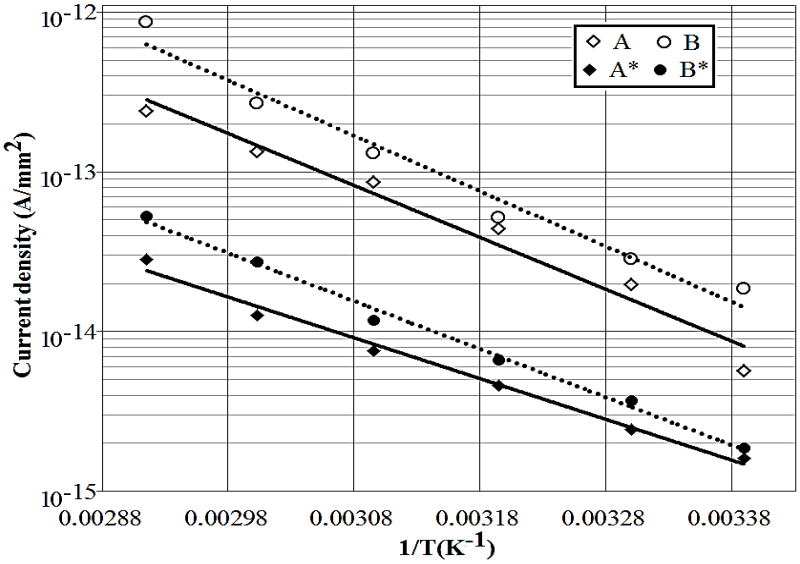

Figure 3.8. Current density (J) vs. reciprocal absolute temperature for silicone rubber materials of different thicknesses. The solid and dotted lines represent exponential fittings of the measured data points.

The dependencies of the current densities on absolute temperature are usually described assuming Arrhenius expression

$$J(T) = J_o exp\left(-\frac{E_a}{kT}\right) \qquad (3.2)$$

where J(T) is the current density at a given temperature, J_0 is a constant, E_a is the activation energy, k is Boltzmann constant, and T is the absolute temperature. Fittings of data presented in Figure 3.7 at constant applied field using (3.2) are shown in Figure 3.8 along with the results of the obtained current densities for thick samples of the same materials. As seen, the data points follow Arrhenius law with slightly different characteristics of the trend lines indicating its applicability for both the silicone rubbers as well as for its different thicknesses. The slopes of the lines representing activation energies are given in Table 3.5. As can be noticed, the values are slightly higher for ATH doped materials than for unfilled silicone rubbers regardless of the thicknesses of samples.

Table 3.5. Activation energies of volume current densities of studied silicone rubbers materials.

Parameter	Materials			
	A	B	A*	B*
Activation energy of volume current density (eV)	0.63	0.69	0.51	0.59

3.6 Surface conductivity measurements at different temperatures

An example of the surface currents measured at room temperature on thick samples of the studied silicone rubbers using electrode configuration in Figure 3.1b is shown in Figure 3.9. As can be seen, time variations of the currents are different for different materials depending on the nature of curing agents and additional fillers. Thus for material A*, the current is almost constant while it starts at much higher magnitudes for materials B* and D* and decreases over a certain range of time until it reaches a steady state. The possible reason for that is the fact that the additional doping of the latter materials with ATH causes an increase in the strength of both surface and volume polarization processes. Therefore, immediately after applying the test voltage, a capacitive current of approximately one order of magnitude higher compared to the relatively pure silicone rubbers is observed. After the initial spike, polarization processes relaxes and finally the current drops to a fairly constant value. For silicon rubber C*, similar behavior is noticed, however, the rate of the decrease of the surface current is much lower compared to ATH doped materials. In general, the features in Figure 3.2 (volume currents) and Figure 3.9 are quite similar for all the materials.

Current-time dependencies recorded for thin samples at room temperature are shown in Figure 3.10. In this case, the times required for surface currents to reach steady state for ATH filled silicone rubbers B and D are shorter than for corresponding counterparts A and C without fillers. These tendencies are very similar to the ones found for the volume currents in corresponding materials and the physical reasons are elaborated in section 3.4.

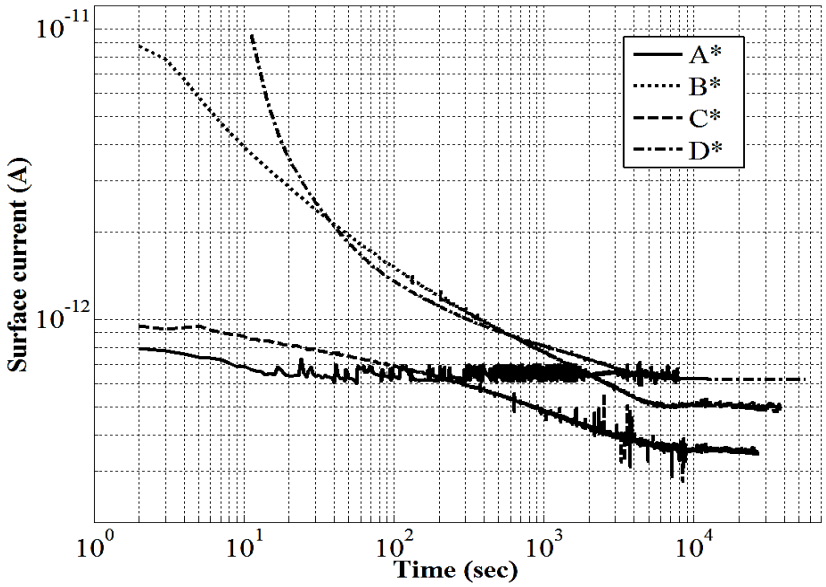

Figure 3.9. Surface currents measured for thick sample of HTV silicon rubbers materials.

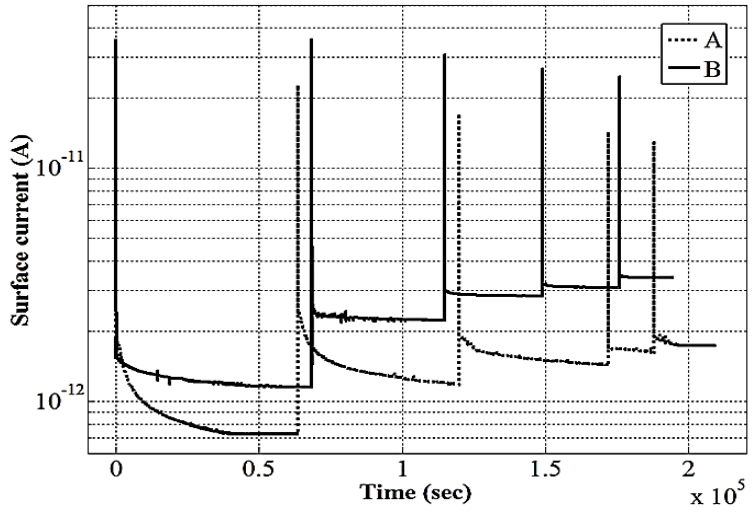

(a)

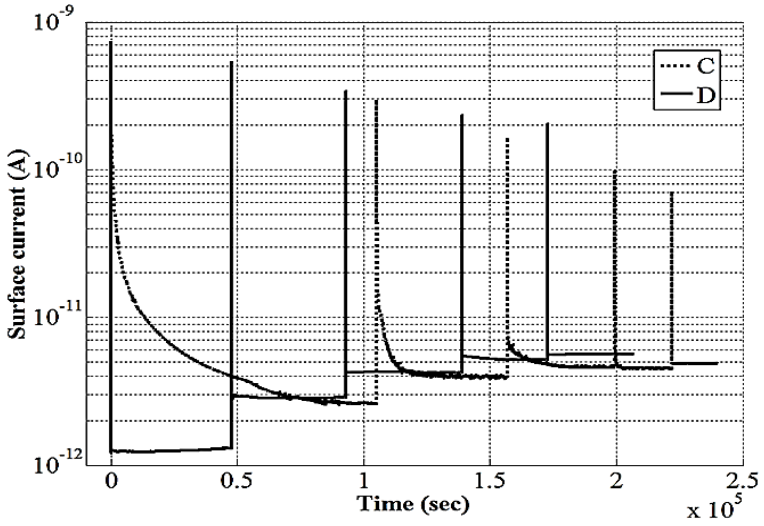

(b)

Figure 3.10. Measured surface currents for materials A, B (a) and C, D (b) at different test voltages. The first spike in both the figures corresponds to the application of 300V, followed by 600, 800, 900 and 1kV.

The surface conductivities are deduced from the magnitudes of the steady surface currents in Figs. 3.9 and 3.10 as

$$K_s = \frac{I}{V*53.4} \qquad (3.3)$$

Here, V is the applied test voltage and I is the steady state value of the surface current (these are reached at different instants for various materials). The constant number "53.4" is the ratio of the effective dimensions of the electrode system. The obtained magnitudes of the surface

Table 3.6. Surface conductivities (K_s) at applied test voltages of 1kV for HTV silicone rubber materials of different thicknesses.

Parameter	Materials			
	A A*	B B*	C C*	D D*
K_s, S	4.5×10^{-17} 1.1×10^{-17}	1.0×10^{-16} 9.5×10^{-18}	9.3×10^{-17} 6.6×10^{-18}	1.3×10^{-16} 1.2×10^{-17}

conductivities for thin and thick silicone rubbers samples are given in Table 3.6. Considering these results, one may notice that the influences of materials compositions (i.e., additional fillers) are rather weak that is opposite to the observation made for bulk conductivities, especially for thin samples.

Dependences of the surface conductivities on the test voltage are shown in Fig. 3.11 and Fig. 3.12. As can be seen in both the figures, the slopes of the curves are either remain nearly constant or decreasing with increasing amplitudes of DC test voltages. From conceptual point of view, a constant line would indicate pure Ohmic conduction that is found to be the case for ATH doped materials, although the line is slightly bending for material B at the later stages of the applied sequential voltages (Figure 3.11). For silicone rubbers A and C, the applicability of the Ohms law is rather questionable.

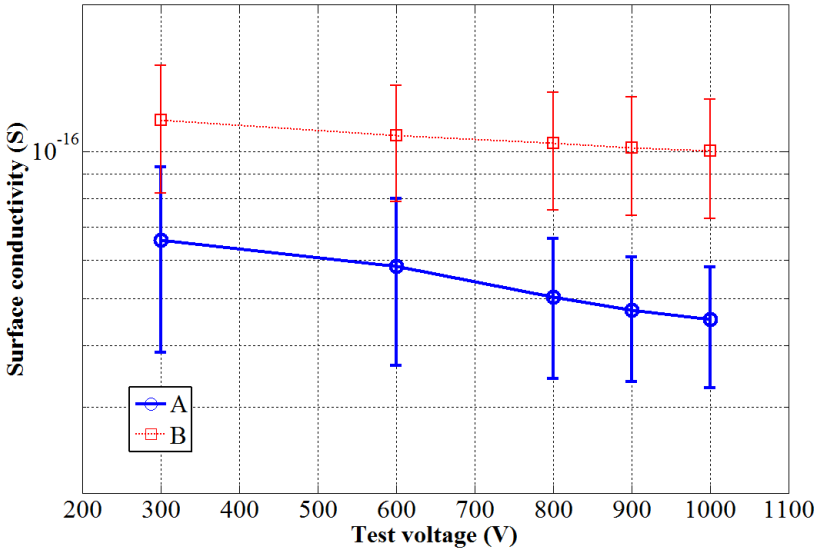

Figure 3.11. Measured surface conductivities of materials A and B at different test voltages. Mean values of three measurements are indicated by markers while error bars show standard deviations.

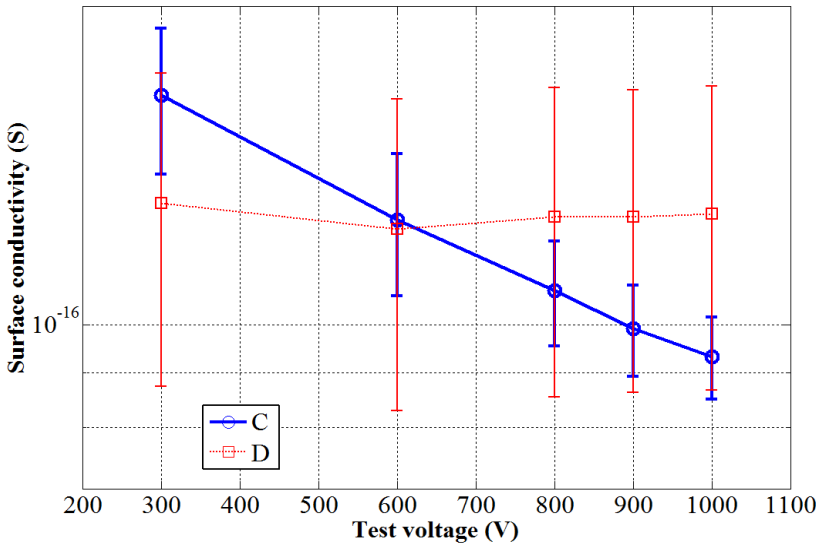

Figure 3.12. Measured surface conductivities of materials C and D at different test voltages.

An example of temperature dependencies of surface currents measured for ATH doped material B is shown in Figure 3.13. As can be seen, the increase of the currents brought about by an ambient temperature variation from 22 ^{o}C to 70 ^{o}C is nearly two times, which is quite weak. On the other hand, for volume currents of the same material, the increase close to two orders of magnitudes was observed.

Taking into account that the surface currents are in general lower than the volume currents under the same experimental conditions, one may expect the influence of the former on surface charge/potential decay is rather weak.

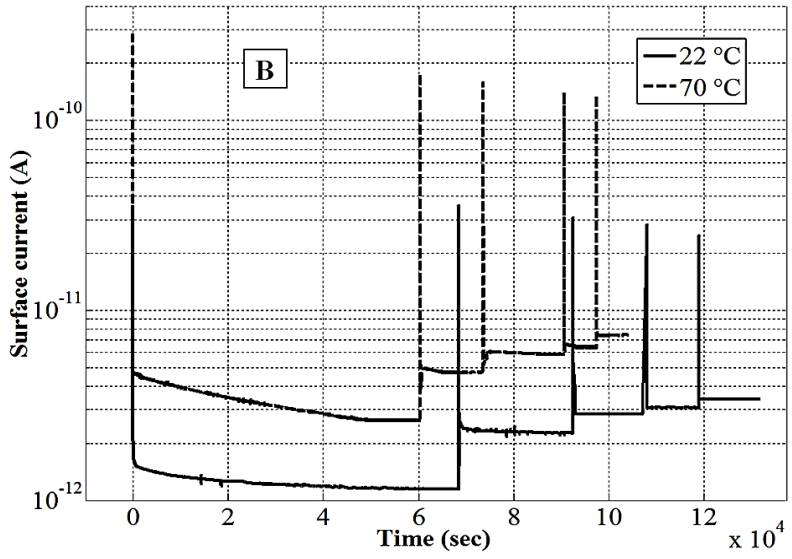

Figure 3.13. Measured surface currents for ATH doped material B at different test voltages and ambient temperatures.

3.7 Dielectric spectroscopy measurements

In general, every dielectric material on both the microscopic and macroscopic levels consists of balanced amounts of positive and negative charges. When material is exposed to an external electric field, the bonded charges start to align along the direction of the field, resulting in the polarization of the material. Different polarization mechanisms (electronic, ionic, dipole, interfacial) can contribute at the macroscopic level and each of them may become active in different frequency range or at different time spans. To understand the polarization processes and to be able to interpret results of dielectric spectroscopy measurements, various models of insulation have been proposed by different authors [87, 88]. An example shown in Figure 3.14 demonstrates the most commonly used equivalent circuit approach within which a material is represented by a combination of capacitive and resistive elements connected to a high frequency capacitance C_∞ and an insulation resistance R_0. The different mechanisms of polarization are represented by the series R_iC_i branches with corresponding characteristic time constants [87].

Dielectric response of a material in time domain can be represented by time dependent relaxation currents (absorption/desorption, polarization/depolarization) and return voltage. In frequency domain, complex capacitance or complex permittivity and dielectric loss factor (tanδ) are used as characteristics of polarization in the material. As long as the insulation material behaves linearly, there exist algorithms that can be used to convert data between the time and frequency domains [87 - 89].

Dielectric response measurements on single layered materials

The dielectric response measurements both on single and double layered materials (will be discussed in section 5.3) were carried out in the frequency range from 0.1 mHz to 1 kHz by means of an Insulation Diagnostic System IDAX 300 and the test cell (resistivity test fixture Keithely 8009) used for the conductivity measurements. The system is equipped with an internal sinusoidal voltage source that can provide test voltages up to 200 V_{peak} (140 V_{rms}). The response current, as a result of the voltage applied to the test object, is measured and used to deduce a complex capacitance. The latter parameter is recorded by the diagnostic system, which is further utilized to obtain the relative permittivity and dielectric loss taking into account the dimensions of the electrodes and thickness of the material sample as

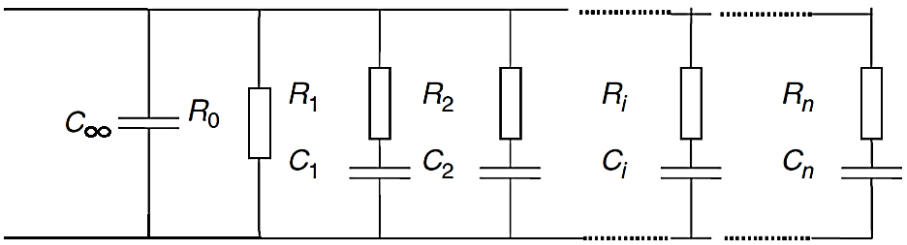

Figure 3.14. Equivalent circuit to model linear dielectrics [87, 88].

$$\varepsilon^* = \varepsilon' - j\varepsilon'' = \frac{C^* L}{A} \tag{3.4}$$

where $\varepsilon^*$and $C^*$are the complex permittivity and capacitance, respectively; $\varepsilon'$and $\varepsilon''$are the real and imaginary parts of the complex permittivity; L is the thickness of material specimens, and A is the area (2290 mm^2) of the electrode used in the test cell.

An example of the frequency dependences of the real and imaginary parts of the complex permittivity measured for studied silicon rubbers is shown in Figure 3.15. As can be seen for

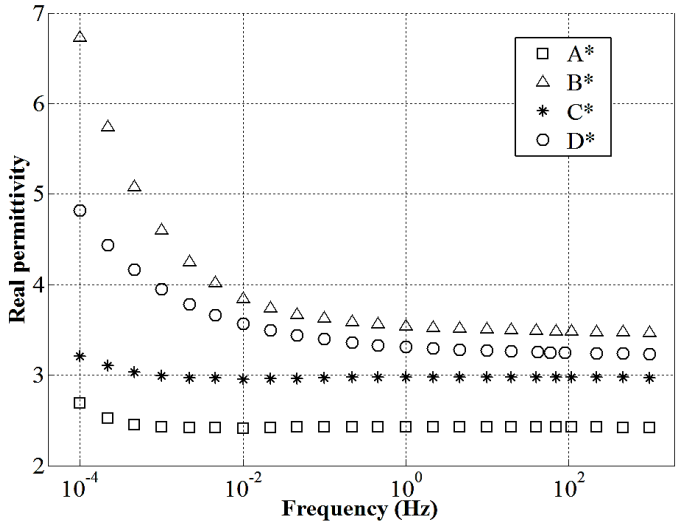

(a)

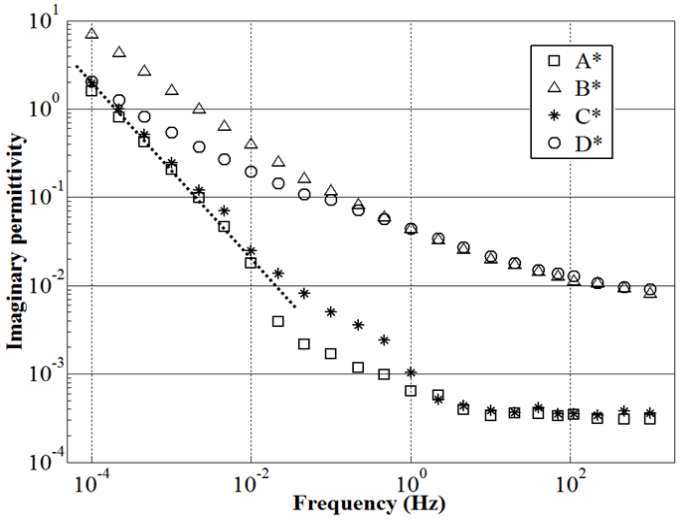

(b)

Figure 3.15. Real (a) and imaginary (b) parts of the complex permittivity for different materials. In (b), the dotted line represents fitting of the measured data points with a slope of -1of unfilled silicone rubber materials.

relatively pure materials A* and C*, the real part is nearly constant in the studied frequency window, although absolute values are different for the materials. This indicates that polarization intensity doesn't change significantly in the selected frequency range. Although, a very weak increase can be found at low frequencies that can possibly be attributed to interfacial polarization at internal interfaces between the polymer base and the fillers (note that silicone rubbers always contain some filler added for mechanical stability, but material B* and D* are also doped with additional amount of ATH). At the same time, one can observe by analyzing the imaginary parts that the frequency dependences for silicon rubbers A* and C* are almost overlapping representing similar losses in both the materials. The dielectric losses are varying with frequency. For ATH doped materials B* and D*, the imaginary parts of the complex permittivitties are almost one order of magnitude higher than for corresponding counterparts A* and C* without fillers at high frequencies close to 1 kHz. However at lower frequencies, the absolute differences are getting smaller and at 0.1 mHz, the losses of almost the same magnitude are found in all the studied materials. In addition to that, the measured data points for silicone rubber A* and C* at lower frequencies (from 10^{-4} Hz to 10^{-2} Hz) are best fitted by a line with a slope equal to -1. This type of behavior is normally allocated to dc conduction [90]

$$\varepsilon'' = \frac{K_{vdc}}{\varepsilon_0 \omega} \qquad (3.5)$$

where K_{vdc} stands for pure dc volume conductivity and ω is the angular frequency.

By analyzing the measured characteristics of ATH doped materials B* and D*, a distinct rise can be noticed at lower frequencies in the real parts of the complex permittivity. Such feature is similar to that resulted from low frequency dispersion (LFD) [61]. This phenomenon is

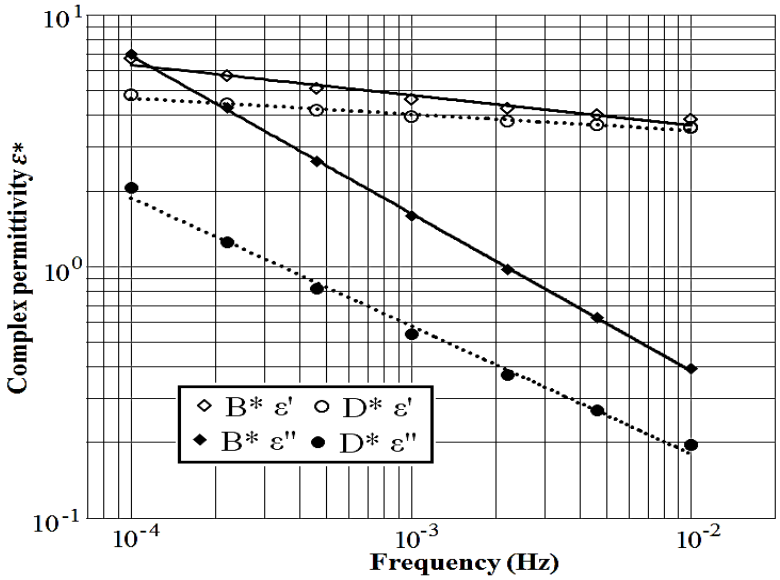

Figure 3.16. Complex permittivity of ATH doped materials. The solid and dotted lines represent power frequency fittings of the measured data points.

associated with accumulation of charges either in the material bulk or at the interface. The significant contents of ATH (50 wt. %) in silicone rubbers B* and D* may give rise to such accumulation of charges at the internal interfaces due to gradients in the dielectric properties of filler particles and base materials. Thus, interfacial polarization may be activated and, consequently, an increase is seen in the relative permittivity at lower frequencies.

In order to interpret further the obtained results, the mathematical treatment proposed by Jonscher [61] is followed. The frequency dependences of the real and imaginary parts of complex permittivity are fitted by power laws and the results are shown in Figure 3.16. It is worth mentioning that the lower frequencies need to be carefully chosen for the fitting and depending upon the range, the characteristics of the fittings may slightly vary. However, assuming that the dielectric properties of silicone rubbers A* and C* are dominated by pure dc conduction in this range, as shown in Figure 3.15, the same frequency window is selected for treating the measured data for ATH doped materials. The results of the fitting can be seen in Figure 3.16 while information on the slopes of the lines and ration of dielectric susceptibilities is given in Table 3.7 (for comparison purpose, the obtained data for silicone rubbers A* and C* is also mentioned in the same table). As seen, the differences between the slopes for relative permittivities and losses in both the materials (B* and D*) are significant and the values for the imaginary parts are far from unity. The latter indicates strong dependence of electrical conductivity on frequency, which is opposite to the attributes of LFD [61]. Further, the ration that corresponds to the fraction of the accumulated charge is much higher than the numbers indicated in the literature (typically in the range of 0.01 to 0.1) [61]. Based on these observations, one may conclude that the measured characteristics of ATH doped silicone rubber materials do not match those associated with low frequency dispersion. Instead, comparing the numbers listed in Table 3.7, it may be argued that it is the dc conductivity that dominates the properties and is accompanied by weak contributions from interfacial polarization. The insignificant effects of the latter phenomenon may be related to the smaller volume fractions of interfaces in the studied insulation materials. However, its role in composites may become important at considerable volume fractions and an example that illustrates such tendency is given in the section 5.3.

Table 3.7. Parameters obtained from fitting the measured dielectric properties of HTV silicone rubber materials using the model described in [61].

Deduced parameters	Materials			
	A*	B*	C*	D*
Slope of ε'	-0.02	-0.12	-0.017	-0.06
Slope of ε''	-0.96	-0.63	-0.93	-0.51
$x'(w)/x''(w)$	----	0.82 - 7.2	----	1.9 - 13.1

4. Materials charging by corona in air and surface potential decay measurements

This chapter focuses on experimental setup and procedures used for analyzing surface charge dynamics on HTV silicon rubber materials samples. Influences of different parameters like amplitudes of dc charging voltage, distance between corona electrode and material surface, material properties on surface potential distributions are investigated. Potential decay measurements on surfaces of the studied materials are performed at different pressures of ambient air in order to evaluate the relative contribution of gas neutralization to the total charge decay as well as to analyze solely the role of solid materials properties on charge dynamics. In addition, characteristics of charge decay on highly resistive materials are examined for exploring mechanisms of potential decay that are not typical for studied silicone rubbers.

4.1 Experimental setup and procedure

The experimental setup was built inside a sealed metallic chamber (~1 m^3) shown in Figure 4.1 (general view) and Figure 4.2 (specific views) that allowed for carrying out the measurements at different gas pressures. The pressure in the chamber was controlled by means of a rotary vacuum pump and a digital manometer (precision of 0.1%) was used for monitoring its level. The conditions in the laboratory during the experiments were practically constant (air temperature 18-20 ^oC, humidity ~50%).

Inside the chamber, a linear positioning system with a movable grounded table carrying a flat material sample was installed and it was connected to an external controller via a low voltage bushing. The charging arrangement included a corona needle, which was used to deposit charges onto the sample. The needle diameter was 0.89 mm with a tip radius of about 0.125 mm. The needle was mounted on a wooden arm and it was connected to an external dc voltage generator through a high-voltage bushing. A schematic view of the charging arrangement is shown on the left side of Figure 4.3.

The surface potential measuring set-up contained a Kelvin's type vibrating probe (Trek 3455ET) installed on the same wooden arm as the corona needle and connected to an electrostatic voltmeter (Trek 341B, ±20 kV) located outside of the chamber. The distance between the probe and the sample was fixed at about 2 mm in order to achieve accurate results. The voltmeter provided a low voltage replica (attenuated by 1000 times) of the probe potential. A voltage divider was used to further step down the potential to a ratio of 4:1 to make it possible for data acquisition system to handle it. In the tests, the positioning system was used to move the sample beneath the charging needle and the probe. Information on the position of the sample and signals

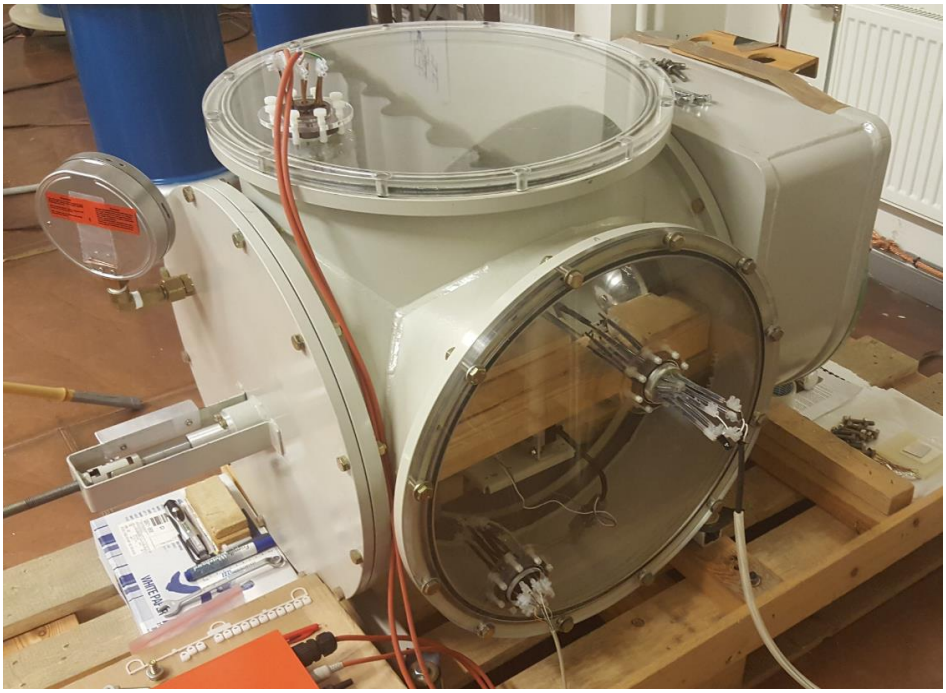

Figure 4.1. General view of the test chamber, inside which the experimental setup comprising charging arrangement and electrostatic probe is assembled.

from the potential probe were communicated to a computer through a data acquisition card. A schematic view of the scanning setup is shown on the right side of Figure 4.3.

A material sample (100 mm × 100 mm × L (thickness) mm) was placed on the grounded movable table inside the test vessel and its open surface was scanned to check if the initial magnitudes of surface potential were sufficiently low (typically below 100 V). For charging, the table was brought to the position such that the tip of the needle was located at the center of the sample. Thereafter, the surface was charged by applying DC voltages to the corona needle for 2 minutes (different amplitudes and polarities were utilized). During charging, air pressure in the test vessel was equal to the external atmospheric pressure. After completing the charging, it was evacuated down to a certain pressure level. Two pressures, 600±10 mbar and ~300±10 mbar, were considered in the present study. Immediately after the charging was completed, the needle was grounded and the table with the sample was brought to the position under the electrostatic probe (which took approximately 30 sec) and the surface potential measurements started. For obtaining distributions of the potential on the surface, the sample was moved under the probe. In the preliminary experiments, it was observed that the charging resulted in symmetrical potential distributions around the point above which the corona needle was located. For this reason, a half of a sample surface was typically scanned along a line starting from the sample edge to its center that allowed for reducing scanning time down to ~5 s. The measurements of the surface potentials were repeated at different instants after the charging. Between the consecutive measurements, the sample was moved to a parking position away from any sharp edges to avoid external disturbances of the surface potential.

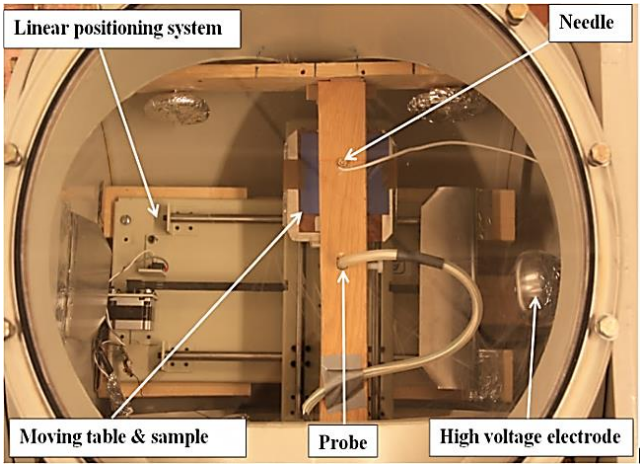

(a)

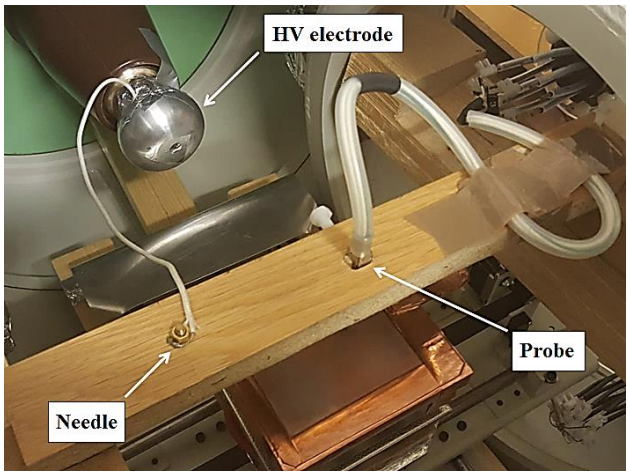

(b)

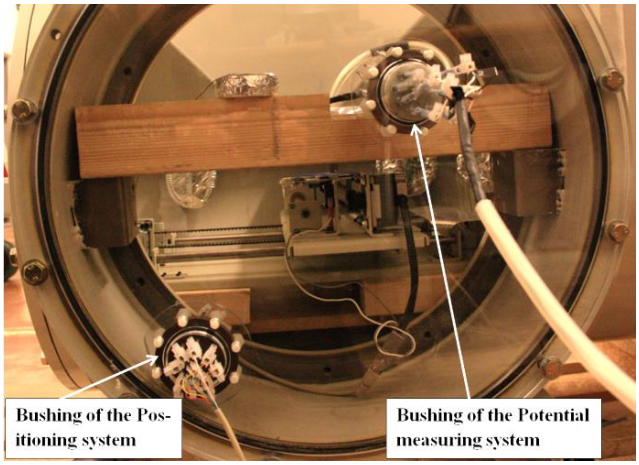

(c)

Figure 4.2. Top (a), inside (b) and side (c) views of the sample positioning system with charging and scanning setups mounted in the test vessel. Note that the charging needle and the probe are beneath the arm and are facing downwards to the sample.

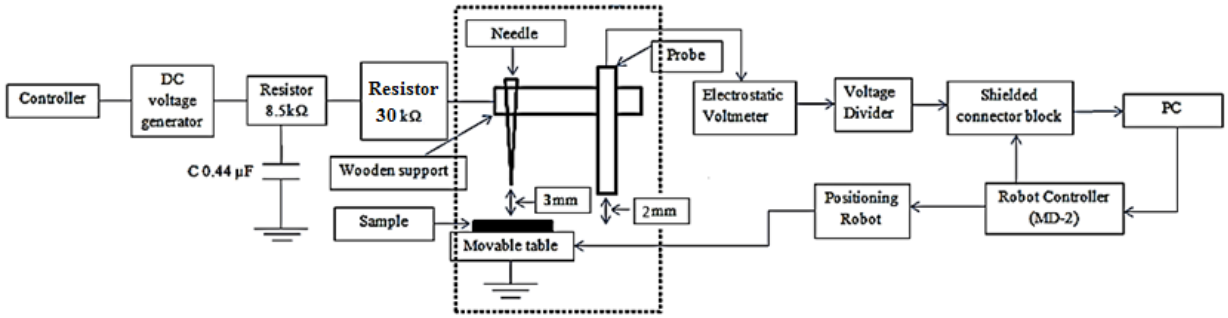

Figure 4.3. Schematic view of charging arrangement and scanning setup for surface potential distribution measurements. The broken line shows the metallic chamber wall.

4.2 Test conditions

Potential decay measurements inside the test vessel were taken at three different pressure levels that allowed for realizing the following conditions for the neutralization of deposited surface charges by air ions:

Natural gas neutralization – this condition inside the test vessel was achieved by taking the decay measurements at ambient pressure. Gas neutralization takes place due to the interaction of surface charges and free ions of opposite polarity arriving from the gas to the material surface. The free counter ions are driven by the electric field induced by the surface charges. The intensity of gas neutralization depends on the amount of ions present in the gas phase as well as on the field strength in the vicinity of the material surface.

Reduced gas neutralization – the relative contribution of gas neutralization to the surface charge decay can be reduced by lowering air pressure inside the test vessel. As mentioned above, one of the reduced pressure levels in the experiments was ~600 mbar. It was chosen due to its practical significance since gas neutralization can be of primary concern for insulation of components of HVDC power transmission systems operating at high altitudes. Thus, HVDC power transmission lines may pass through high mountain areas, see e.g. [91] where altitudes up to ~4300 m are mentioned. Under such conditions, air pressure is reduced in ~40% as compared to its normal atmospheric level. The relative contribution of the gas neutralization to the surface charge decay on insulating polymeric materials has not been investigated under such conditions.

Negligible gas neutralization – refers to the situation where the potential decay takes place solely due to solid material properties. This condition was achieved by measuring the decay characteristics at ~300 mbar air pressure inside the test vessel.

In addition to the above mentioned test conditions, surface potential decay measurements were also performed on double layered material samples (see chapter 5) as well as at elevated temperatures (will be discussed in chapter 6).

4.3 Determination of background densities of ions in air at different pressures

Measurements of density of ions in air inside the pressure chamber are quite difficult due to the limited gas volume and a necessity to connect external devises to internal ion counters. Therefore, an alternative way for its evaluation was chosen: two sufficiently large parallel plate electrodes separated by a certain distance were placed in the test vessel, a certain dc voltage was applied and a current between them was measured using e.g. Keithley 6517A electrometer. The obtained currents at different air pressures were further post-processed to deduce the density of charge carriers. It is worth mentioning that the currents measured in this way were extremely low and were close to the sensitivity level of the electrometer. Thus, recording current in the linear region of voltage-current characteristics of air [26] was not possible and, therefore, currents corresponding to the initial phase of an exponential region (corresponding to formation of electron avalanches) were considered. The developed experimental setup and procedure as well as obtained results are presented below.

Experimental setup and procedure

The test setup consists of a pair of parallel electrodes of Rogowski shape (diameter 100 mm, separation 8.5 mm) placed inside the metallic chamber. One of the electrodes was connected to the external HVDC generator through a high-voltage bushing while another one was connected to Kiethely electrometer 6517A via dedicated bushing.

In the experiments, the pressure inside the test chamber was reduced down to a certain level using vacuum pump and then the voltage was applied. The voltage was increased in steps and the corresponding current was recorded. At each step, a spike in the current was observed (was identified as a capacitive current) and, therefore, the current was allowed to relax to a constant value before the next voltage step was applied. The same procedure was repeated at different air pressures.

Ion current measurement at different air pressures

The measured currents are shown in Figure 4.4. As can be seen, the slope of the lines gets steeper with the drop in the pressure level. Also, the data points at a particular applied voltage have lower values at reduced air pressures, though the electric field (reduced value) is much higher.

The current density resulted from the drift of charge species between the electrodes inside the test chamber can be expressed as

$$J = q\mu nE \qquad (4.1)$$

Here, μ is the average mobility, n is the concentration of charge carriers and E is the electric field. As seen from Figure 4.4, the leftmost points on the curves represent the lowest field

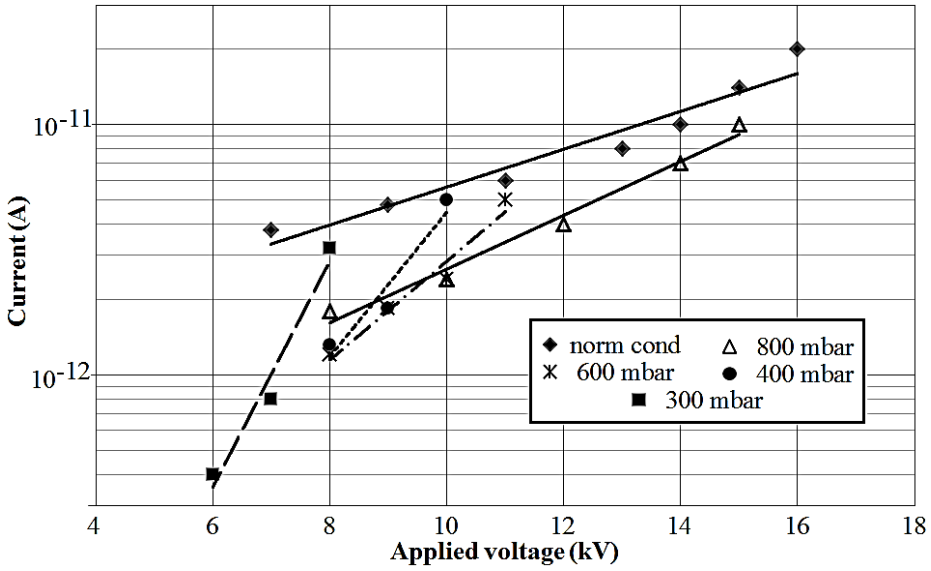

Figure 4.4. Ion current measured at different air pressures. The solid and broken lines are the exponential fitting of the experimental points.

strength (applied voltage divided by the gap distance) indicating the current level close to that due to background ionization processes only. However, the measured quantitity tend to increase when the applied field becomes stronger that corresponds to the initiation and intensification of electron impact ionization in air, i.e., to the appearance of Townsend's discharge. This process can be mathematically represented as

$$n = n_0 e^{\alpha d} \qquad (4.2)$$

Here, n_0 is the background ion density, α is the Townsend first ionization coefficient, and d is the gap distance between the two electrodes. In principle, equation (4.2) can be used for obtaining n_0 provided that the dependence of α on field strength is well defined. Howerer, the applied fields in the experiments were weak and well below the lowest magnitude for which values of α are reported in the literature [92]. Therefore, the measured data were treated according to (4.1) by considering only the initial point on each profile. Using the mobility μ = 2 cm^2/Vs [93], the estimations resulted in the initial densities n_0 listed in Table 4.1. As one can observe, the concentration at normal pressure n_0 ~ 20 cm^{-3} is well below than the commonly accepted value

Table 4.1. Ion density obtained inside the test vessel at different ambient pressures using (4.1).

Parameter	Pressure, bar				
	1	0.8	0.6	0.4	0.3
n_0, cm^{-3}	20	7	5	5	2

~10^3 cm^{-3} [94] for open air. Such significant difference can be attributed to a screening effect of the grounded metallic vessel which attenuates the intensity of external factors (terrestrial radiation, cosmic rays) responsible for the background ionization of the gas. The reduction of the pressure down to 300 mbar yielded a significant drop (~10 times) of the ions density, which can be related to the decrease of the gas concentration, i.e. the number of molecules available for ionization. Note that the mentioned values (Table 4.1) at lower pressures are overestiamted due to the fact that the measured currents don't result from pure background ionization processes, as seen from Figure 4.4, and the actual numbers may be even lower. Hence, the amount of ions which may contribute to surface charge relaxation/decay is negligible under such conditions and thus, charge dynamics on materials samples can be solely considered due to solid material properties.

4.4 Surface charging

Different experiments were performed to analyze the influences of various factors like dc voltage amplitude, polarity, needle electrode gap distance as well as material properties on the resulting surface potential distributions. The obtained results are presented in the following sections.

4.4.1 Effect of charging voltage magnitude

Surface potential distributions for silicone rubber E* obtained with different amplitudes of the negative dc charging voltages at distances of 1 mm and 3 mm between the needle tip and the material surface are shown in Figure 4.5a and Figure 4.5b, respectively. Note that the charging arrangement used, shown in Figure 4.2, provided a symmetrical distribution of surface potential around the center of the sample above which the corona needle was located. Therefore, the potential profiles are shown for a half of the scanned path and the arrows indicate the position of the corona needle. A complete profile can be obtained by mirroring the distributions around the central point. As can be seen, for 1 mm gap distance, all the potential profiles are characterized by a maximum value that move towards the zero co-ordinate with higher applied voltages and, therefore, causes an increase in the area covered by the charge spot. Further, it can be noticed that the resulting distributions are saddle shaped, which have been observed in other studies, see e.g. [3, 95]. Such feature can be attributed to overcharging of the surface right below the needle tip that may lead to back discharges after switching off the charging voltage neutralizing part of the deposited charges. The neutralized area is defined under the curve between the maximum magnitude of surface potential and central point where the corona needle is placed. Since, with the increasing charge spot, the area covered by the electric field lines is getting larger, therefore, causing an increase in the intensity of back discharges.

For the distance of 3 mm between the needle and the sample, similar distributions as that for 1 mm gap are obtained. However, stronger spread in the surface potential can be observed as compared to the previous case. For the charging voltage of -3 kV, the potential distribution is bell shaped, however, the profile is transformed into saddle shape at -5 kV and it becomes even more

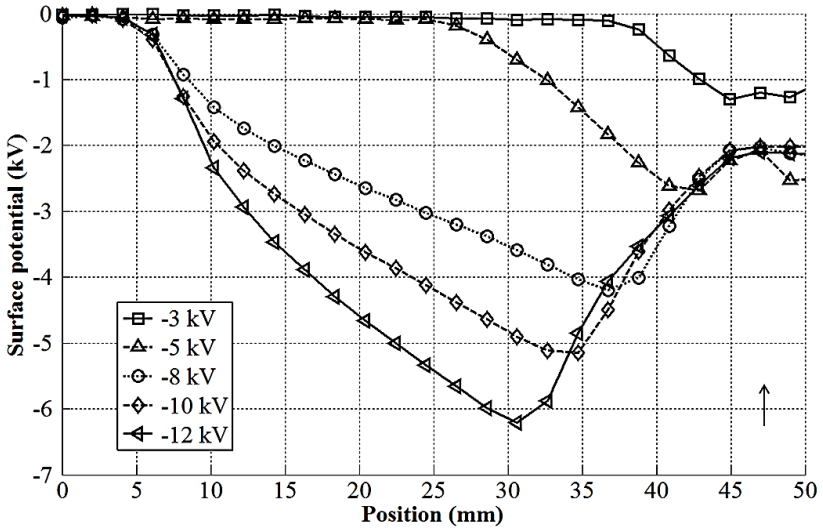

(a)

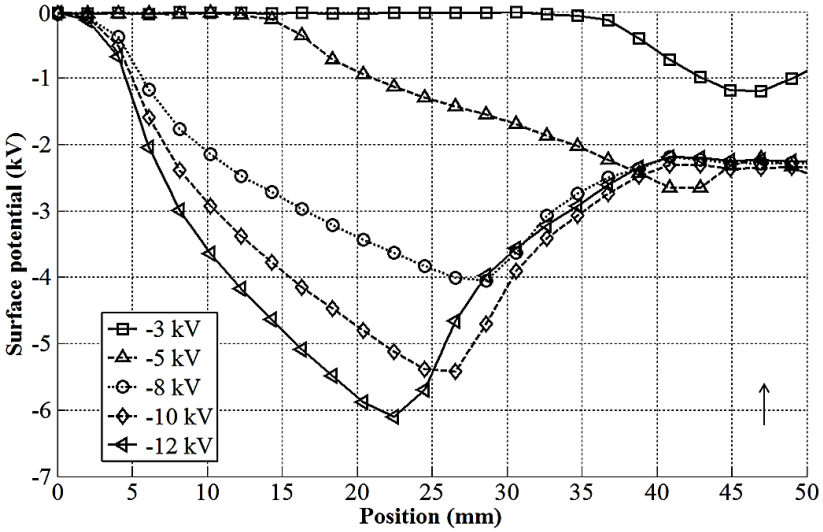

(b)

Figure 4.5. Surface potential distributions for material E* obtained with different amplitudes of the negative dc charging voltages at needle electrode to surface gap distances of 1 mm (a) and 3 mm (b). The arrow indicates the location of the corona needle during charging (the center of the sample).

prominent as the corona voltage approaches -12 kV. Also, it can be noticed that with the increasing gap distance the back discharges become more intense and, therefore, causes an increase in the neutralization area.

From the above demonstrations one may suggest that increasing either of the two parameters (voltage amplitude or needle-sample distance) results in a larger area of the charged spot and larger spread of the surface potential.

It important to mention here that in the rest of the study, voltage amplitudes of ±12 kV and needle-sample distance of 3 mm were used in the charging procedure.

4.4.2 Effect of materials properties

Potential distributions measured on flat samples of HTV silicon rubber materials at normal ambient air pressure after charging are presented in Figure 4.6. As it is seen, all the obtained profiles are characterized by a maximum magnitude appearing at distances 20-30 mm from the edge of the sample and reduced potentials at the center of the sample. Despite of the non-uniform surface charging, the obtained potential profiles allow for establishing certain regularities. Thus, it can be observed that the distributions for both polarities of the charging voltage have in general similar shapes. However, the magnitudes of the surface potential at negative polarity are slightly higher. This reflects larger amount of negative charges which are accumulated on sample surface. Furthermore, the measured potential distributions demonstrate that surfaces of the materials used could be charged in different ways and up to different levels depending upon their properties. Thus, one may notice a correlation between the materials parameters provided in Table 3.2, Table 3.3 and Table 3.6 and the surface potential distributions – the lower are the values of surface and bulk conductivities, the larger is the size of the charged spot on the surface and the higher is the peak value of the potential.

In addition to the demonstrated factors, influences of other parameters like time duration of the applied voltage, level of ambient air pressure, pre-stressing of insulators etc. were also evaluated on surface charging and the results of such measurements can be found in [3, 47, 96].

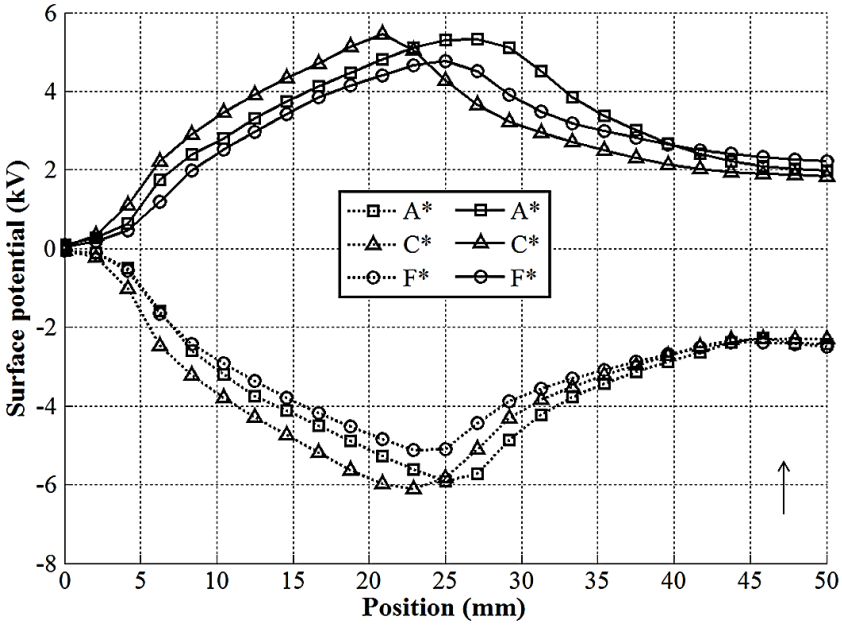

Figure 4.6. Measured surface potential profiles at atmospheric pressure at 30 s after charging. Broken and solid lines show the negative and positive distributions respectively.

4.5 Surface potential decay

Effects of various parameters such as air pressure, polarity of deposited surface charges and influence of solid materials properties on surface charge dynamics were investigated. Depending on the surrounding environment and material related properties, SPD measurements took a time span from a couple of minutes to couple of weeks. The obtained results are described in the following sections.

4.5.1 Potential decay at various pressures of ambient air

An example of the surface potential distributions measured at two ambient pressures inside the test chamber on thick sample of ATH doped material B* is shown in Figure 4.7. Similar data collected for other materials can be found in [47]. It is worth to mention that each experiment under similar conditions was conducted at least three times. The recorded potential magnitudes at different locations on the material surfaces were post-processed to get mean values. The data in the figure are shown with error bars representing standard deviations while the mean values are connected by lines and represent potential distributions. As can be seen, the deviations from the mean surface potential magnitudes at different instants during the decay process are not significant indicating good repeatability of the results.

As can be noticed from the measured distributions, the magnitudes of V_s decrease with time without lateral spread of the charged spot. This indicates that contribution from surface conduction to the potential/charge decay is negligible. Furthermore, comparing the recorded profiles at different ambient pressures, it can be observed that the decay process takes longer time at reduced air pressure. This can be attributed to the reduced amount of free ions in the test vessel, as was demonstrated in section 4.3 above. The weak effects of both the surface leakage and gas neutralization suggest that bulk conduction is the most probable mechanism affecting potential decay under conditions of the present study.

The non-uniformity of the measured distributions (arising due to the charging method used) allowed for obtaining potential decay characteristics at different locations on sample's surfaces, i.e., at its different initial magnitudes and thus induced fields in the material. These non-uniformities, however, do not contain strong gradients (discontinuities) and are within the range which could be successfully resolved by the potential probe used. In case of uniform surface charging, obtaining field dependencies of decay characteristics or other associated parameters (e.g. conductivities) would require a number of separate experiments. Moreover, non-uniform surface potential/charge profiles can be considered as more common practical situation than uniformly distributed potentials/charges, which may seldom appear on real insulating surfaces.

Decay of the maximum magnitude of surface potential

Normalized surface potential decay characteristics obtained for the locations corresponding to the maximum values of V_s on samples of different materials are shown in Figure 4.8. As can be seen,

the decay process is strongly affected by the material properties. Thus, the time needed for the reduction of the potential down to 50% of its initial value is the shortest for material B*, it is approximately four times longer for material C* and in more than ten times longer for material E*. This correlates well with the measured bulk conductivities of the materials (Table 3.2 and Table 3.3). As seen, the fastest decay is for the relatively most conductive material (B*) while the slowest is for the most resistive one (E*). The polarity of the deposited charges does not seem to affect the decay process significantly (compare corresponding curves in Figure 4.8a and 4.8b).

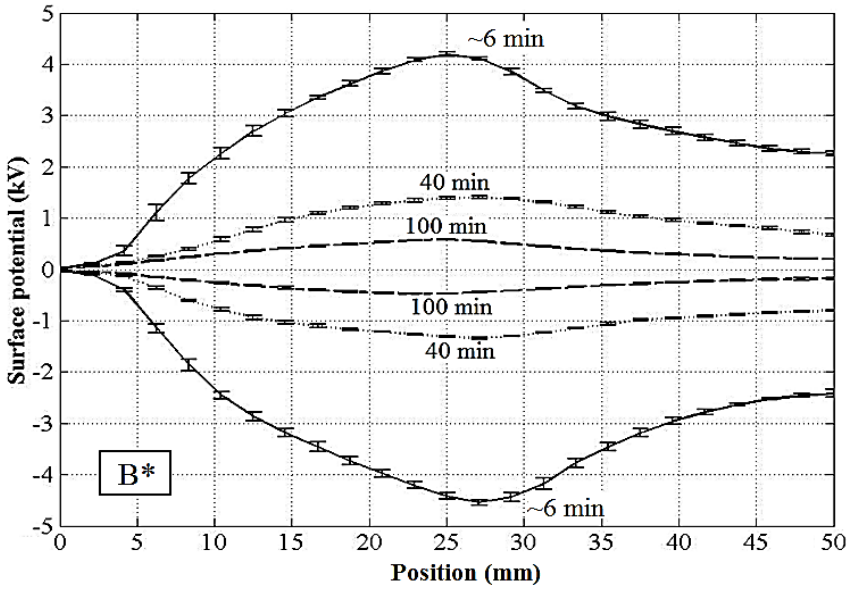

(a)

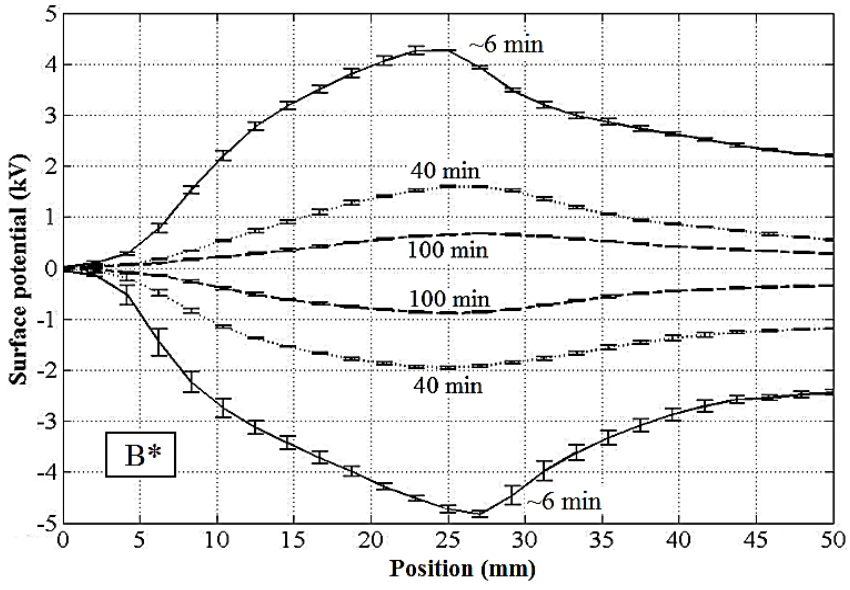

(b)

Figure 4.7. Measured surface potential distributions at different time instants during the decay process on material B* at normal (a) and 300 mbar (b) air pressure.

As seen in Figure 4.8, the charge decay becomes slower at the reduced pressure levels for all the materials and both polarities of deposited surface charges. Further, one can also observe that the potential vanishes faster at the beginning of the process when its magnitudes are relatively high. This is clearly seen in Figure 4.9 where the decay rates, dV_s/dt, deduced from the measured characteristics are presented. At normal pressure and higher magnitudes of surface potentials, stronger electric fields are induced within the gas volume thus making the arrival of free counter

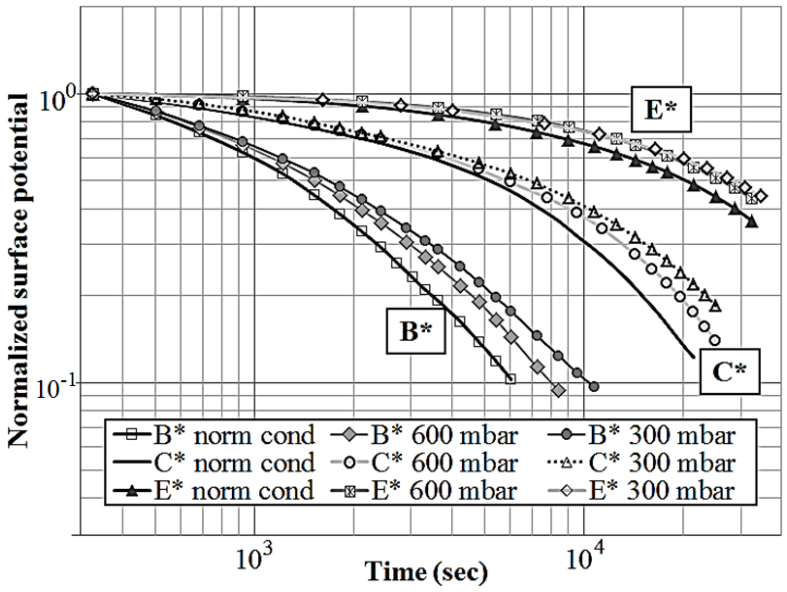

(a)

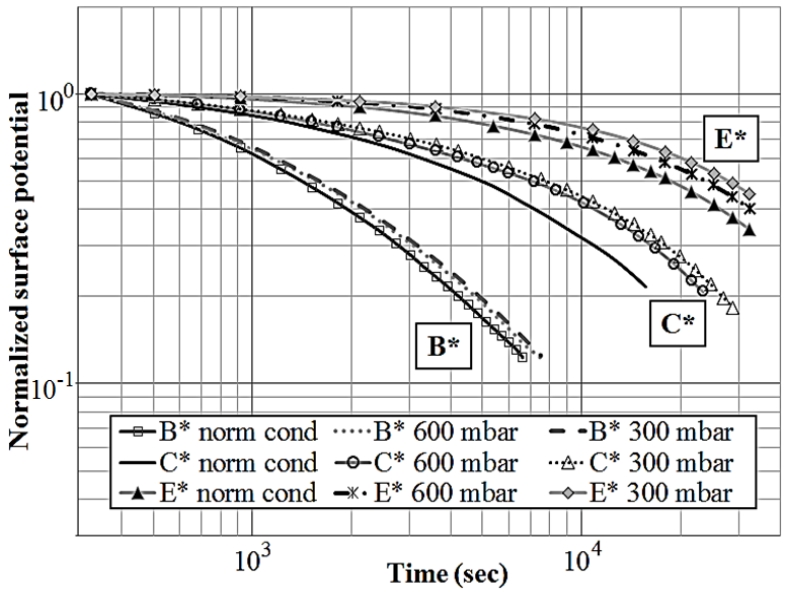

(b)

Figure 4.8. Surface potential decay characteristics for different materials at different air pressures for (a) negative and (b) positive charging. The surface potential is normalized to its maximum value corresponding to the first measured point.

ions present in air and neutralization of the deposited charges more efficient. However, at lower magnitudes of V_S, the potential derivatives decrease and tend to merge into the same region (encircled areas). These findings may suggest that the distributions, presented in Figure 4.7, will deplete faster at the region where maximum values of *Vs* exist compared to the periphery of the profiles. The reduction of air pressure yields smaller decay rates without bringing a major change in the shapes of the characteristics indicating overall weak contributions of the gas neutralization to the total charge decay. The relative differences between the potential derivatives at different air

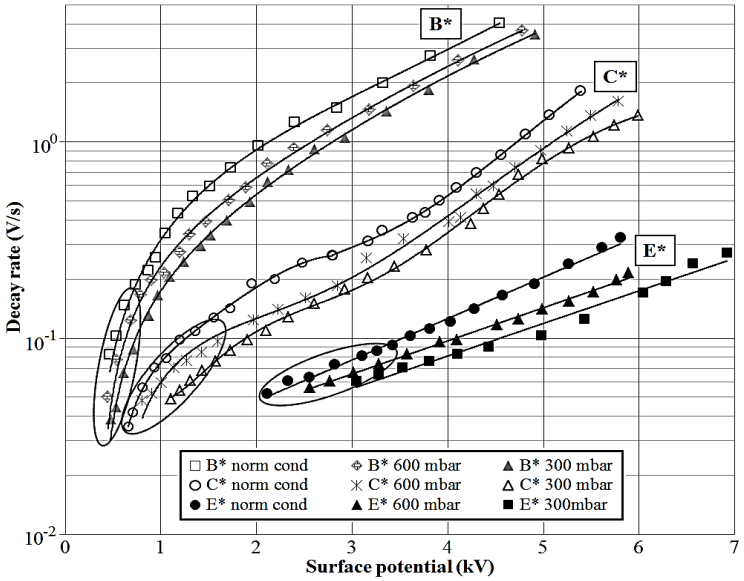

(a)

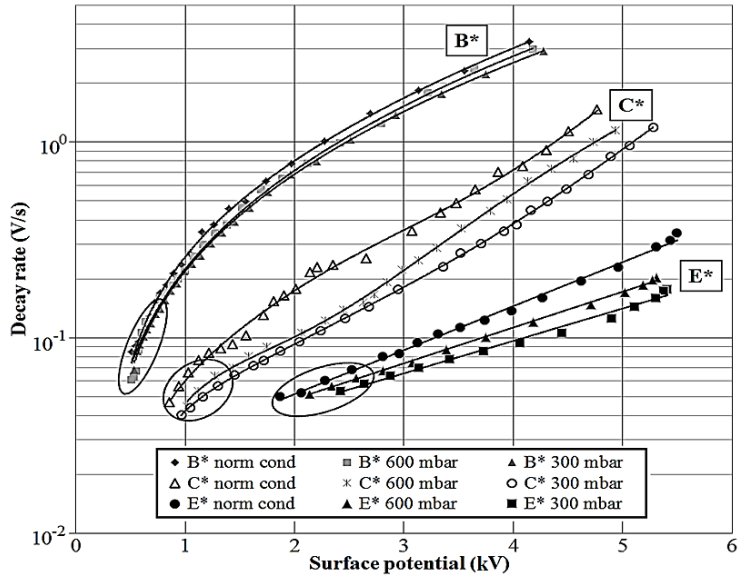

(b)

Figure 4.9. Decay rates of surface potentials at (a) negative and (b) positive charging for different materials and gas pressures. The solid lines represent the results of fitting.

pressures are similar for all the studied materials. The exception is the set of data for silicone rubber B* at positive polarity (Figure 4.9b) where one can observe just small deviations due to the change in gas pressure. The reason for this is unclear and requires further analysis.

4.5.2 Influence of material properties

In order to analyze solely the role of solid material properties on SPD process, normalized decay characteristics obtained at 300 mbar ambient pressure for thin and thick samples of silicone rubber materials in Figures 4.10 and 4.11 were utilized. It can be inferred from Figure 4.10 that different material compositions and thus the bulk properties play a deterministic role in controlling the decay process. For materials containing additional amount of ATH filler (B and D), the decay profiles are quite similar. However, the characteristics for original silicone rubbers (A and C) are different, which can be attributed to the differences in their properties brought about by the various nature of curing agents. It is noticeable also that the time required for neutralization of deposited surface charges can be correlated with the volume conductivities of the materials (Table 3.2). Thus the decay is fastest for material D characterized by the highest conductivity among the studied materials. At the same time, the lower conductivity of material A (by almost one order of magnitude) yields much longer time for surface potential to vanish. Quantitatively, time to halving the surface potential (50% of its initial value) is approximately 2 times longer for material C and more than 5 times longer for material A than that for material D.

Data for thick samples, shown in Figure 4.11, demonstrate similar features as observed for thin samples of the same materials. Thus, relatively shorter time can be noticed for charge decay on additionally doped materials compared to silicone rubbers without fillers. Likewise for the thin materials, the time interval required for the potential to drop down to half of its initial values can be linked to the magnitudes of the volume conductivities (see Table 3.2).

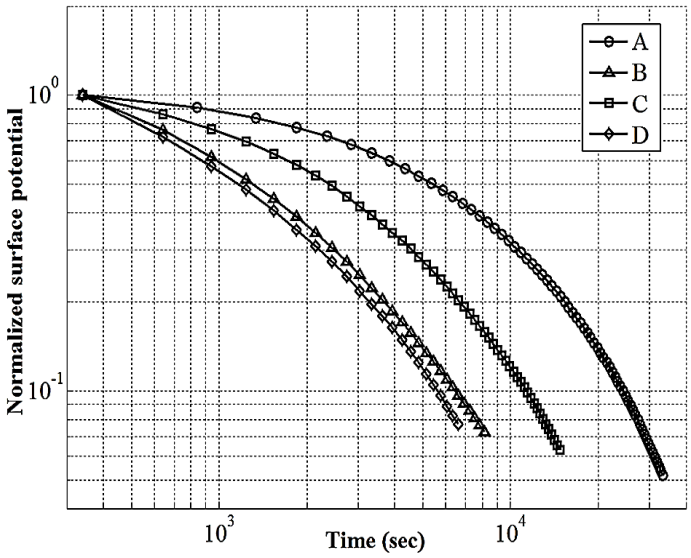

Figure 4.10. Normalized surface potential decay characteristics obtained at 300 mbar ambient pressure for thin samples of HTV silicone rubber materials.

In spite of the similarities found in the SPD and its correlation with the materials' conductivities, there exist some non-matching features. For instance, for thin samples of materials B and D, the decay is similar even though the conductivities differ by nearly 2 times. On the other hand for thick samples of materials C* and D*, the values indicated in Table 3.2 are very close (only the digit after the decimal point is different), however, clear dissimilarities can be observed in the decay profiles. In addition to that, comparing the right most cures (Fig. 4.10 and Fig. 4.11), fast decay can be noticed for silicone rubber A compared to material C* while the conductivity of the

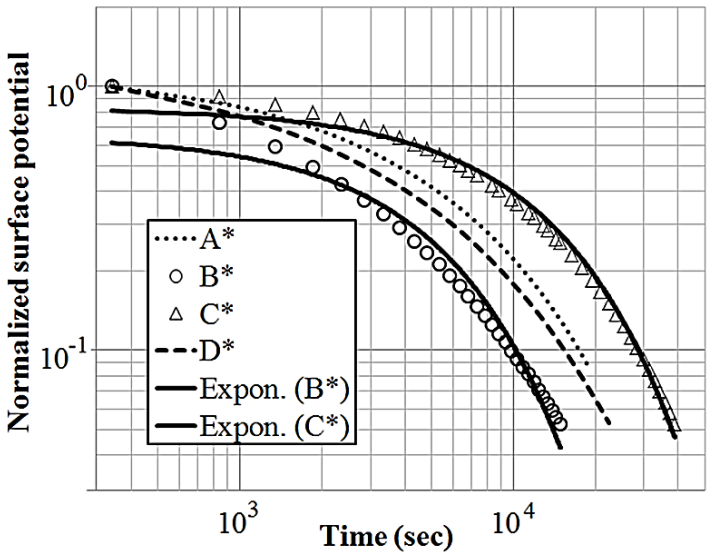

(a)

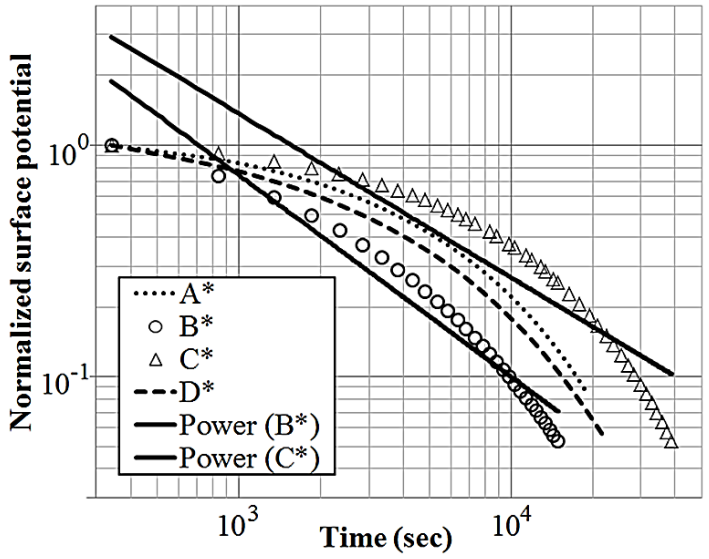

(b)

Figure 4.11. Surface potential decay characteristics for thick samples of silicone rubbers fitted with (a) exponential and (b) power laws. The dotted lines and markers represent the experimental data while the solid lines show the fits.

Table 4.2. Parameters obtained from fitting surface potential decay characteristics measured on HTV silicon rubber samples.

Materials	$a \cdot \exp(b \cdot t)$		$c \cdot t^d$	
	a	b	c	d
A*	0.940	– 0.00014	18.47	– 0.47
B*	0.935	– 0.00027	38.57	– 0.61
C*	0.918	– 0.00008	18.68	– 0.45
D*	0.887	– 0.00016	26.23	– 0.53

former is lower than the latter one (Table 3.2). These attributes may not be explained based on the single values in Table 3.2, and, therefore, bulk conductivities in an extended range of electrical fields are required to be examined to make better interpretations of the decay profiles.

A number of mathematical representations have been proposed for analyzing the role of bulk conduction processes on SPD. Thus, it has been shown in [25, 38] that exponential decay characteristics are typically associated with stable conduction process (constant intrinsic conductivity) while other mechanisms (charge injection, slow polarization, etc.) result in power law type dependences. Incorporating this approach for analyzing the measured data, fittings of the different types were executed and are shown in Figure 4.11 by solid lines (note that the results are provided for the most and least conductive silicone rubbers). The fitting parameters are provided in Table 4.2. As seen in the figure, the measured SPD profiles are better fitted by the exponential functions (Figure 4.11a), covering either a major portion of the data points (materials C*) or at least an essential part of them (materials B*). However, one common feature is that the solid lines follow well the measured decay curves at the latter stages. As for the fitting with power laws, the agreement with experimental data is poor (Figure 4.11b). Based on these observations, one may suggest that intrinsic conduction is mainly responsible for the surface potential/charge decay in most of the thick materials. Similar results were obtained for the thin samples, Figure 4.12, which provided higher induced fields levels during decay for the same magnitudes of V_S.

Though the fittings do provide some useful information, however, they include uncertainties due to the fact that single exponential or power law fit may not be enough to get an agreement with experimental data for the entire SPD profile. Employing piecewise functions of either form usually provide good match. However, this approach may have drawbacks. In particular, it may not be capable of providing trend lines for the data points corresponding to early stages of SPD (see plots above), which is of critical importance for making proper comparisons. In addition to that, a good match achieved by fitting may not be enough to claim a dominant effect of a certain

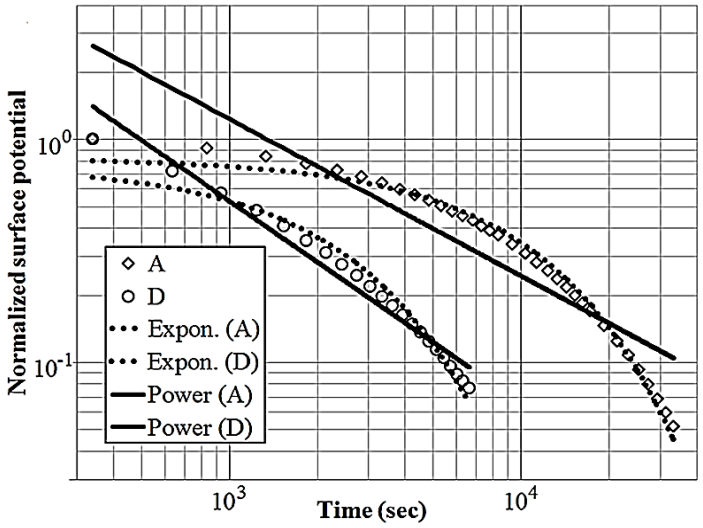

Figure 4.12. Results of fittings of SPD with exponential and time power laws for thin samples of silicone rubbers. The markers represent the experimental data while the solid and dotted lines show the fits.

SPD mechanism. The consequence of these, especially the latter fact, is that other types of analysis than simple curve fitting should be carried out in order to determine the main process relevant for a given material at given experimental conditions. Therefore in the present study, measured and computed SPD characteristics on silicone rubbers (will be discussed in section 8.3.1) are compared that allowed for making better assessments than the approach used above.

The rates of potential decay for the studied thin and thick material samples obtained utilizing the data shown in Figure 4.10 and Figure 4.11 are presented in Fig. 4.13 and Fig. 4.14 respectively.

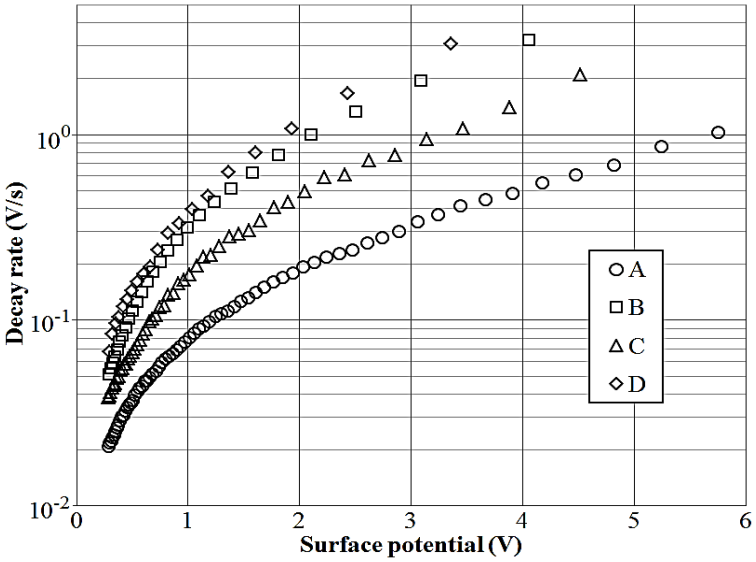

Figure 4.13. Surface potential decay rates for thin samples of silicone rubbers calculated from the data shown in Figure 4.10.

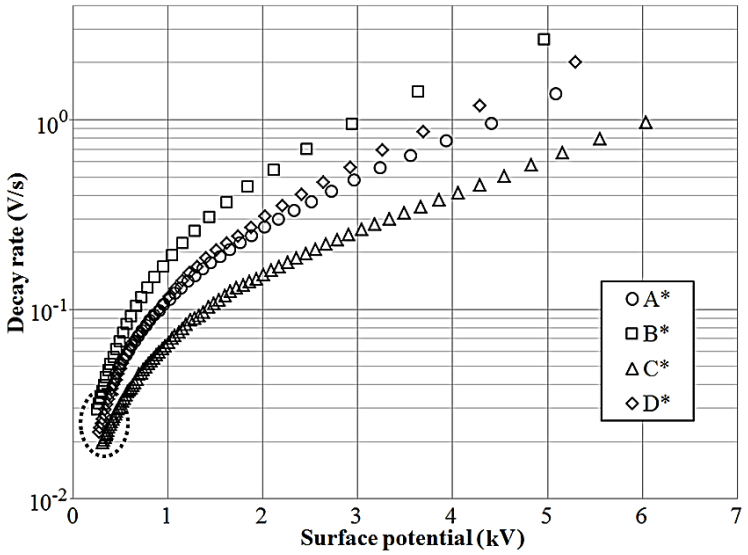

Figure 4.14. Surface potential decay rates for thick samples of silicone rubbers calculated from the data shown in Figure 4.11.

As can be seen, the rates increase with increasing magnitudes of V_s for all the materials that suggests an enhanced conduction in the bulk due to stronger internal fields induced by higher surface potentials. Essential differences in the characteristics can be observed depending on the materials properties and thicknesses of samples (i.e. strengths of electric fields). Thus, for the most conductive and most resistive thin silicone rubbers (D and A), the rates corresponding to the surface potential of ~3.5 kV (for material D it is the right most data point) differ nearly by one order of magnitude, which is almost the same as the differences in the conductivities of these materials (Table 3.2). Similar correlations can be observed for thick materials (Figure 4.14). However at the leftmost region, the features of the decay rates in Fig. 4.13 and Fig. 4.14 are slightly different. For thick samples, they decrease and tend to merge into the same region (encircled areas) indicating weak influence of materials conductivities on their magnitudes. On the other hand for thin silicone rubbers, differences may still be observed even though the electric fields are quite weak. Note that the scale used in both the figures is semi-logarithmic and, therefore, needs to be considered while describing the features of the decay curves.

4.6 Surface potential decay on highly resistive materials

Cross-linked polyethylene (XLPE) belongs to the class of materials that are used in cable insulation and other high voltage applications due to its excellent electrical properties in particular extremely high resistance. This section focuses on understanding of physical mechanisms responsible for potential decay on flat XLPE samples.

The measured properties of XLPE are given in Table 4.3 and details of the conducted measurements can be found elsewhere [47]. In the experiments, the volume current was below the lower limit that can be accurately determined by the measuring device used (Keithley 6517A

Table 4.3. Electrical characterization and thickness of XLPE [47].

Material	K_v , S/m	K_s , S	ϵ_r	L, mm
XLPE	$< 1 \times 10^{-15}$	4.8×10^{-18}	2.2	2.1

electrometer) and thus it was not possible to obtain the magnitude of K_V. The extremely low bulk conductivity may cause appearance of other decay mechanisms such as surface conduction, which so far has not been observed on silicone rubber materials (section 4.5).

Distributions of surface potential measured at different time instants during the decay process at normal and 300 mbar ambient pressure are shown in Fig. 4.15 and Fig. 4.16, respectively. As can be seen in both figures, not only the maximum magnitude of surface potential decreases with time, but also, there exist a lateral spread of the charges along the material surface. Since bulk conductivity of XLPE is extremely low, charges may not escape through the material bulk or, in other words, physical processes in the bulk may not be considered as a major contribution to the potential decay. Instead, the tangential component of the electric filed induced by deposited charges activates surface conduction that causes their lateral spreading. Also at normal pressure (Figure 4.15), surface charges are neutralized due to the arrival of free counter ions present in the surrounding volume that, however, requires relatively long times. The effect of these two mechanisms causes a decrease in the magnitude of surface potential, particularly at the location corresponding to the peak value. Further at 300 mbar air pressure (Figure 4.16), gas

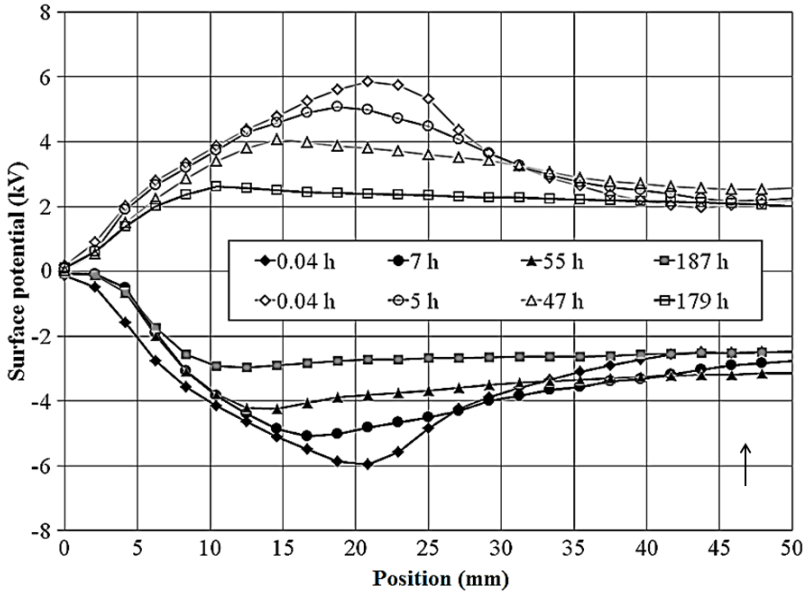

Figure 4.15. Measured surface potential distributions at different time instants during the decay process on XLPE at normal air pressure. Arrow indicates the position of the corona needle.

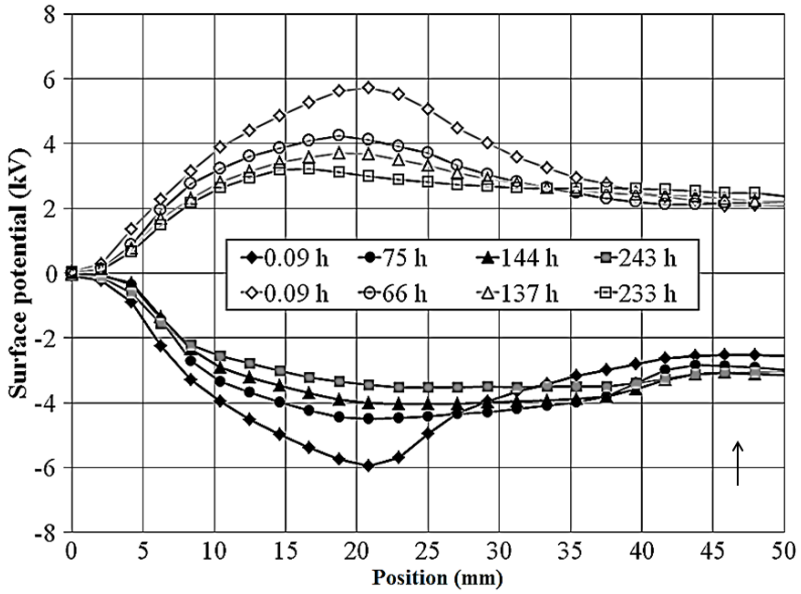

Figure 4.16. Measured surface potential distributions at different time instants during the decay process on XLPE at 300 mbar air pressure.

neutralization is insignificant as described earlier in section 4.3 and thus, charge decay may be attributed to surface conduction only. The latter effect that causes the potential on the material surface to approach to a nearly uniform value can be clearly observed for potential profiles recorded at long times after charging.

According to equation (2.1), potential distributions in this case (flat samples) provide direct images of the surface charge densities. Hence, there is no way for deposited charges to escape from the surface at reduced air pressure. Therefore, the area under each curve that gives the total accumulated charge remains almost the same as seen in Figure 4.16 for longer instants.

Normalized surface potential decay characteristics obtained for the locations corresponding to the maximum values of V_s utilizing the data presented in Fig. 4.15 and Fig. 4.16 are shown in Figure 4.17. Comparing the characteristics for different pressures, it can be observed that the decay process takes longer time at reduced air pressure. Thus, the time needed for halving the surface potential (50% of its initial value) at ~300 mbar is nearly 100 h longer as compared to that at atmospheric pressure. The reason could be due to the fact that the former provides a significant decrease in the number of free ions in the gas phase at its reduced density, demonstrated in section 4.3, and thus, strongly minimizes the intensity of gas neutralization. Under these conditions, charge decay is solely considered due to material properties. Further, due to extremely low electrical conductivity the decay process is very slow and, consequently, for the maximum potential to reach to half of its initial value, the required time is approximately 300 hours. The polarity of the deposited charges does not seem to affect the decay process significantly (compare corresponding curves in Figure 4.17a and 4.17b).

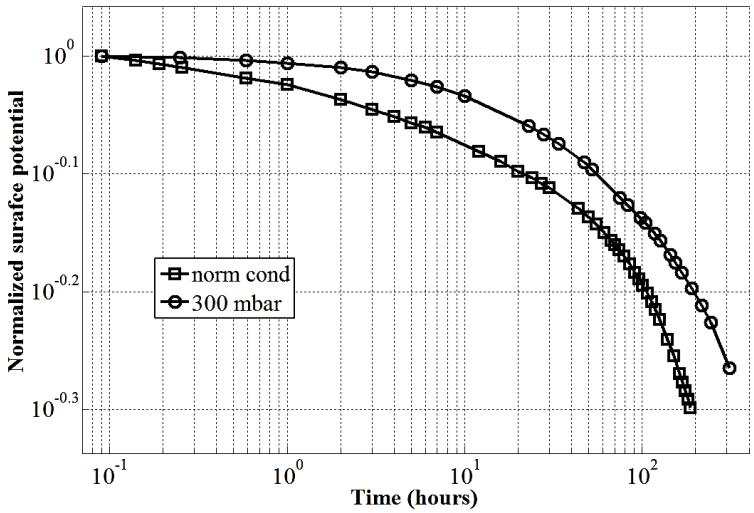

(a)

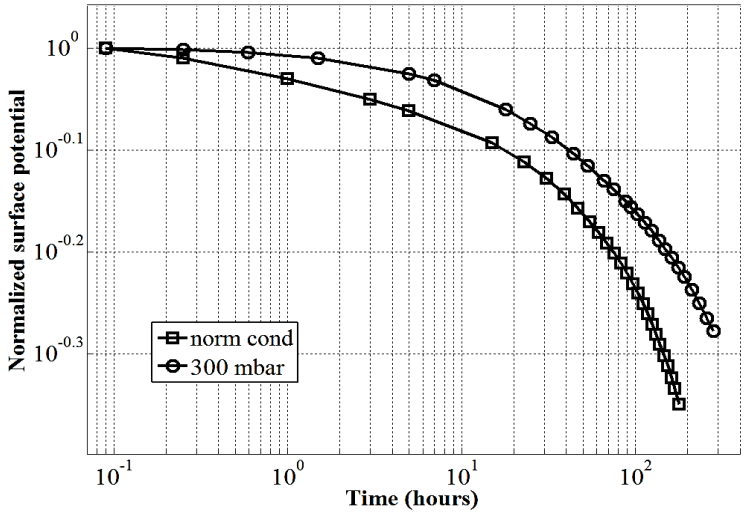

(b)

Figure 4.17. Surface potential decay characteristics for XLPE at different air pressures for (a) negative and (b) positive charging. The surface potential is normalized to its maximum value corresponding to the first measured point.

5. Measurements on double layered structures

This chapter focuses on surface potential decay (SPD) on double layered materials and their dielectric properties. Measurements performed on sandwich structures are compared to those of individual samples for analyzing possible effects of macroscopic interfaces between the layers on the obtained characteristics. In addition to that, layered structures of the studied silicone rubbers are modelled using Maxwell-Wagner capacitor theory and the output of simulations is compared to the experimental results. Influences of measured properties of materials and that of externally introduced charge densities on numerical outputs are analyzed.

5.1 Role of interfaces in composite insulators

In practice, insulation systems may exist in the form of composites e.g. air/gas-solid, solid-solid, base material and filled particles, layered structures of different dielectrics etc. and, hence, interfaces between materials could be of different scales, types and volume fractions [81, 97]. Presence of interfaces leads to existence of possible defects, gradients in materials' dielectric properties, occurrence of charge trapping sites. A lack of knowledge on thicknesses of interfacial layers in different systems makes their analysis rather complex. Additional processes can become essential if insulation is made of layers of different materials, which is very common in practice. In such systems and especially in the case of HVDC conditions, the role of internal contact surfaces become of particular importance due to possible accumulation of charges and associated with it interfacial polarization. Interfaces, under the conditions of considerable volume fractions and strong electric fields, may affect various physical processes and even control properties of insulting materials including dielectric permittivity as well as losses in the system. In addition to that, it may influence decay of charges and, respectively, potentials and fields on open surfaces of the insulation that control its flashover performance.

5.2 Preparation of sandwich structures

For the purpose of examining the role of macroscopic interfaces in composite insulators, samples of different materials were attached to each other to form layered structures. A good contact between the layers was usually achieved thanks to the sticky nature of the studied silicone rubbers which was even more enhanced by spreading a small quantity of isopropanol over the surfaces before putting them in contact. After preparation, the samples were short circuited (grounded) and placed beneath a weight for a significantly long time to get rid of tribocharges. The double layered samples with different combinations of materials were prepared to analyze the effects of conductivities, additional fillers and structural differences (order of the layers) on surface charge decay and dielectric properties.

5.3 Characterization of double layered materials

The frequency dependences of the dielectric constant measured with various double layered materials´ samples made of the studied silicone rubbers are shown in Figure 5.1. The dielectric constants of single layered materials are also provided in the same figures for comparison. As seen, if a thin layer of the same material is placed on the top of the base layer to form double layered samples, the increase of the low frequency permittivity is more significant than that found for individual materials. This reflects presence of interfacial charges between the layers (see data for A/A* and D/D*). Nevertheless, the changes in the permittivities are small and can be correlated to the small amount of charges that appear as a result of weak gradients across the

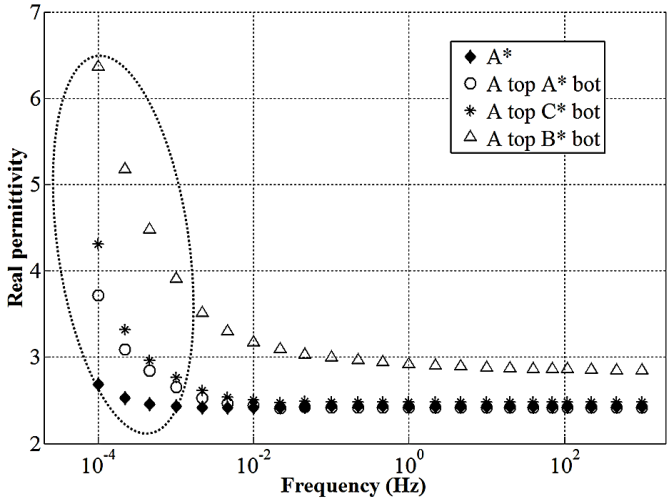

(a)

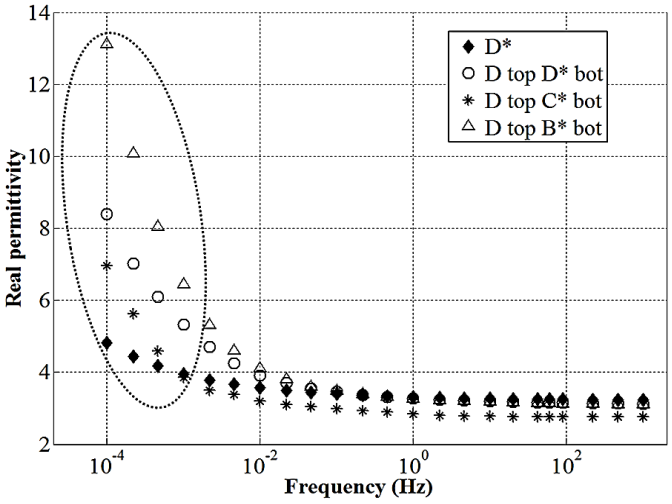

(b)

Figure 5.1. Dielectric constants obtained for single and double layered samples. In (a) and (b), the top layers are made of unfilled and ATH doped HTV silicone rubbers respectively.

interface. However, the amount of interfacial charges in a double layered structure made of two different materials may become significant and lead to larger differences in the dielectric constants. This can be observed in Figs. 5.1a and 5.1b for the combinations A/B* and D/B*, respectively. As seen, the permittivities at the lowest frequency increase in more than 2.5 times as compared to single layered materials.

Frequency dependences of the imaginary parts of the complex permittivities are shown in Figure 5.2. For better illustration and due to the fact that interfacial effects and contributions of dc conductivity come into picture only at lower frequencies, a frequency range from 10^{-4} Hz to 10^{-2} Hz is selected. As can be seen, the dielectric losses in the layered structures are much higher as

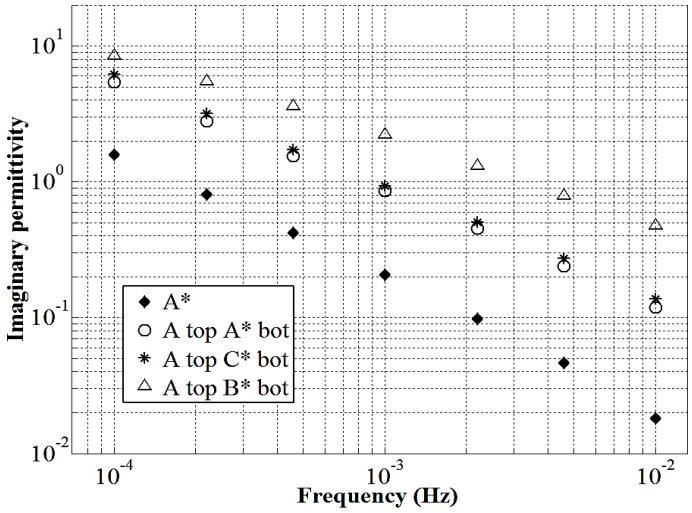

(a)

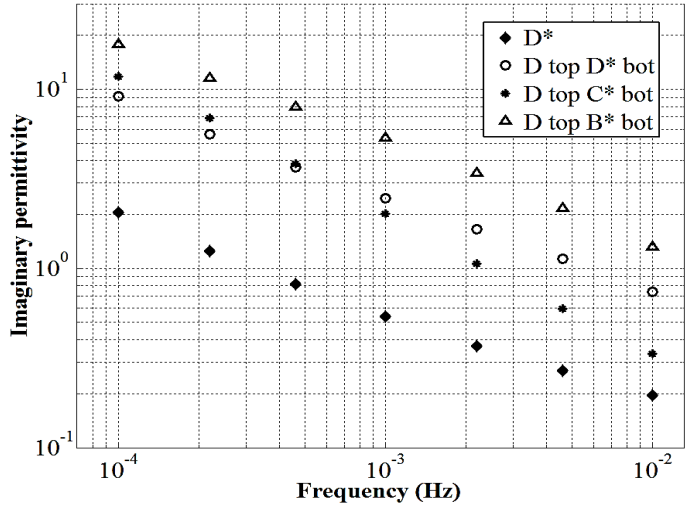

(b)

Figure 5.2. Imaginary part of the complex permittivity obtained for single and double layered samples. In (a) and (b), the top layers are made of unfilled and ATH doped HTV silicone rubbers respectively.

compared to that for individual materials. Further, the magnitudes of the imaginary parts are strongly influenced by the properties of bottom layers, in particularly by their conductivities. Since material B* is the most conductive amongst the studied thick silicone rubbers (Table 3.2), highest losses are observed for the combinations A/B* and D/B*. The increase at the lowest frequency is more than 4 times and ~10 times, respectively, as compared to single layered materials. By considering the scaling factors for both the real and imaginary parts, one can argue that by combining layers of different materials, the dielectric losses are affected stronger than the dielectric constants.

The common property of the characteristics in Figure 5.1 and Figure 5.2 is the fact that the measured data points for the layered structures at lower frequencies lay outside the borders defined by the results of individual materials (Figure 3.15). The appearances of such features are somewhat unique in the sense that they cannot be explained by taking into account effective parameters (averaging materials properties over the system), which otherwise are well discussed both in terms of theory and mathematical equations for describing the properties of composite materials [98]. One possible way of explanation could be thorough introducing extra amount of charges at the macroscopic interfaces between the layers. The results of such estimations are presented in section 5.5. Further, the physical processes that may support the hypothesis (additional charges at the interface) are reported in the next section 5.4.

The exception to the above described features is the set of data for combination A/B* that shows approximately the same values (both real and imaginary permittivities) as obtained for silicone rubber B* (section 3.7) at the left-most frequencies.

5.4 Surface potential decay characteristics

A schematic view of charging arrangement for double layered structures is shown in Figure 5.3. In the experiments, scanning was performed before the actual measurements to check if the initial magnitudes of surface potentials were sufficiently low (typically below 100 V) that may appear at open interface due to tribocharges, finger contacts during sample placements on movable grounded table (see section 4.1), etc. Afterwards, open surfaces of the sample were subjected to negative corona discharges generated at ambient conditions from a needle located at 3 mm above its center. Upon completing the charging process, the decay of surface potential was recorded at $3\times10^4\pm10^3$ Pa (300±10 mbar) air pressure inside the test chamber for the purpose of examining materials related properties on charge dynamics. The whole experimental procedure is described in detail in section (4.1). For layered structures, the measurements were conducted for different thicknesses of the top (exposed to the corona source) and the bottom (in contact with the grounded electrode) layers in the samples.

Normalized surface potential decay characteristics obtained for the locations corresponding to the maximum values of *Vs* on single and double layered samples of different materials are shown in Figure 5.4. As discussed earlier (section 4.5.2), one may notice clear correlation between the rates of the decay process and magnitudes of the bulk conductivities for single layered samples. Thus,

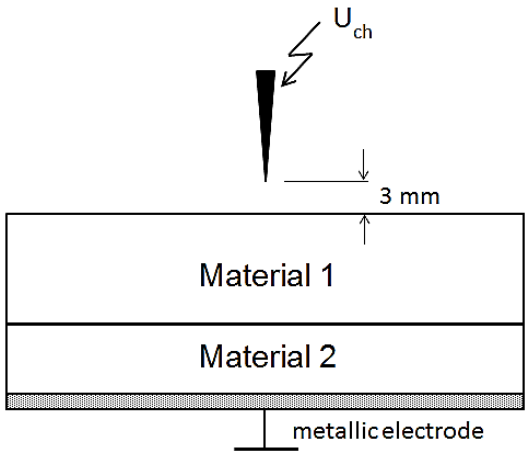

Figure 5.3. Schematic view of charging arrangement for double layered structures. Materials marketed with symbols 1 and 2 represent the top and bottom layers respectively.

higher conductivity (Table 3.2) of sample A* as compared to that of A leads to faster decay and similar trend exists for samples of ATH filled materials D and D* (see Figs. 5.4a and 5.4b, respectively). Recall that silicone rubbers A* and A are the same materials and the latter one represents thin samples. The attributes of the decay profiles for these materials are in accordance with the deduced parameters from volume currents measurements (see section 3.4).

The results of the measurements performed on double layered samples demonstrate that in case of sandwich structures made of silicone rubber A and A* (Fig. 5.4a), the SPD speeds up with respect to the decay on the single layers, regardless of the placement of thin or thick samples at the top (exposed to corona) or the bottom (grounded) positions. It can however be observed that the shift of the decay curve towards shorter times is more pronounced in case of a more conductive bottom layer, i.e. for A/A* combination (dashed line in Fig. 5.4a). On the other hand, the decay characteristics for the sandwich structures made of samples D and D* are bonded by the curves for individual materials (Fig. 5.4b), i.e. the SPD is faster than it is for the more resistive silicone rubber D* and slower than for the most conductive material D.

The common property of the characteristics in Fig. 5.4 for the double layered structures made of the same material (i.e., A/A*, A*/A, D/D*, D*/D) is the fact that the decay rate increases if more conductive layer is used for the bottom of the sample which is in contact with the grounded metallic plate. A possible explanation of this observation could be through an enhanced injection of charge carriers from the metallic electrode into a more conductive base layer, which also provides more effective transport of the injected charges to the internal interface as compared with the case of less conductive material. Further, a fraction of the injected carriers is transported through the interface and the top layer. While reaching the open surface of the sample, the transported charges contribute to neutralization of the charges deposited by corona. In this way, charge injection into material bulk complements intrinsic conduction and may influence surface potential decay. As for the carriers remaining in the bulk of the sample between the layers, they form interfacial charge, which maintains continuity of the electric flux and thus the current

through the sample. In general, the accumulated interfacial charges define the amount of charge delivered to the open surface of the sample and, thus, it is natural to expect variations of SPD characteristics depending upon properties of internal interfaces. An example illustrating the effect is shown in Fig. 5.4, where the decay curves for the compositions A/B (Fig. 5.4a) and D/B (Fig. 5.4b) are presented. As seen, the decay is significantly faster than it is for the double layered samples made of the same type of materials. Recall from section 3.2 that silicone rubber B is actually material A doped with ATH similarly to D, however, it has been manufactured using different curing agent. Due to these features, one may expect increased number of trapping sites

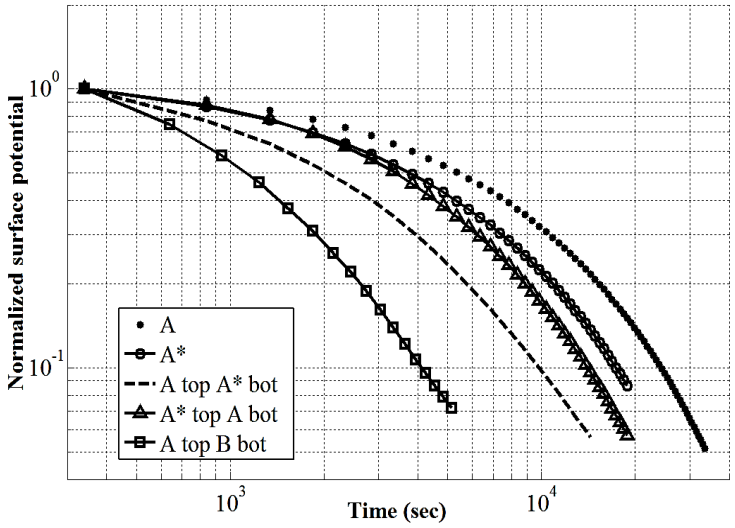

(a)

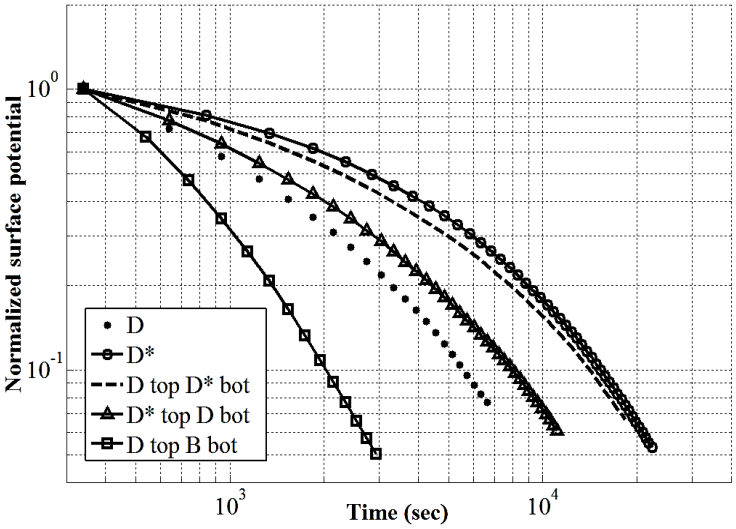

(b)

Figure 5.4. Normalized surface potential decay characteristics measured on single and double layered samples. In (a) and (b), the top layers are made of unfilled and ATH doped HTV silicone rubbers respectively.

on the interfaces that giving rise to charge trapping and de-trapping, recombination, etc. Since these processes are activated only in the double layered systems, it is natural that they do not contribute in the measured macroscopic properties of individual materials as can be noticed from section 4.5.2. Thus, based on the values of the conductivities in Table 3.2, one may expect that the decay for the structure A/B would be faster than for the combination A/A* (since both B and A* are used as bottom layers and B is more conductive that A*) that corresponds to the experimental observations (Fig. 5.4a). However, the decay characteristics for the samples D*/D and D/B show opposite trend despite of the fact that material D is more conductive.

Regarding the contributions of polarizations mechanisms (interfacial type in the studied single and doubled layered materials) to the measured potential decay on samples of silicone rubbers, one should mention the following. As has been demonstrated with the help of fittings (section 4.5.2) that the decay characteristics are dominated by materials conductivities rather than polarization. Therefore, the latter in the individual materials may be assumed as stabilized or in other words equation (2.6) can be used to fully describe the results. On the other hand, for the combination of materials, effects of polarization may no longer be discarded due to the following reasons.

The concept of effective properties (averaging materials properties over the system) can be utilized only if the measurements on mixtures (composites) are bounded by the results of individual materials. Since for the layered structures, dielectric permittivities (see Figure 5.1) laid outside the boundaries, therefore, decay characteristics presented in Figure 5.4 cannot be explained using (2.6) by replacing the parameters (K_v and ε_r) with effective terms (K_v^{eff} and ε_r^{eff}). Instead, the rate of potential decay, can be approximated as (following (2.2) and neglecting the space charge effects)

$$\frac{\partial V_s(t)}{\partial t} = -\frac{K_v V_s(t)}{\varepsilon_0} - \frac{L}{\varepsilon_0} \cdot \frac{\partial P}{\partial t} \qquad (5.1)$$

Equation (5.1) implies that potential decay is caused by a collective effect of intrinsic conduction and polarization processes. The latter one may be reflected in the permittivities of the materials, namely in their increased magnitudes at lower frequencies as demonstrated in the previous section 5.3. Thus, the strong contributions of the second term on the right hand side of (5.1) in combination with the relatively high conductivity of the bottom layers (Table 3.2) may describe the drastic speed up of SPD in Figure 5.4.

As known, SPD rates dV_s/dt presented in a log-log coordinate system and fitted by two power time laws with an average slope nearly equal to -1 are typically associated with three different physical mechanism (dipolar relaxation, charge injection and detrapping) [38]. A description of mathematical model providing a link between the decay rates and absorption current, governed by dipolar relaxation, is given in section 2.3.3 and for the other two processes, related theories can be found in [24, 38]. For the studied materials, the contributions of charge injection and

detrapping to the potential decay are negligible due to low energies of deposited surface charges, weak induced electric fields, low ambient temperature and relatively large thicknesses of the samples. The leftover mechanism can be taken into consideration and significantly influence SPD characteristics on layered structures as elaborated in the above paragraphs. Following this, the obtained results are presented below and discussed in the light of theories developed for single layered materials.

Decay rates VS time plots

Surface potential decay rates, dV_s/dt , calculated utilizing the data presented in Figure 5.4 are shown in Figure 5.5. As seen, the data points can be fitted by two straight lines in log-log

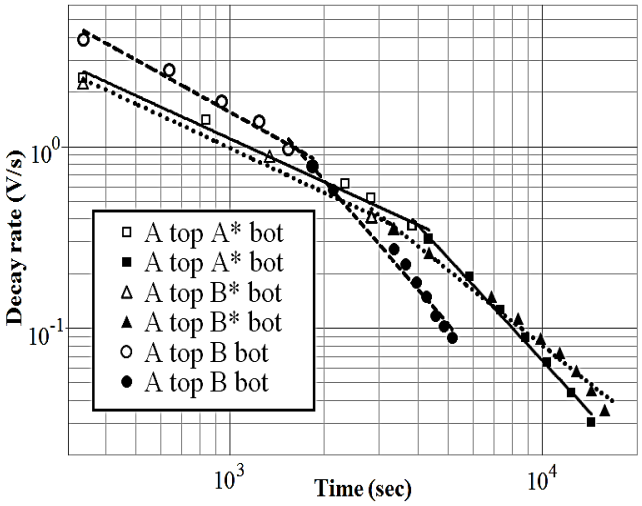

(a)

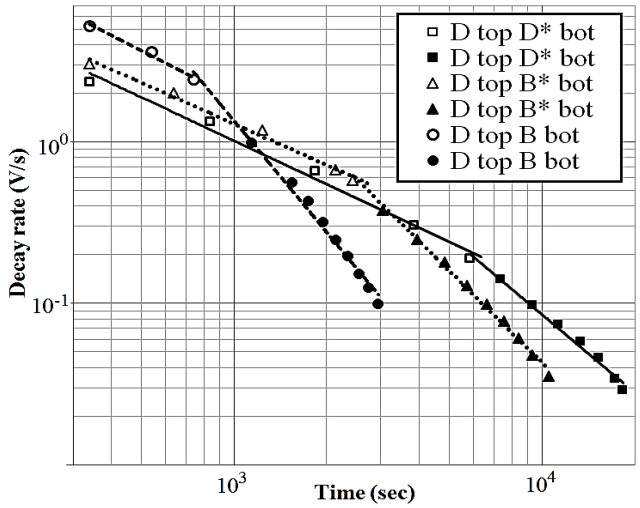

(b)

Figure 5.5. Decay rates of surface potentials for silicone rubbers (a) A and (b) D with different base layers. The solid and broken lines are the fittings of the decay characteristics with time power laws.

coordinate system indicating power-law time dependencies. The knee point that corresponds to the intersection of the trend lines is observed to be strongly affected by the compositions and properties of bottom layers, in particularly by the conductivities. Thus, it appears earlier for more conductive bottom layers. Information on the approximate instants at which the pieces of the fitting curves meet is given in Table 5.1, along with the other parameters obtained from fitting by equation (2.5). As seen, the earliest times appear for the combinations A/B and D/B. For the latter case it advances even to 740 sec, which is much shorter compared to the transit time (t_T) observed in other studies [51]. Although, it is worth to mention that characteristic time t_T is a feature of single layered materials and depending on the dominant effect of the decay mechanisms it is uniquely defined [38]. In addition to that, another features associated with t_T is the change of the slopes of the trend lines with slopes less than -1 on the left and larger than -1 on the right represented by $-(1-\alpha_1)$ and $-(1+\alpha_2)$ respectively. Since the data shown in Figure 5.5 is for double layered materials and commenting on the estimated times (Table 5.1) is rather complicated at this stage of analysis, therefore, the term knee point is used instead of transit time. However, the same notations are used for slopes (Table 5.1) due to the fact that it merely indicates numerical values.

Examining the numbers in Table 5.1 in the 2nd column, which refer to the slopes on the left of the knee point, one can notice that values are below and close to -1 that is in accordance with the criterion mentioned above. On the other hand, the slopes on the right of the knee points, represented by $-(1+\alpha_2)$, are much larger than -1 for most of the cases. Taking this into account, even if the average value of the two slopes is considered, the whole criterion will still not be fulfilled and for the combinations A/B and D/B, the deviations will be even more significant.

Table 5.1. Parameters obtained from fitting potential decay rates on double layered materials using equation (2.5).

Double layered materials	$-(1-\alpha_1)$	$-(1+\alpha_2)$	t_k, sec
A/A*	-0.79	-1.87	3840
A/B*	-0.81	-1.37	2920
A/B	-0.95	-1.99	1690
D/D*	-0.89	-1.61	6090
D/B*	-0.85	-1.89	2570
D/B	-0.97	-2.31	740

The obtained results indicate that physical processes associated with SPD in double-layered samples are much more complex than in individual materials and, therefore, require special treatment and deeper analysis.

5.5 Modelling of layered structures using MW-theory

Accumulation and relaxation of interfacial charges in layered systems is normally described by Maxwell-Wagner (MW) theory of interfacial polarization [99]. Within this concept, interfaces are assumed to be ideal and the amount of interfacial charges is defined by macroscopic materials´ properties. Thus, the density of charge accumulated on the interface between materials 1 and 2, which in the present work corresponds to top and bottom layers respectively, at test voltage U_0 is provided as

$$\rho_s = -\frac{(K_{v2}\varepsilon_{r1}\varepsilon_0 - K_{v1}\varepsilon_{r2}\varepsilon_0)}{L_2K_{v1} + L_1K_{v2}} U_0 * (1 - e^{-t/\tau}) \qquad (5.1)$$

$$\tau = \frac{(L_2\varepsilon_{r1}\varepsilon_0 + L_1\varepsilon_{r2}\varepsilon_0)}{L_2K_{v1} + L_1K_{v2}} \qquad (5.2)$$

Here, ρ_s represent interfacial charge density, and τ is the time constant of the system. Charge accumulation on macroscopic interfaces in the studied layered structures can be revealed, e.g., by utilizing results of dielectric spectroscopy measurements, which are shown in section 5.3. As discussed above in section 5.4, internal interfaces between layers of materials may introduce additional trapping centers and enhance accumulation of interfacial charges thus increasing dielectric constants at lower frequencies, which were found 2.5 times higher compared to the individual materials (Figure 5.1).

In order to quantify the effect of interfacial charges on real permittivity of two layered structure D/B*, computer model describing electrostatic fields in the materials has been developed and implemented using Comsol Multiphysics software package. Actual parameters of the materials from Table 3.2 were utilized. The results of the calculations are provided in Figure 5.6 (only low frequency region is shown). As seen, the frequency dependence of the dielectric constant computed based on materials´ parameters only (dashed line with circles) deviates from the measured curve (solid triangles) especially at lowest frequencies. Note that this case corresponds to Maxwell-Wagner (MW) capacitor theory with the interfacial charge density given by (5.1). To obtain better fit to the experimental data, some scaling factor was introduced and corresponding uniform surface charge density was assigned to the interface between the layers. The dependencies obtained by using factors 15, 25 and 60 in (5.1) are presented in Figure 5.6 where the trend in the results is shown by the arrow. The additional charges cause modification of the electric fields in both the top and bottom layers. As can be seen, with involvement of extra quantities of interfacial charges, the simulations may provide permittivity values close to the

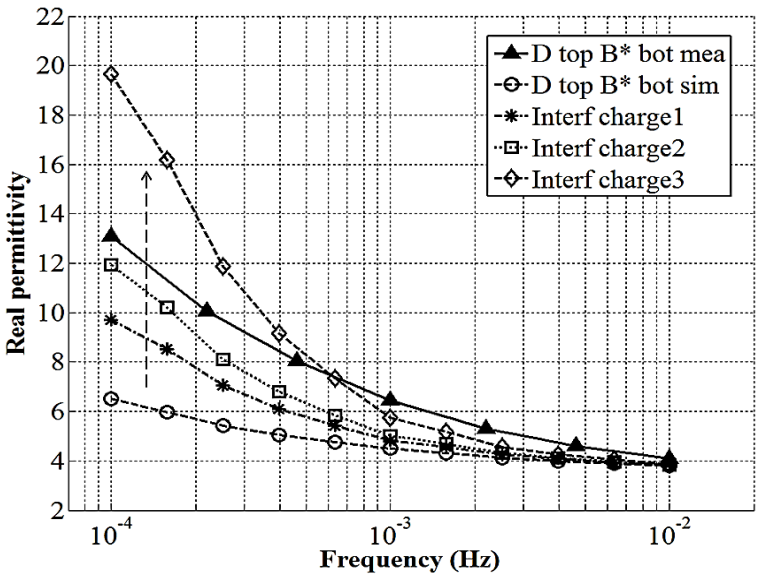

Figure 5.6. The measured and computed profiles of dielectric permittivity of double layered structure. The results of the simulations were obtained with the MW-model accounting for the dielectric properties of both the materials. Also, numerical output is shown for amplified charge densities introduced at the interface.

measured ones. However, introducing such modifications doesn't reflect the actual physics of the interfacial processes and a more accurate model involving, in particular, description of charge transport through the material (including multi-layered structures) need to be developed.

6. Surface potential decay at elevated temperatures

This chapter focuses on experimental setup and procedure used for conducting measurements of surface potential decay at elevated temperatures. Modifications introduced in the earlier described test chamber (section 4.1) for controlling and implementing temperature variations inside the setup are highlighted. Decay characteristics obtained for HTV silicon rubber materials of various thicknesses and compositions are analyzed.

6.1 Temperature effects on electrical properties of insulating polymers

Analysis of thermal effects in insulating systems has received special attention due to its practical relevance, in particular, increasing demand put on the performance of polymeric materials in applications with a wide range of temperatures. In addition, such analysis allows for exploring fundamental properties (e.g. electrical conductivity, dielectric permittivity, etc. [83, 100]) and characteristics (e.g. surface charge accumulation, potential decay, etc. [36, 101, 102]) of insulating materials.

Under HVDC conditions, conductivity of insulating materials become of particular importance due to its dominant role in controlling the distribution of electrical fields across the insulation materials. It is strongly coupled to temperature and field variations. Gradients in dielectric properties associated with differences in temperatures between the insulation terminals and field assisted thermionic injections at metal-material interfaces may cause accumulation of charges inside material bulk [83, 103, 104]. Formation of space charges may affect the applied electrical fields causing overstressing of the materials that may even lead to breakdown of insulation systems [11, 105].

Temperature dependences of surface potential decay have been utilized for studying various properties of insulating polymers. It includes evaluation of bulk conductivity of highly resistive materials (e.g. epoxy), which otherwise was not possible to obtain with standards measurements of volume currents [82]. Similarly, it comprises analysis of the nature of traps (electrons or holes) their densities as well as distributions of energies [106, 107]. Determination of the latter parameters may play essential role in diagnosing the materials as the energy depth of the traps identify the chemical or physical defects in the polymers [108]. In addition, they are strongly related with the charge transport processes (traps in disordered materials significantly influence charge carrier trapping, detrapping, recombination, etc.), understanding of which is important for proper design of HVDC insulation systems.

6.2 Experimental setup and procedure

For conducting SPD measurements at elevated temperatures, modifications were introduced into the earlier described experimental setup (see section 4.1). A hot plate 140 mm×140 mm (PZ 35 ET, Harry Gestigkeit Gmbh) was installed inside the test chamber on the moving table and was fed from the control unit (2680 SR) via low voltage busing as shown in Figure 6.1. It provided constant temperatures on the surface which was adjusted with the precision of ±0.5 °C. Before actual measurements, material samples of different thicknesses were placed on the hot plate and the calibration was performed to check for uniformity of thermal conditions of the material. For this, two resistive temperature detectors (RTD) were mounted at two different positions on sample surface (in the middle and at the edge). The temperature sensors were connected to a Fluke 88464A precision electrometer via the same bushing. The results of the calibration for different temperatures of the hot plate and at low pressure inside the chamber are provided in Table 6.1. As can be noticed for relatively thin sample of silicone rubber, the readings obtained with the RTDs are quite close to the adjusted temperatures on the hot plate and, therefore, possible effects associated with temperature gradients in the material bulk can be neglected. However for thick material, the differences are larger and approaches to 8 °C for the maximum studied temperature of the hot plate. These may possibly affect the results of surface charge dynamics and associated with it properties of materials. Nevertheless, it has been found that temperature gradients are considerable only at field strengths close to a certain threshold, above which space charges may accumulate in the materials [103]. Taking into account the range of the

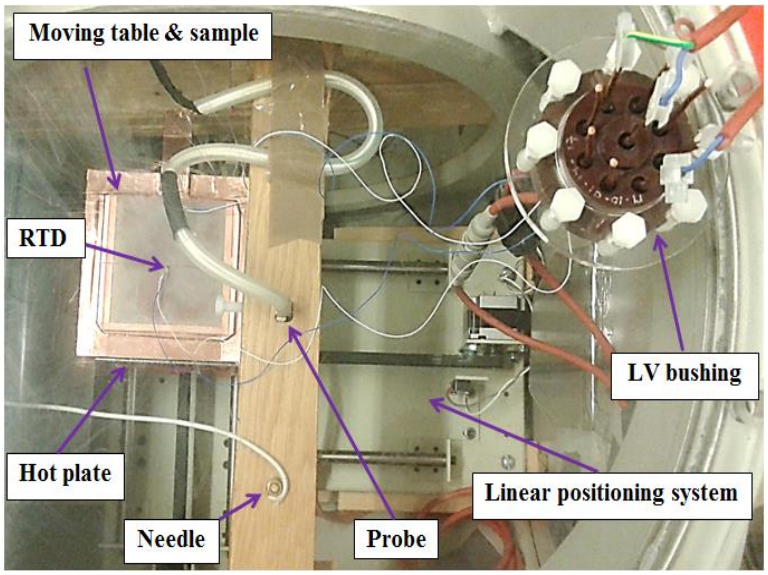

Figure 6.1. Top view of the sample positioning system with charging and scanning setups mounted in the test vessel. Material sample is placed on the top of hot plate and RTD's are installed at two positions on its surface. Note that charging needle and the probe are beneath the arm and are facing downwards to the sample.

Table 6.1. Measured temperatures on material samples at different temperatures of the hot plate.

Plate temperature (°C)	Surface temperature (°C)			
	Thin sample(~0.25mm)		Thick sample(~2.3mm)	
	RTD_{mid}	RTD_{edge}	RTD_{mid}	RTD_{edge}
40	39.8	39.2	39.1	38.9
60	59.6	58.8	56.3	55.4
70	69.0	67.9	64.4	63.5
80	78.3	76.8	72.1	71.0

studied electrical fields (section 7.2) especially on thick materials that are well below the threshold values, space charge effects for the conditions of the present work can be ignored.

For charge decay measurements at elevated temperatures, slightly different procedures were followed as compared to the experiments at room temperature (section 4.1) as well as depending on the materials thicknesses (Table 3.2). For thin silicone rubbers, first, a desired temperature of the hot plate was adjusted and material sample was left for 30 min on its surface to allow for steady state thermal conditions. Further, corona charging was performed as described earlier in section 4.1. Afterwards, pressure inside the test vessel was reduced down to $3\times10^{4}\pm10^{3}$ Pa (300±10 mbar) and SPD measurements were conducted. It is worth mentioning that for each increment of hot plate temperature, the magnitude of charging voltage was slightly increased in order to get similar initial potentials as those obtained at normal conditions for comparison purpose.

For thick materials, one more step was added to the procedure described in the above paragraph. Since, the gradients across the insulation terminals are found to be larger (Table 6.1) compared to thin materials especially at higher temperature. Therefore, settings on the hot plate were adjusted in a manner to get similar average temperatures to those of thin sample. Although, another option could be to consider similar temperature gradients, however, due to the lack of data on such analysis as well as average values being more meaningful, the latter criterion was selected.

6.3 Influence of elevated temperatures on surface potential decay

Normalized potential decay characteristics obtained for silicone rubber materials A and B at different temperatures are shown in Figure 6.2. As can be observed, the effect of the temperature is rather strong. Surface potentials vanish much quicker at elevated temperatures causing shifting of the decay curves to the left. The features in the characteristics are different for different

materials. Thus for silicone rubber A, the time needed for the potential to drop down to half of its initial value at elevated temperatures is reduced more strongly as compared to material B which is doped with additional amount of filler. This effect is quantified in Table 6.2 where the information on the exact time spans is given. As can be seen, the total reduction, considering the measured data at 22 °C as a reference, is ~12 times and ~5 times for materials A and B respectively. Based on this observation, one can conclude that thermal activation of bulk conductivity (responsible for neutralization of deposited surface charges) for rubber A is stronger than for ATH doped material B (see Table 7.6, compare activation energies for these materials obtained from SPD based technique).

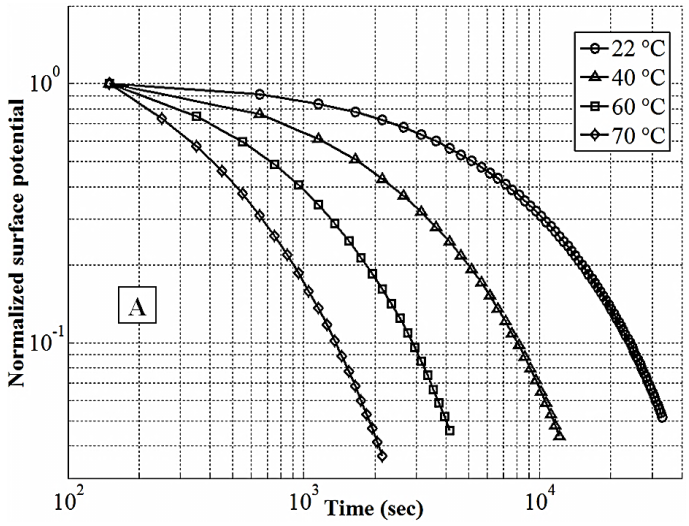

(a)

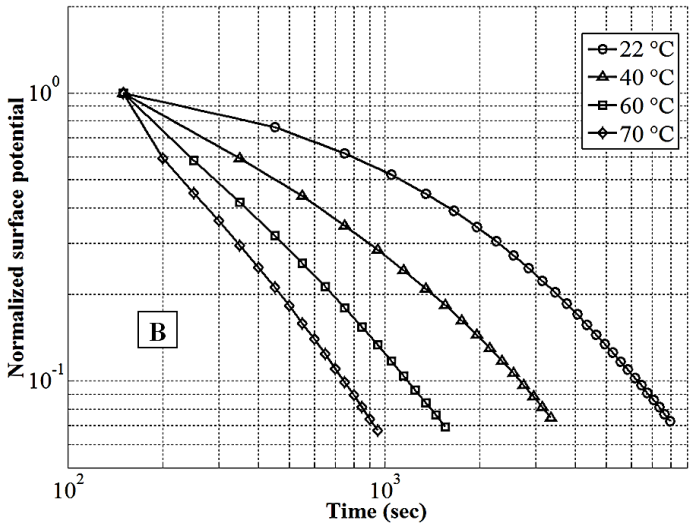

(b)

Figure 6.2. Normalized surface potential decay measured at different temperature settings of hot plate for silicone rubber A (a) and ATH doped material B (b).

Table 6.2. Times (sec) needed for the potential to drop down to half of its initial values at different average temperatures for HTV silicone rubber materials.

Average temperature in the materials (°C)	Silicone rubber materials			
	A	B	A*	B*
~22	5200	1120	3690	1620
39.9	1750	450	1640	730
59.8	700	290	560	420
69.5	420	230	370	310

Data obtained for thick samples of unfilled silicone rubber A* and ATH doped material B* are shown in Figure 6.3 and Figure 6.4, respectively. As can be seen in both figures, the shift of the SPD curves to the shorter instants is similar to that noticed for thin samples of the same materials. Thus, smaller variations in decay time can be observed for additionally filled silicone rubber B* compared to its counterpart A* without filler. Quantitatively, the scaling factors between the minimum and maximum studied temperatures for the duration required for halving the surface potential (50% of its initial value) are ~10 and ~5 times for rubbers A* and B* respectively. These factors are very close to the ones mentioned above and are the same for materials with additional amount of filler (B and B*). At the same time, by comparing the strengths of electrical

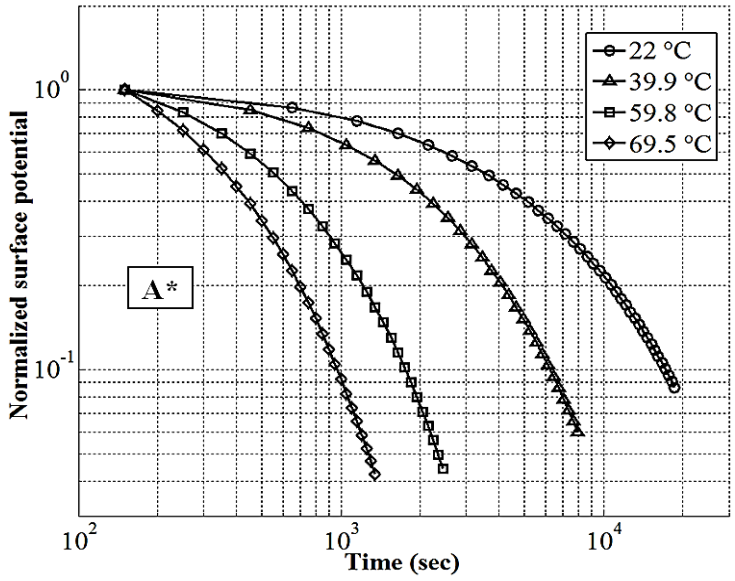

Figure 6.3. Normalized surface potential decay for unfilled silicone rubber A*. The legends show average temperatures in the materials obtained at different settings of the hot plate.

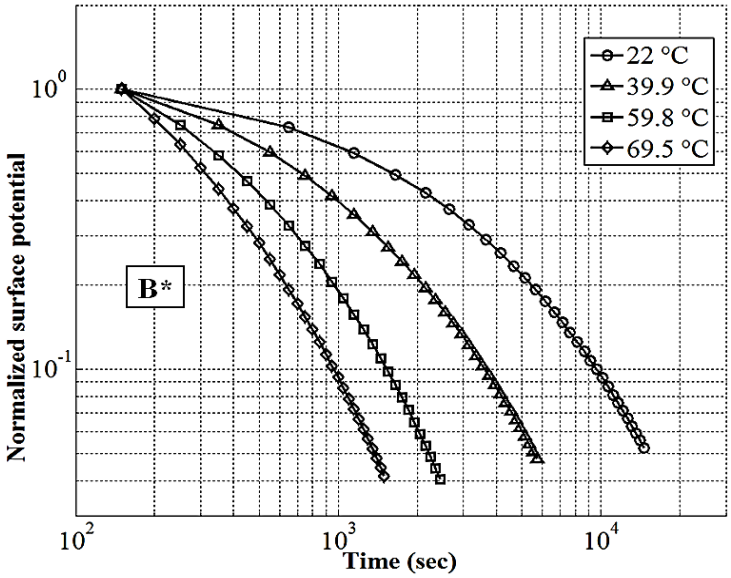

Figure 6.4. Normalized surface potential decay for ATH doped material B*. The legends show average temperatures in the materials obtained at different settings of the hot plate.

fields, a reduction by ~7 to ~9 times (see Table 3.2) can be noticed for thick materials compared to that for thin samples. These observations may indicate that the thermal activation of materials conductivity assists the decay process, independently of the internal field strengths. However, one finding requires further investigations, namely, the smaller changes induced in the decay on filled materials at elevated temperatures, although, it contains additional amount of ATH particles in the bulk. The latter should have caused more rapid neutralization of the deposited surface charges in comparison to the unfilled materials, as observed at room temperature, which is not found to be the case at least for studied silicone rubbers.

7. Evaluation of material properties from potential decay characteristics

As described above, DC electric conductivity of insulating materials is usually deduced from steady-state volume currents measured on samples placed between metallic electrodes. Results of such measurements typically accommodate undefined effects of processes on metal-material interfaces as well as contributions from capacitive currents, elimination of which requires very long measuring times. In this chapter, a complementary technique based on surface potential decay characteristics is presented and discussed. The method is herewith used for characterization of the studied silicone rubber materials of different thicknesses at room as well as at elevated temperatures. Field dependent conductivities retrieved with the proposed approach are compared with those measured by standard method at different test voltages and thermal conditions. Bulk conductivities within a wider range of field strength are estimated from SPD data that is hard to realize in standard measurements. Temperature dependences of the conductivities deduced from both the techniques are fitted using Arrhenius law and activation energies are compared with known values. A comparative study is performed to elaborate the weaknesses and strengths of both the methods. In addition to that, Poole-Frenkel model is utilized to describe field dependences of conductivities and its applicability is examined for the studied materials.

7.1 Surface potential decay as a complementary technique

Measurement of SPD can be utilized as a powerful tool for characterizing insulating materials provided that the relative contribution of the physical processes to the total charge decay is determined. It is commonly accepted that potential decay on polymeric surfaces under normal conditions is governed by three mechanisms, namely, bulk and surface conduction and neutralization by atmospheric ions [31, 109]. In the present study, the contribution of the latter can be considered as negligible due to low gas pressure and screening effect of the metallic enclosure. The surface conduction is not significant as well that is reflected by the extremely low surface conductivities of the materials (Table 3.6). Hence, the observed SPD can be attributed solely to bulk conduction that is also confirmed by the good agreement obtained between the results of experiments and simulations (will be discussed in section 8.3.1).

Field dependent materials conductivities are typically obtained from standard measurements (as described earlier in section 3.4) performed at different test voltages. To realize this, a sample is placed between two metallic electrodes with fixed potentials and a current through the material is recorded. Alternatively, results of surface potential decay measurements can be utilized provided that potential magnitudes at each instant correspond to voltages applied across a material sample induced by deposited surface charges (this is the situation in the present experiments where one

side of the sample was always grounded during the measurements). It is worth mentioning that this approach yields a dynamic apparent conductivity (due to the decaying potential) that may differ from equilibrium value. The latter can be, in principle, obtained from standard voltage-current measurements at sufficiently long times (which may reach ~5 days for the studied materials, see section 3.4) required for mitigating capacitive current component through the sample. In practice, however, such long-lasting measurements are not feasible and are usually interrupted when it is decided that the capacitive current is sufficiently low thus resulting in conductivity values which may (or may not) be close to equilibrium magnitudes. Hence, both approaches are characterized by some uncertainties in the results. However, the method based on surface potential decay may be preferable for obtaining field dependent conductivities due to the fact that the potential decay is a natural process controlled only by properties of the material and surrounding gas. Under conditions of the present study, the influence of the latter is minimized and the effect of surface conduction can be neglected as discussed above. Therefore, field dependent bulk conductivities of the studied materials obtained utilizing the model (2.6) - (2.8) are demonstrated in the following sections.

Before presenting any data, it is worth mentioning that conductivities from SPD based technique in all the figures below refer to the magnitudes calculated with dielectric permittivity of the materials at 50 Hz, otherwise, specifically mentioned. The sensitivity of the results to variations of this parameter is evaluated in a separate section 7.5.

7.2 Comparison of conductivities of studied materials obtained with different methods

The field dependences of K_v for studied thin samples of silicone rubbers deduced from surface potential decay method utilizing data shown in Figure 4.13 are presented in Figure 7.1 along with the results of standard measurements (SM) of volume currents. As can be seen, the technique based on SPD characteristics provides conductivity values which are of the same orders of magnitude as the outputs from the standard measurements. Taking into account that the latter cannot be considered as a true reference due to the reasons discussed earlier (section 3.4), such agreement between the results can be considered as acceptable. In order to quantify the discrepancies, the percentage deviations calculated with respect to SM data are provided in Table 7.1. As seen, the overall discrepancies are within the range $\pm 30\%$ except for material B, where they are higher. It is worth mentioning that such deviations are quite natural and close to the level of uncertainties appearing in practice when measuring conductivities of highly resistive materials. Thus, the results in Figure 7.1 and Table 7.1 suggest that SPD can be seen as alternative method for determining materials conductivities. Note also that the total time needed for electrical characterization of the studied insulating materials using SPD was significantly shorter than that required by standard method. Thus as mentioned earlier in section 3.4, time to reach a true steady state dc volume current in material C might reach few days while the time required to conduct

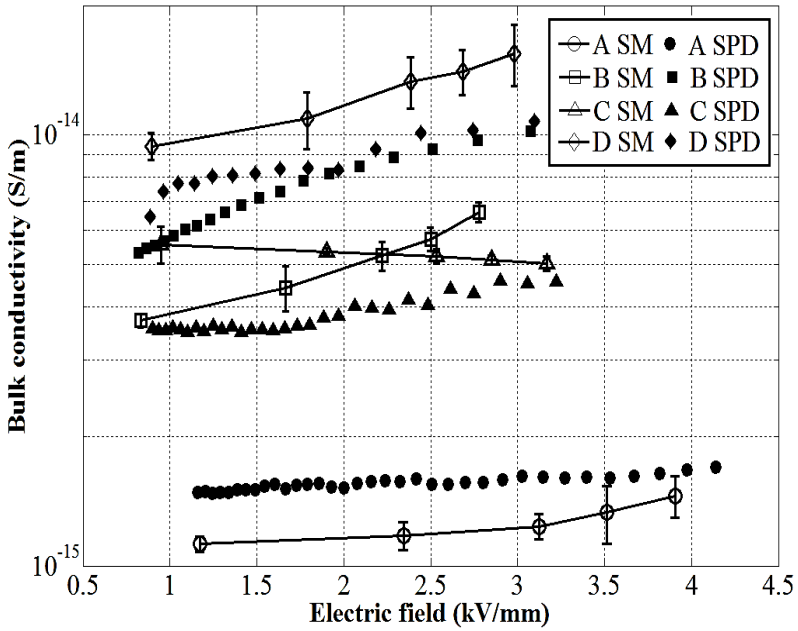

Figure 7.1. Bulk conductivities of the thin materials deduced from the measured surface potentials (marked as SPD) and obtained from standard measurements (SM) of volume currents. Error bars for SPD are not displayed due to weak scattering in the measurements as shown in Figure 4.7.

surface potential decay experiments (which would yield similar results) is just a couple of hours (section 4.5.2).

As one may notice from Figure 4.13, the corona charging resulted in the maximum magnitudes of the surface potentials up to 5-6 kV depending upon material type. Such magnitudes of V_s are much higher than the maximum dc test voltage of 1 kV applied during conventional measurements to induce measurable volume currents through the materials. In principle, the test voltage in the standard measurements can be increased provided that discharges from the metallic

Table 7.1. Deviations of the values K_v obtained from SPD characteristics from the output of standard measurements.

Material	% deviations				
	300V	600V	800V	900V	1 kV
A	-30.6	-33.5	-29.9	-20.6	-12.6
B	-43.9	-67.3	-68.6	-54.7	-46.5
C	36.57	29.0	22.9	9.9	8.9
D	29.67	23.0	24.1	26.9	30.6

electrodes in air are prevented. Presence of such discharges (which may cause even a breakdown in gas) is a limiting factor for implementing conventional measurements at high fields. It can be avoided by, e.g., immersing the test cell into oil that, however, makes realization of the setup rather complicated. In addition, a special care should be taken to minimize effects of charge injection from both metallic electrodes which may occur under strong electric fields. Space charges may accumulate in the solid dielectrics even at lower fields, especially for filled materials, as demonstrated by the bend of lines shown in Figure 3.5. In this respect, the SPD based method seems to be more flexible in establishing voltage (field) levels during testing which change with time in a natural way being controlled by the conductive properties of the material. Also, one of the electrodes (and thus one of macroscopic metal-material interfaces) is omitted in the experiments arrangement. In addition, SPD technique provides a possibility to obtain conductivity values in a certain range of applied fields from a single SPD characteristic. The actual range is defined by the maximum V_s recorded after charging and its minimum value corresponding to time at which the SPD measurement is completed. To illustrate this, the full set of conductivities K_v for the studied materials deduced from corresponding SPD characteristics using (2.6) is presented in Figure 7.2 (data obtained from standard method are also shown for comparison). As seen, the range of the applied fields spans oven one decade. This allows for observing clearly the tendency of the conductivities of the studied materials to increase with increasing field strength. It is notable that the magnitudes of K_v of unfiled rubbers A and C are quite different (A is more resistive), but their increase with the field is even stronger than exponential, especially for material A. In contrast, conductivities of ATH-filled rubbers B and D

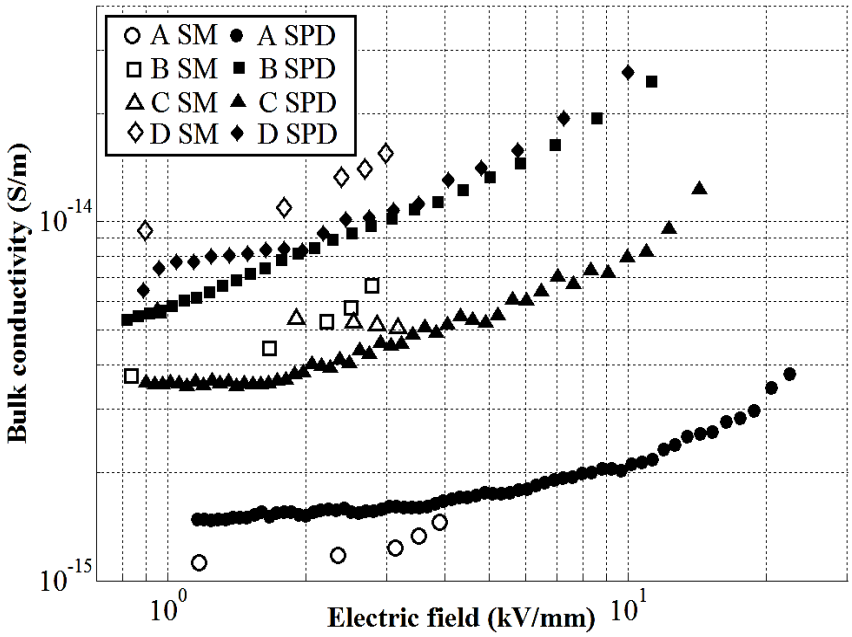

Figure 7.2 Bulk conductivities obtained from SPD characteristics for an extended range of electric fields along with the results of standard measurements (SM).

are higher than that of pure materials and are practically equal at the field strength exceeding ~2 kV/mm that can be attributed to a dominant effect of the filler. In general, the effect of field on conductivities of the studied HTV silicone rubbers is quite weak and leads to variations of K_v values within one order of magnitude or even less. However, SPD experiments can be performed at higher levels of charging voltages thus providing a reliable way for obtaining intrinsic materials conductivities in a wider range of the fields that is hard to realize using the standard method.

7.3 Field dependences of bulk conductivities

The dependences of the conductivities on electrical field (induced by deposited surface charges) shown in Figure 7.2 may occur due to field-assisted transport of charged species through the material associated with different physical processes, e.g., charge trapping and de-trapping, ionization of impurities resulting in ionic conduction, space charge accumulation, etc. Such mechanisms can be activated if the field strength within a material induced by deposited surface charges becomes strong enough [52, 68, 110] or even at relatively low fields if, e.g., charge trapping is concerned. If expression (2.7) is used to represent field dependent conductivity, an overall effect of these processes is to be reflected by the exponential factor β. Thus, its smaller values indicate weak exponential behavior of the bulk conductivity (zero limit corresponds to a constant conductivity) and vice versa for higher values of β. A discussion regarding the applicability of Poole-Frenkel model and estimated values of β for the studied materials can be found in the next section 7.4.

As it was already mentioned with regards to Figure 4.11, the intrinsic conduction of studied materials is the dominant mechanism of potential decay in the present study. This implicates that field dependent bulk conductivity of the insulating materials should only be a function of the magnitude of surface potential, which is different at various radial positions on the material surface due to non-uniform charging. In other words, if different locations on the material surfaces that correspond to different initial potentials are selected, the curves of the calculated bulk conductivities must overlap. In order to validate this, the magnitudes of the conductivity of ATH doped material B and unfilled silicone rubber A obtained at different locations on samples surfaces are shown in Figure 7.3. Note that the conductivities are presented as functions of $V_s^{1/2}$ following equation (2.7). As can be seen, the deviations of the data are not significant for both the materials and the conductivity values increase with increasing magnitude of surface potential.

Deviations in the field dependent conductivity values calculated from potentials measured at different points on the surface have been also observed in another study [111], where field strengths induced by the deposited surface charges were much higher as compared to the present case. Such discrepancies can be attributed to space charge effects or charge injection into the material bulk which may contribute to the intrinsic conduction.

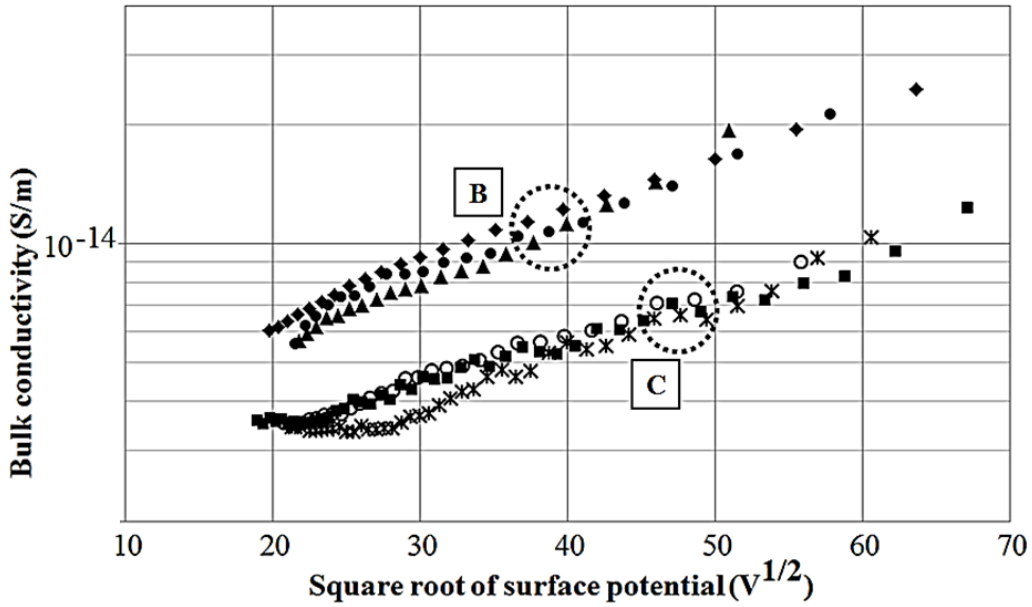

Figure 7.3. Conductivities of materials B and C deduced from the surface potentials measured at three different locations on the sample separated on a distance of 5mm from each other.

Deduced bulk conductivities of thick materials

Field dependent bulk conductivities deduced from the surface potential decay characteristics measured on the thick silicone rubber materials are shown in Figure 7.4 as functions of square root of surface potential ($V^{1/2}$) following equation (2.7). As it is seen, the obtained conductivity values increase with increasing surface potential similar to that in Figure 7.3. For the studied samples, depending on materials compositions and thus their bulk properties, a region with practically linear increase at relatively low values of V_s is followed by an exponential rise at higher values (fitted by the dotted lines in the semi- logarithmic scale used). The magnitude of V_s corresponding to the transition is different for different materials, but it is lower for higher overall conductivity values. Thus for ATH doped material B*, which is the most conductive among the studied thick silicone rubbers (Table 3.2), the non-linearity is of exponential type even for surface potentials as low as ~300V. Similar characteristics can be observed for rubber D* that is also additionally filled with ATH, however, the exponential increase is slightly weaker compared to material B* (see Table 7.2, compare experimental β). On the other hand for unfilled materials A* and C*, both regions exist and the transition point appears to be at V_s ~1.5 kV and at V_s ~2.2 kV, respectively. Recall from Table 3.2 that the magnitudes of the conductivities for materials A*, C* and D* obtained from standard measurements are practically the same, however, the field dependencies are quite different. This indicates that SPD based technique allows for distinguishing between properties of materials with very different compositions which may not be possible to identify based on single values of conductivities obtained from standard measurements (Table 3.2).

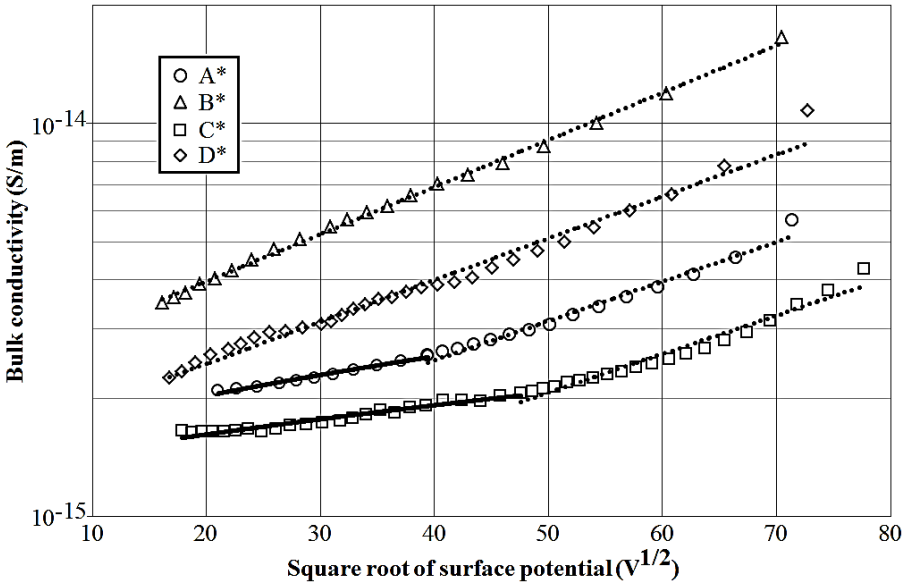

Figure 7.4. Field dependent bulk conductivities of thick silicone rubbers deduced from the measured surface potentials, markers fitted by dotted lines represent the exponential part of the dependence while solid lines are for the linear part.

7.4 Examining the applicability of Poole-Frenkel conduction model

It was mentioned earlier in section 2.3.3 that field dependencies of bulk conductivities can be explained by employing Poole-Frenkel (PF) conduction model. To examine its applicability for the studied materials, the parameters shown in Table 7.2 (calculated by fitting the exponential branches in Figure 7.4 utilizing equation (2.7)) can be analyzed. As seen, the smallest PF factor is found for material C* while the strongest exponential dependence is observed for material B* containing additional amount of filler. The discrepancies can be related to different material specific physical processes (among those mentioned above in section 7.3) which can be

Table 7.2. Parameters obtained from fitting field dependent conductivities of thick silicone rubber materials utilizing the model (2.6) - (2.8).

Parameter	Material			
	A*	B*	C*	D*
K_{v0}, fS/m	1.11	2.41	0.69	1.55
β *exp*erimental $\times 10^{-2}$	2.31	2.76	2.26	2.45
β theoretical $\times 10^{-2}$	3.99	3.30	3.59	3.62

Table 7.3. Parameters obtained from fitting field dependent conductivities of studied thin materials utilizing the model (2.6) - (2.8).

Parameter	Material			
	A	B	C	D
K_{v0}, fS/m	1.11	3.65	2.27	3.86
β *exp*erimental$\times 10^{-2}$	1.37	2.98	2.34	3.26
β theoritical$\times 10^{-2}$	11.90	8.31	9.6	9.01

intensified in stronger fields induced by higher surface potentials. Note that factor β is involved in the exponential term (2.7) and even small differences in its values may drastically change the behavior of the dependent variable. Nevertheless, the values of β for all the materials estimated from surface potential decay characteristics are of the same order of magnitude as the values obtained from equation (2.8) indicating that the field dependent conductivities may obey Poole-Frenkel model. However, by examining data obtained with thinner samples of the same materials and thus for stronger induced fields (shown in Table 7.3), noticeable differences can be seen between the theoretical and experimental values of β. Therefore, it may be concluded that the conductivities of the studied silicone rubbers are field dependent, however, the dependences $K_v(V^{1/2})$ can be quantitatively described by Poole-Frenkel model only at relatively low fields.

7.5 Sensitivity analysis of the effect of dielectric permittivity

As follows from equation (2.6), evaluations of materials conductivities from SPD characteristics require adopting a certain value of the dielectric permittivity. In order to estimate the influence of the latter, bulk conductivities obtained with two different dielectric constants of the materials are shown in Figure 7.5 (set of data for each material is indicated by the encircled areas) along with the results of standard measurements. For the sake of clarity, the results are presented for silicone rubbers A and B which are characterized by different frequency dependent permittivities (see Figure 3.15). As expected, the shift along the vertical axis is quite weak for unfilled material A due to weak variations of the dielectric permittivity in the studied range of frequencies. On the other hand, for additionally filled material B, the output of equation (2.6) is observed to be strongly affected by the values of permittivity. Thus at 50 Hz, the deviations between the results of the two approaches are weak (Table 7.1). However, the difference increases when the conductivities are evaluated using the magnitudes of the dielectric constants at 10^{-4} Hz (Figure 7.5). By applying ε_r corresponding to the low frequency for obtaining the conductivity of material D which is also ATH doped, the agreement with the result from the standard measurements is even better. Taking into account the two contradictory findings, i.e. the

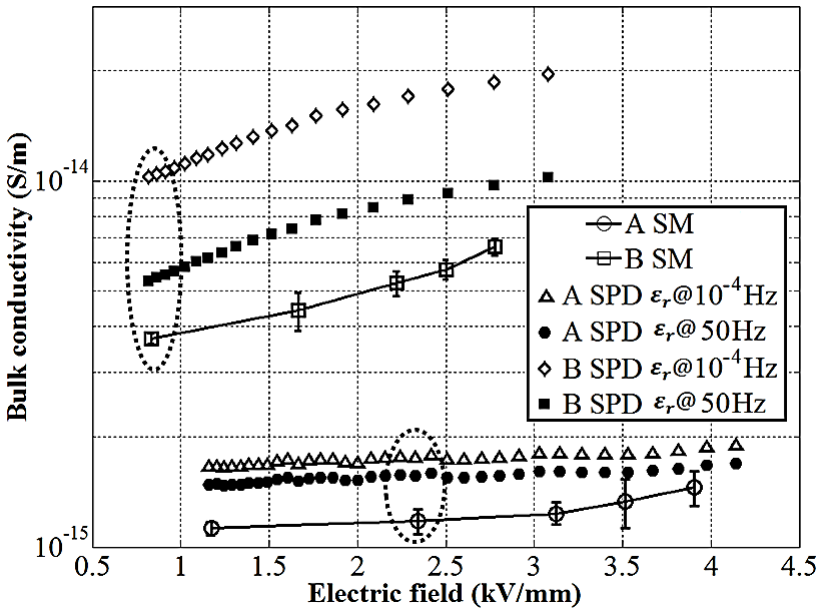

Figure 7.5. Bulk conductivities of the thin silicone rubbers estimated from SPD method with two different permittivities of the materials at 50 Hz and 10^{-4} Hz. The results of SM are shown for comparison purpose.

significant differences and very good match between the results of the two methods for filled materials B* and D*, respectively, making conclusions concerning the accuracy of the SPD based technique is rather difficult at this stage of the analysis.

7.6 Electrical characterization of silicone rubber materials at elevated temperatures

The volume conductivities of materials A and B calculated from (2.6) using SPD data in Figure 6.2 are presented in Figure 7.6 along with the results of the standard measurements. Note that for the sake of clarity, data points from both the methods are indicated by encircled areas. As can be seen, the conductivities of both materials are strongly dependent on thermal conditions. The increments in K_v caused by each step in temperature are not equal regardless of the method used indicating non-linear dependences of $K_v(T)$.

By analyzing the total increase in conductivities in Figure 7.6 for the studied range of temperatures, it may be noticed that the spread lies within two orders of magnitudes. Further, comparing the individual results achieved by means of the two mentioned approaches, a shift in both directions can be seen reflecting the situations of either surface potential decay technique provide relatively higher conductivities or the other way round. However, one finding is common for both the materials that standard measurements of volume currents results in higher conductivities at elevated temperatures. A possible source of such trends may be linked to the thermal expansion of soft samples, pressed between the two electrodes, in resistivity test fixture

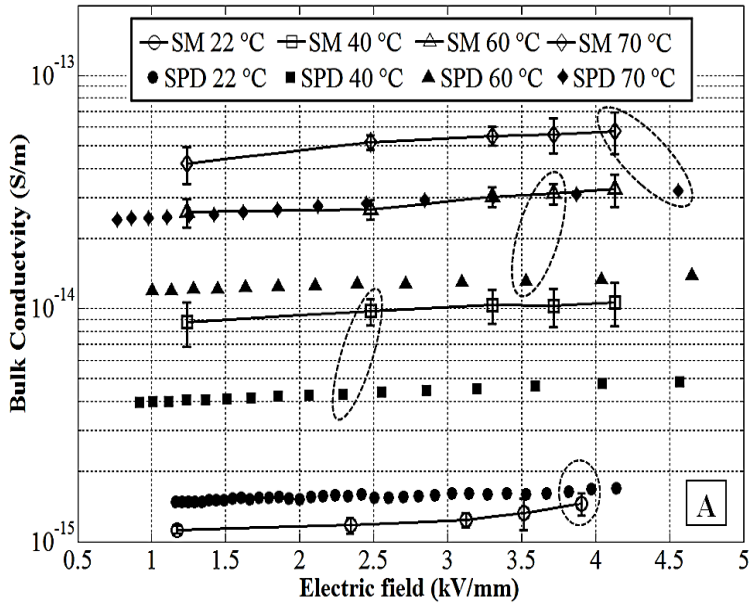

(a)

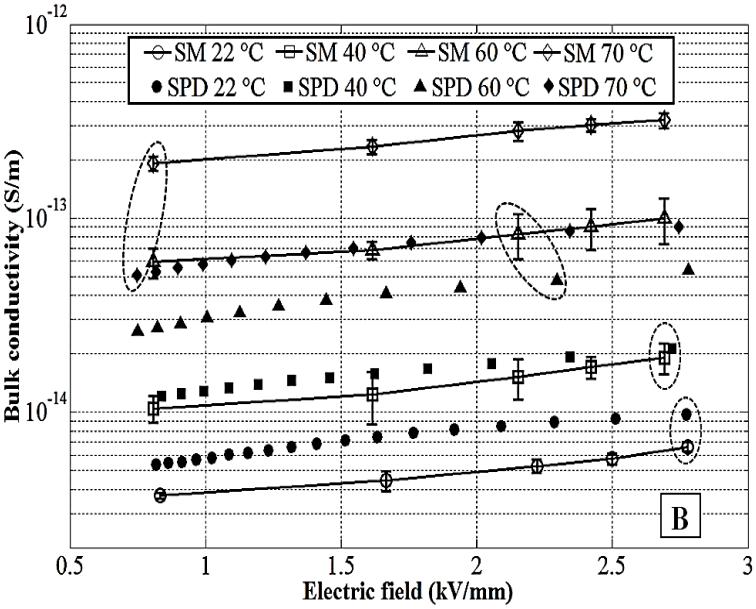

(b)

Figure 7.6. Bulk conductivities of silicone rubber A (a) and ATH doped material B (b) deduced from SPD characteristics and obtained from standard measurements (SM) of volume currents at different temperatures.

and pressure may vary depending on the thickness of materials. The consequence is that the affective area of samples under test may decrease leading to enhanced electrical fields and thus higher magnitudes of volume currents. The overestimated values of the bulk conductivities are further confirmed with the help of simulations (see section 8.3.3) that produced unrealistically faster decay compared to experiments. When using SPD technique, deformation of the sample is

Table 7.4. Deviations of the values K_v of material A obtained from SPD characteristics from the output of standard measurements at different levels of studied temperatures.

Temp (°C)	% deviations				
	300V	600V	800V	900V	1 kV
22	-30.6	-33.5	-29.9	-20.6	-12.6
40	53.7	55.1	56.1	54.4	55.2
60	52.9	52.1	57.1	57.9	58.7
70	40.2	45.1	45.6	44.7	44.5

Table 7.5. Deviations of the values K_v of material B obtained from SPD characteristics from the output of standard measurements at different levels of studied temperatures.

Temp (°C)	% deviations				
	300V	600V	800V	900V	1 kV
22	-43.9	-67.3	-68.6	-54.7	-46.5
40	-15.1	-27.1	-16.5	-12.7	-11.8
60	53.9	40.4	46.9	46.6	45.9
70	72.3	69.9	71.7	71.5	71.7

avoided. The percentage deviations calculated with respect to the data obtained from standard measurements are provided in Table 7.4 and Table 7.5 for materials A and B, respectively. As seen, the maximum discrepancies are close to those obtained at room temperature shown in Table 7.1, although the sign is different. This indicates that SPD technique provides meaningful results even at elevated temperatures.

Temperature dependences of conductivities of polymers is usually described by Arrhenius law as

$$K_v(T) = K_{v0} exp\left(-\frac{E_a}{kT}\right) \qquad (6.1)$$

where $K_v(T)$ is the bulk conductivity at given temperature, K_{v0} is a constant, E_a is the activation energy, k is Boltzmann constant, and T is the absolute temperature. Exponential fittings of the

data presented in Figure 7.6 at constant applied field using (6.1) are shown in Figure 7.7a. As seen, the conductivities obtained with both the methods follow Arrhenius law with slightly different slopes of the trend lines indicating its applicability for both the materials. The activation energies of volume conductivities estimated at two different magnitudes of surface potentials and test voltages are provided in Table 7.6. As can be noticed, values deduced from conventional measurements are slightly higher than those obtained from SPD technique. The differences for ATH doped material B are comparatively larger than for unfilled silicon rubber A. Nevertheless, the obtained energies are close to the known values [112, 113]. This again confirms the

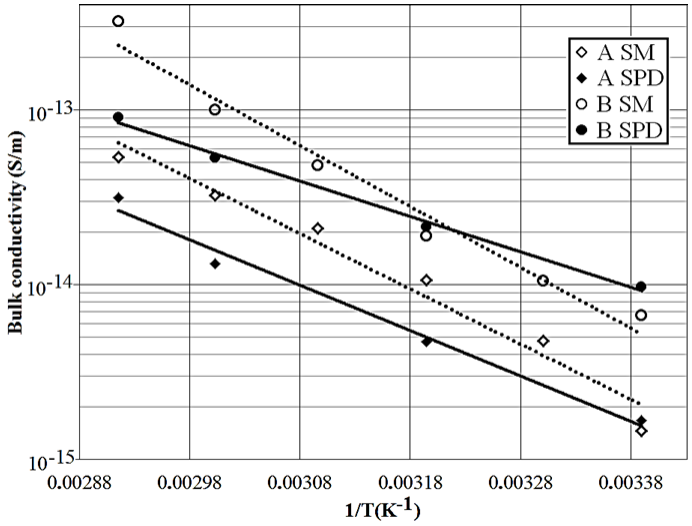

(a)

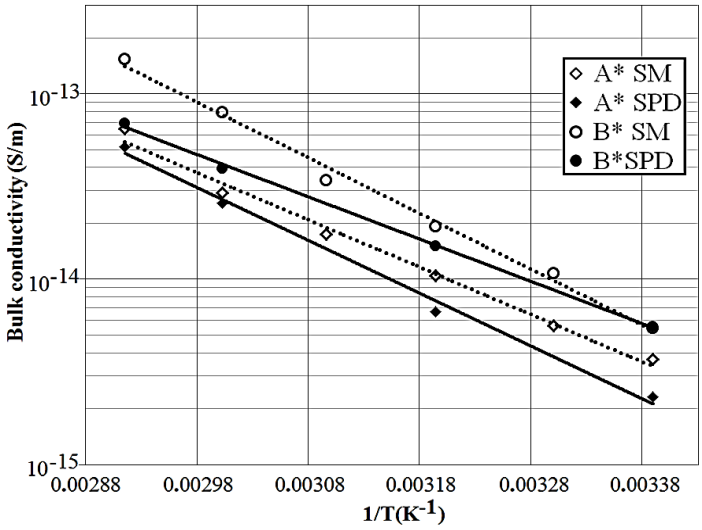

(b)

Figure 7.7. Bulk conductivities vs. reciprocal absolute temperature for thin (a) and thick (b) materials of silicone rubbers. The solid and dotted lines represent exponential fittings of the results of SPD technique and SM of volume currents respectively.

Table 7.6. Activation energies of volume conductivities of studied silicone rubbers materials.

Material	Activation energy of volume conductivity (eV)			
	SPD_{300V}	SPD_{1kV}	SM_{300V}	SM_{1kV}
A	0.49	0.52	0.67	0.63
B	0.49	0.41	0.71	0.69
A*	0.54	0.57	-	0.51
B*	0.49	0.45	-	0.59

possibility to utilize SPD method as a complementary and even more accurate tool for examining electrical conductivities of insulating materials.

In order to analyze similar data for thick silicone rubbers, the measurements shown in Figure 7.7b were utilized. As seen, conductivities evaluated from both the methods are quantitatively in good agreement at all the studied temperatures and, thus, supporting the experimental results demonstrated throughout this chapter. Further, activation energies (Table 7.6) are found to be close to the known values and differences for relatively pure material (A*) are smaller than that for additionally filled material (B*). These features match with those noticed for thin materials (Figure 7.7a). However, one characteristic is slightly different that is the weak spread of energies for thick materials as compared to thin samples (Table 7.6). For the latter, it may strengthen the fact that the results of the standard measurements of the volume currents are overestimated (Figure 7.6 and Figure 7.7a) as described earlier in this section. On the other hand for materials A* and B*, thermal expansions compared to the total thicknesses may be negligible resulting in close matching of the energies.

7.7 Comparison of the standard method with surface potential decay technique

Based on the demonstrations and analysis of estimated conductivities for HTV silicone rubber soft materials from standard measurements (Chapter 3) and surface potential decay technique, a comparative analysis is performed that is summarized in Table 7.7.

Table 7.7. Comparative analysis of standard measurements of volume currents and surface potential decay technique for evaluating conductivities of studied silicone rubbers.

Standard measurements (SM)	Surface potential decay technique (SPD)
1. SM may take significantly long times. In the present study, experiment for one of the material was conducted for 5 days to complete one set of measurements.	**1.** Time span of the experiments can be reduced to a large extent using SPD technique without affecting significantly the magnitudes of the measured conductivities.
2. Estimated conductivities from SM may include uncertainties if charging currents are interrupted prior to the mitigation of polarization processes.	**2.** It is practically impossible to completely negate other potential decay process that may also affect the final results.
3. SM is free of assumptions, related to materials, required for evaluating bulk conductivities.	**3.** SPD may require certain assumptions e.g. uniform surface charge density, relative permittivity at 50Hz, negligible effect of a measuring probe etc.
4. Voltage limitations of SM make it hard to estimate conductivities at higher field strengths that are most likely to appear in practical situations.	**4.** SPD based method seems to be more flexible in establishing stronger fields by utilizing higher corona voltages.
5. Obtaining field dependencies of bulk conductivities from SM would require a number of separate experiments to be performed especially on thick materials.	**5.** Non-uniform distributions of surface potentials may facilitate this process by selecting different locations on materials surfaces that correspond to different initial voltages (fields).
6. SM for a variety of materials may result in practically the same conductivities or relatively weaker spread of data as observed for the studied silicone rubbers and, thus, lack the strength of making effective representation.	**6.** SPD based technique collect conductivities for a certain range of fields (constituting a set of data points) that allows for making clear distinctions between the results of materials of very different compositions.
7. SM may possibly cause space charge effects, especially at higher electric fields and thus make it hard to estimate intrinsic conductivity that is a more natural parameter of insulation materials.	**7.** SPD reduces the risks of space charge effects due to lower energies of deposited surface charges and thus ensures estimations of intrinsic conductivities.
8. Resistivity box in SM of volume currents may induce mechanical errors (thermal expansion of samples), especially at elevated temperatures, and hence overestimate the magnitude of conductivities.	**8.** SPD based technique is more reliable and accurate due to the fact that it avoid pressing of material samples.

8. Potential decay modeling

This chapter focuses on simulation of potential decay on studied materials accounting for charge leakage through material bulk and along gas-solid interface. The results of the experimentally obtained SPD characteristics are compared with the numerical outputs. Results of a parametric study aiming at identifying the influences of the volume and surface conductivities of the materials as well as that of the dielectric permittivities on surface potential decay are examined. Filed dependent bulk conductivities obtained from standard measurements of volume currents for the studied thin samples are used as input for the model.

8.1 Physical background and computer implementation

As mentioned earlier, it is commonly accepted that charge/potential decay on insulating materials may occur due to volume and surface conduction in/on the solid material and due to neutralization of surface charges caused by free charge species within gas phase. Under normal conditions, all the three decay mechanisms act simultaneously and it is a difficult task to distinguish between their individual contributions to the total effect. In the present study, the influence of gas phase is eliminated by considering the dynamics of surface potentials at reduced gas pressure that provides a low number of ions in the gas volume, as demonstrated in section 4.3. Such approach allows for analyzing solely the role of solid material on surface charge behavior, which can be affected by several processes in the solid, e.g. dipolar relaxation, intrinsic conduction, de-trapping, etc. [24, 40]. For the studied HTV silicon rubber samples, the experimentally obtained surface charge/potential decay curves were well fitted by exponential type of dependences (section 4.5.2) that indicated dominant role of intrinsic conduction in SPD. In order to further analyze the influences of volume conductivities as well as to suggest a range of relevant parameters at which the contribution of surface conduction may be considerable, potential decay model presented earlier in section 2.4 was utilized.

Equation (2.15) was solved numerically using simulation tool Comsol Multiphysics, which is based on finite element method. The equation was implemented in a 1D axially symmetric model as the measured surface potential distributions were found to be symmetrical around the mid position of the sample (location of the tip of the corona needle). In the selected 1D approach, the computational domain (line) represented the gas-solid interface and all the material parameters were taken as being independent of the sample thickness. The coefficients in (2.15) were calculated using characteristics of the material samples shown in Table 3.2 and Table 3.3, and the surface potential profile measured immediately after completing the gas evacuation (3 min after charging) was used as the initial condition (marked as 0 min in the plots below).

8.2 Comparison of the experimental and simulation results

The experimentally obtained potential distributions at different instants during the decay process and the output from the simulations are shown in Figure 8.1a and Figure 8.1b for thick samples of materials C* and E*, respectively. Recall that material C* is more conductive than E* (compare the properties in Table 3.2 and Table 3.3). As it was already mentioned in section 4.5.1, the lateral spread of the charged spots on surfaces of the materials is negligible even at long times after charging that leads to the conclusion that the contribution from surface conduction to the charge decay is insignificant. Hence, the observed time variations of the surface potential are affected solely by bulk conduction. This is also confirmed in general by the results of the simulations shown in Figure 8.1. As seen, the calculations yielded similar tendency in the time

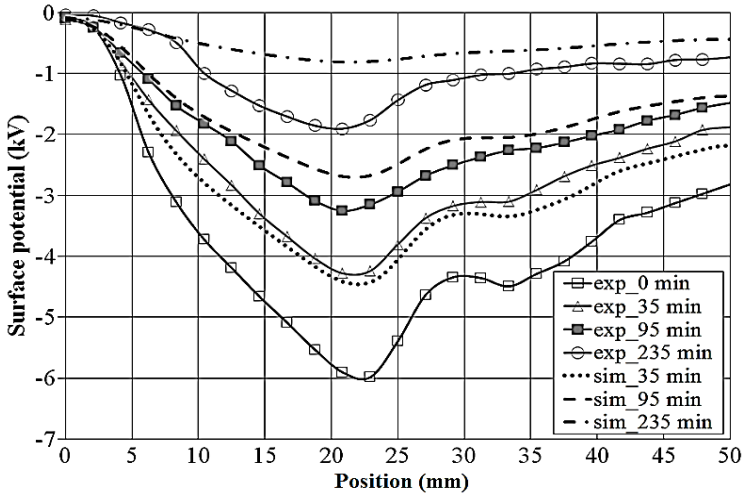

(a)

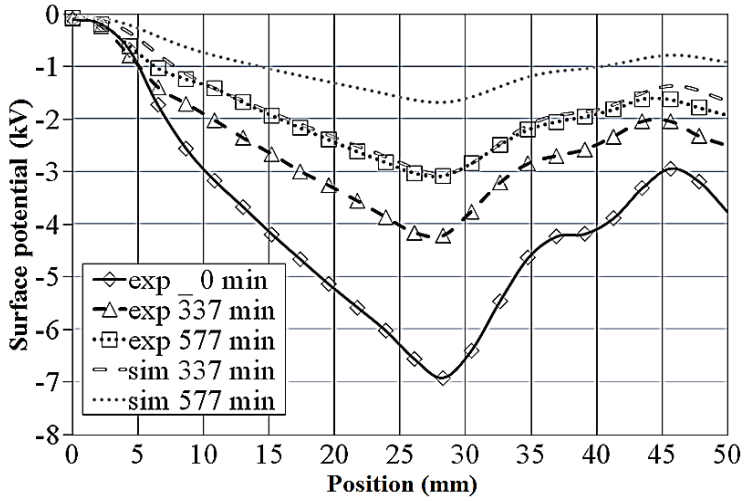

(b)

Figure 8.1. Measured and simulated surface potential profiles on C* (a) and E* (b) materials at 300 mbar at different times after charging.

evolution of the potential profiles as observed in the experiments. Quantitatively, the agreement is quite good at short instants but becomes rather poor at the long times after charging. Thus in Figure 8.1b, the distribution calculated for 337 min is almost overlapping with the experimental profile for 577 min indicating that the actual potential decay is much slower than the calculated one. The discrepancies may arise due to the fact that the fixed conductivity values from Table 3.2 and Table 3.3 obtained at 1 kV test voltage were used in the simulations. In the experiments, however, the electric field in the material induced by the deposited surface charges may become strong enough to activate field-dependent conduction mechanisms in the bulk. In this case, taking into account that the measured potentials (and thus charges) are unevenly distributed along the surface, one can expect a certain dependence of the bulk conductivity on the location on the sample surface. This allows to suggest that field-dependent conductivities should be used in (2.15) instead of the constant values. Results of the implementation of this hypothesis in the model are presented below.

8.3 Effects of material properties on surface potential decay

8.3.1 Analysis of the effect of field dependent bulk conductivity

Field dependent conductivities of the studied thin materials obtained from standard measurements of volume currents, as discussed in section 3.4 and presented in Figure 7.1, were adopted into the model and initial conditions were kept the same. For obtaining the numerical outputs, locations on the sample surfaces corresponding to the potentials of ~1 kV were selected that indicate the same maximum test voltage as was applied in the conductivity measurements. The results of the simulations are illustrated in Figure 8.2 as normalized SPD characteristics for the materials showing most significant variations. Experimental data are provided for comparison. As it is observed, the regularity mentioned earlier is confirmed, i.e., the higher conductivity of the material leads to the faster potential decay.

The plots in Figure 8.2 also demonstrate the results of the performed simulations. As can be seen, incorporating field dependencies of $K_v(E)$ obtained from standard measurements into the model yielded good agreement (especially at short instants) between the computed and experimental SPD curves. For quantitative comparison, the times for reduction of surface potential to a half of its initial value obtained from both the methods and percentage deviations with respect to experiments are indicated in Table 8.1. As seen, the deviations are less than 20% for all the silicone rubbers except for material B (SPD curves are shown in Figure 8.3). The discrepancies may arise due to uncertainties in the decay measurements at lower potentials, numerical errors, and scattering in the measured volume conductivities. In addition to that, equation (2.15) and, hence, numerical output is dependent on dielectric permittivity, which needs to be properly selected as its value is varying with frequency, especially for filled materials. A detail study on the sensitivity of this parameter is carried out in the next section. Nevertheless, for the performed simulations with the dielectric constants ε_r corresponding to 50Hz, the differences in times (Table

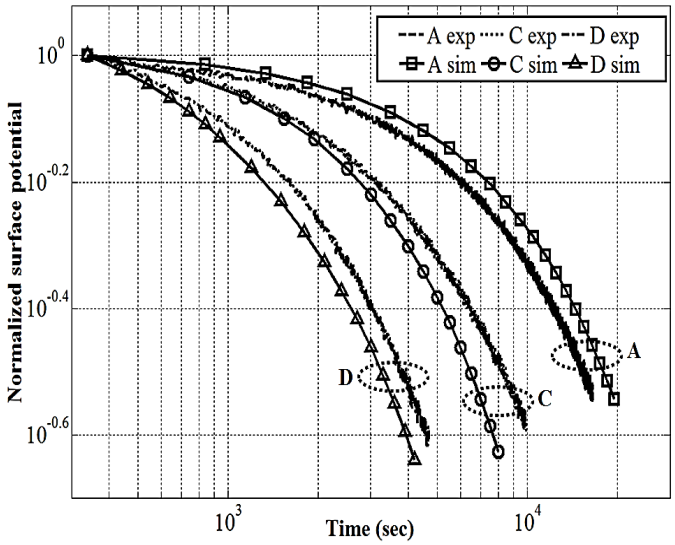

Figure 8.2. Measured and computed profiles of SPD for thin samples of HTV silicone rubbers. The results of the simulations were obtained with the model accounting for the field dependent conductivities of studied materials.

8.1) resulted from the two approaches are quite small. This reveals that the measured SPD characteristics on silicone rubbers can be well explained taking into account field dependent conductivities of materials.

As mentioned earlier in section 7.2, it is not trivial to estimate bulk conductivities for stronger electrical fields, in particular, due to limitations of the conventional measuring setup (e.g., discharges from electrodes may occur due to high test voltages and should be avoided). On the other hand, the initial values of surface potentials in a decay experiment can be high and depends on the charging voltage magnitude and material properties as demonstrated in section 4.4. Therefore, extending the above approach to estimate numerical outputs that can be compared with the decay profiles recorded during the entire period of the measurements, similar to the one shown in Figure 4.10, is rather difficult.

Table 8.1. Times to reach a half of the initial magnitude of surface potential and percentage deviations with respect to experimental data.

Materials	$t_{50\%}^{exp}$ sec	$t_{50\%}^{sim}$ sec	Δ %
A	9110	10920	-19.86
B	2770	3500	-26.35
C	4600	4000	13.04
D	2280	1950	14.47

8.3.2 Sensitivity analysis of dielectric permittivity of studied materials

Normalized SPD characteristics obtained from simulations performed with two different dielectric constants of the materials are shown in Figure 8.3 along with the experimental data. The results are presented for silicone rubbers with dissimilar characteristics of the profiles of permittivities (see Figure 3.15). For obtaining the numerical outputs, the procedure described in the first paragraph of section 8.3.1 was followed. As expected for unfilled silicone rubbers, simulations produce approximately the same results due to the fact that the dielectric permittivity for this material change very slightly in the studied range of frequencies (Figure 3.15). On the other hand for ATH doped material B, using the value of ε_r corresponding to 50 Hz yields weak deviations in the SPD curves (see Table 8.1). However, they increase if the dielectric permittivity measured at 10^{-4} Hz is utilized. Recall that the rate of the potential decay is inversely related to dielectric constants (2.15). Therefore, the decay profiles for both the materials shift to the right (to longer instants) when higher values of permittivities are adopted.

Based on the results of the simulations, it can be argued that it is the dielectric constant at 50 Hz (this value reflect minimized effects of interfacial processes, see section 3.7) which support the experiments. Moreover, it has been demonstrated that slow polarization (e.g. interfacial phenomenon) don't contribute significantly to the measured potential decay (section 4.5.2) on studied materials of silicone rubbers.

8.3.3 Influence of elevated temperatures

Normalized surface potential decay obtained for the locations corresponding to the maximum values of *Vs* on samples of unfilled and ATH doped silicone rubbers at different ambient temperatures are shown in Figure 8.4 and Figure 8.5 respectively. The results of the simulations

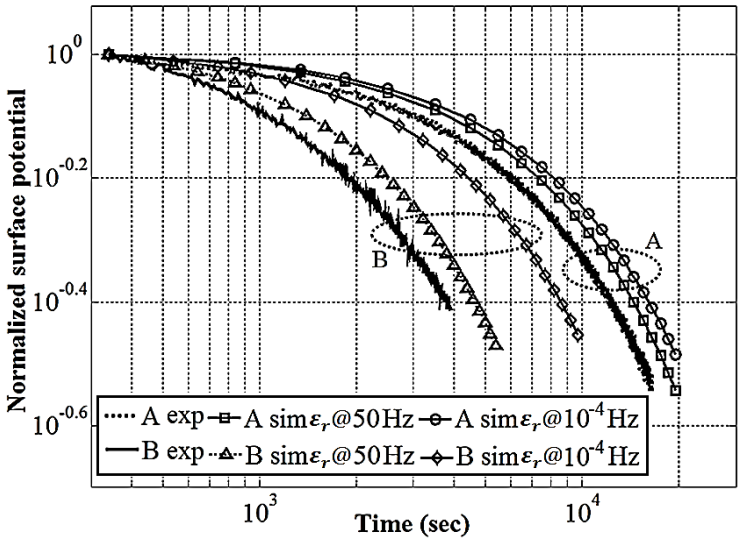

Figure 8.3. Measured and computed profiles of SPD for thin samples of HTV silicone rubbers. The results of the simulations were obtained with two different permittivities of materials at 50 Hz and 10^{-4} Hz.

performed with fixed conductivities deduced from the standard measurements (section 7.6) at 1 kV test voltage are represented by markers with solid lines. Further, for the sake of clarity, arrows are shown that indicate the direction in which numerical outputs deviate from experimental data. As seen, the decay profiles are strongly affected by the ambient temperatures variations. Detail discussion on the measured decay characteristics can be found in section 6.3.

One may notice deviations of the numerical outputs from the measured characteristics which depend on the materials compositions and thicknesses. For material A* that represents thick sample of a relatively pure silicone rubber, the simulations agree partly with the experiments at lower temperatures (20 °C and 40 °C) and the deviations are observed at the later stages of the

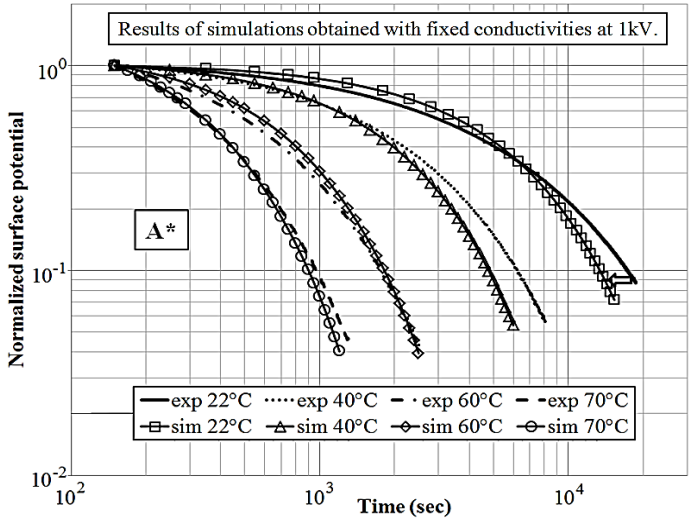

(a)

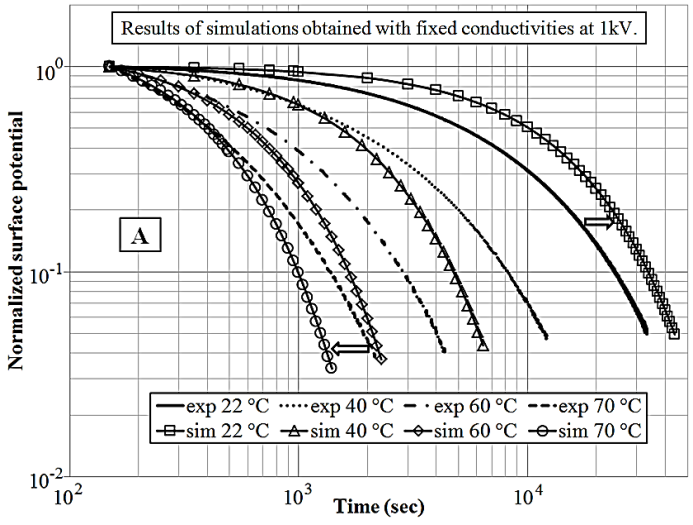

(b)

Figure 8.4. Measured and simulated surface potential profiles on thick (a) and thin (b) materials of unfilled silicone rubbers. The arrows indicate the direction in which numerical outputs deviates from the experiments. The legends show average temperatures in the materials.

decay. However at elevated temperatures, good agreement is observed between the computed and experimental SPD curves for the entire decay time. On the other hand for the thin sample of the same material (A), the simulated decay is slower or faster than that in the experiments depending on the temperature and the deviations are quite significant.

Data for materials containing additional fillers are shown in Figure 8.5. As can be seen, simulations do not match the experiments for any portion of the SPD curves regardless of the thicknesses of samples. For silicone rubber B*, the differences between the results of the two approaches are noticeable and it increasing even more for thin material B. At room temperature, the discrepancies can be minimized by incorporating field dependent conductivities of materials

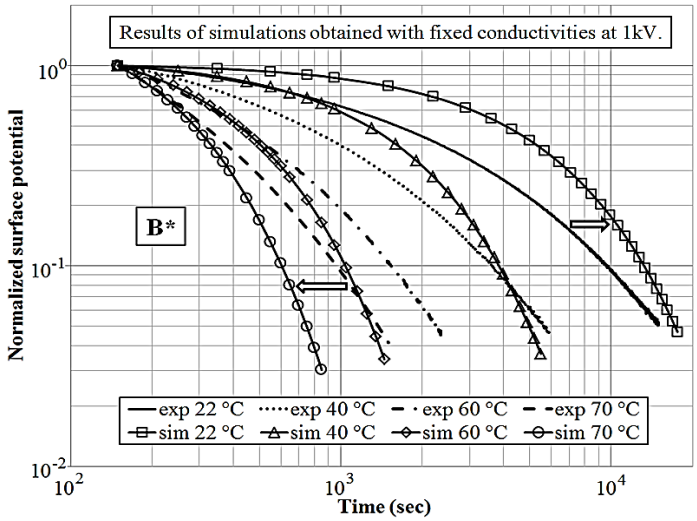

(a)

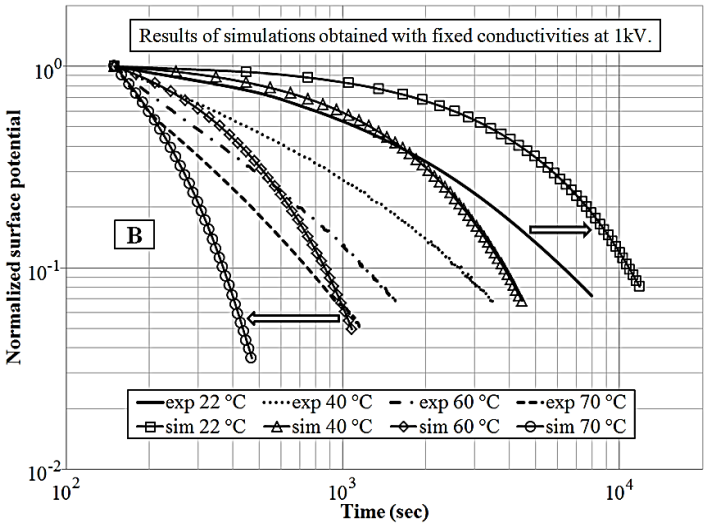

(b)

Figure 8.5. Measured and simulated surface potential profiles on thick (a) and thin (b) materials of ATH doped silicone rubbers. The arrows indicate the direction in which numerical outputs deviates from the experiments. The legends show average temperatures in the materials.

into the decay model as described earlier in section 8.3.1. However at elevated temperatures, the simulated decay for most of the studied materials is faster than the experimental one. The fastest decay is observed for material B (compare the leftmost curves in Figure 8.5b). A possible explanation for these observations could be related to the inaccurate parameters that are used as input for the simulation model. Thus, the numerical outputs are strongly dependent on the conductivity K_v (2.15) and, therefore, the large deviations reflect the fact that the magnitudes of the conductivities obtained using volume currents are overestimated as discussed in section 7.6. The exception to this is the set of data for the unfilled silicone rubber A*, where a good fit is observed between the measured and computed SPD profiles at elevated temperatures.

8.3.4 Contribution of surface conduction to potential decay

A parametric computational study was performed in order to analyze the influence of surface conductivity on surface potential profiles as well as on the potential decay. In the calculations, the bulk conductivity of 10^{-15} S/m and the thickness of the material sample 2 mm were used that corresponded to E* material, the least conductive one. The curve marked as "0 min" from Figure 8.1b represented the initial conditions. The computed variations of surface potential profiles obtained with two different values of surface conductivity are shown in Figure 8.6 for two instants after charging. It was found from the simulations that for the given conditions, the influence of surface conductivity could only be feasible when its magnitude exceed ~10^{-17} S. As it is shown in the figure, the enhanced surface conduction intensifies charge spreading along the surface and may even result in a crossover of the surface potential profiles (curves for $K_s = 10^{-15}$ S). It also could yield a faster potential decay (note that the measured surface conductivity for E* material is equal to $5 \cdot 10^{-19}$ S, Table 3.3).

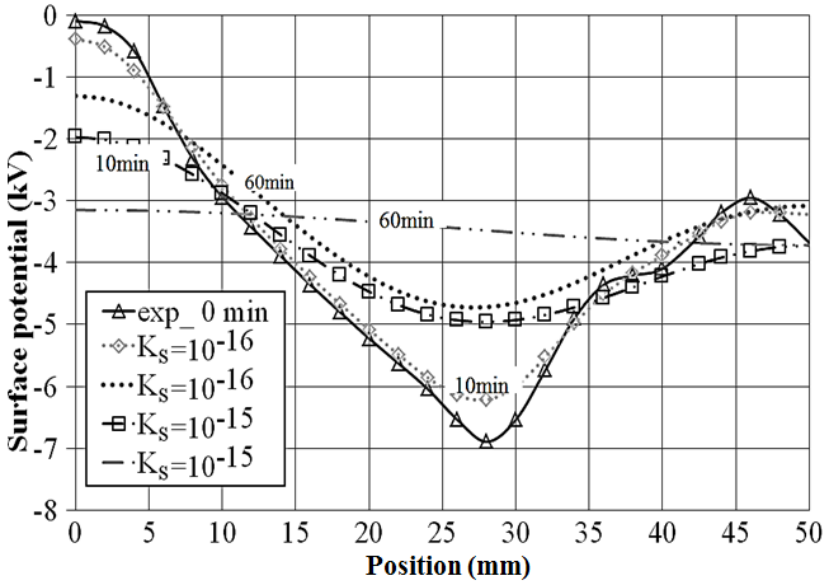

Figure 8.6. Simulated distributions of surface potential at different times after charging and various surface conductivities.

9. Conclusions

The studies performed within the thesis work aimed at increasing understanding of surface charge dynamics on insulating polymers and their electrical characterization. For this, several types of HTV silicon rubbers intendant for use in HVDC applications were utilized. Effects of different factors such as ambient air pressures, elevated temperatures, materials electrical properties, presence of fillers as well as influences of macroscopic interfaces between the materials layers on surface potential decay were investigated. Electrical characterization of the studied polymers has been performed by measuring volume conductivities and dielectric permittivities. For the former, standard method and SPD technique were utilized and a comparative analysis of advantages and drawbacks of the both approaches has been conducted. Computer models of SPD accounting for charge leakage through material bulk and along gas-solid interface have been developed. The results of the performed simulations were compared with the experimentally obtained SPD characteristics. Conclusions drawn from each of these studies are summarized below.

Surface charging

Corona charging from a needle electrode resulted in bell- or saddle-shaped distributions of surface potentials on flat material samples. The latter appeared when charging voltage exceed a certain threshold value. An increase in the voltage amplitude provided a larger area of the charged spot and larger spread of surface potential. The profile of the deposited charge was also dependent upon material properties. Thus, lowering bulk conductivities of the material resulted in a higher peak value of the surface potential while an increase of surface conductivity led to a larger expansion of the potential (charge) over gas-solid interface. The differences in the peaks of negative and positive surface potentials were within 10% that indicated a weak dependence on the polarity of applied voltage.

Surface potential decay under different experimental conditions

Surface potential decay measured at different pressures of ambient air allowed for quantifying the role of gas neutralization in the total charge decay as well as for analyzing solely the effect of solid materials properties on surface charge dynamics. The experiments demonstrated that the amount of ions present in gas affected SPD and it was inhibited at reduced air pressures inside the test vessel as well as at decreased magnitudes of the surface potential. It has been found that gas neutralization caused a pronounced difference in the decay characteristics obtained on material samples with relatively low conductivity. The decay rates were found to be weakly dependent on the polarity of deposited surface charges.

The recorded profiles of the surface potential on the pre-charged HTV silicon rubber samples have demonstrated that the magnitudes of V_S decreased with time while the shapes of the

distributions were in general preserved during the decay process. This indicated that bulk conduction was the dominant mechanism of the potential decay under conditions of the present study. Furthermore, fitting the measured SPD characteristics by different functions provided the best fit obtained with exponential function that confirmed the dominant role of the intrinsic material conductivity in the observed dynamics of the surface potential. To examine the effect of surface conductions, additional experiments have been performed with the material having extremely low bulk conductivity (XLPE). In this case, a pronounced lateral expansion of the charged spot over sample surface was recorded, which resulted in almost even surface potential distributions at long times after charging. This was attributed to the fact that bulk conduction was rather weak and surface conduction process played a dominant role in surface charge/potential decay in this case.

Surface charge decay on studied silicone rubber materials was found to be strongly affected by temperature. It has been shown that thermally activated bulk conduction intensified SPD process at elevated temperatures, independently of the induced field strength.

Studies on double-layered samples of HTV silicone rubbers

SPD on double-layered (sandwiched) structures was found to be faster than on single materials samples and was controlled mainly by the conductivity of the base layer, which was in contact with the grounded metallic electrode. It has been argued that injection of charges from metal-material interfaces might contribute to the intrinsic conduction in the material forming a mechanism for supplying charges from the bulk to the surface of the sample and thus governing SPD under conditions of the experiments. It has been suggested that internal interfaces between layers of materials may introduce additional trapping centers and enhance accumulation of interfacial charges that, in combination with the relatively high conductivity of the bottom layers, may describe the drastic speed up of SPD process. Dielectric spectroscopy measurements revealed that by combining layers of different materials, an increase in dielectric constants up to 2.5 times compared to individual materials can be achieved. The performed computational analyses showed that such effect cannot be explained by means of classical Maxwell-Wagner model and introducing additional charges at the internal interfaces was necessary to reach an agreement between the computed results and experimental data.

Evaluation of material properties from standard measurements and potential decay characteristics

Electrical bulk conductivities of HTV silicone rubber based materials have been determined by measurements based on standard and SPD procedures. It has been demonstrated that the both methods yielded comparable results both under normal conditions as well as at elevated temperatures. The measurements of the volume currents (i.e. standard procedure) conducted at different amplitudes of the applied dc test voltages revealed that mitigation of polarization processes is time consuming and is affected by composition of the material and applied electric field strengths. In contrast, the technique based on surface potential decay allowed for obtaining field dependence of material conductivity from a single SPD characteristic thus significantly

reducing the time span of the experiments. In addition, it was shown that the SPD based approach provided much wider range of the fields for analyzing field dependent intrinsic conductivities than that suggested by the conventional method. Temperature dependences of bulk conductivities of the materials obtained by both methods were of Arrhenius type and the activation energies were found to be in reasonable agreement and close to known values. The results of the study allowed for concluding that SPD technique can be proposed as an alternative and even more accurate method for the electrical characterization of insulating materials for high voltage applications.

Field dependencies of the conductivities of the studied materials were further analyzed using Poole-Frenkel model. It has been found that it provided acceptable match between the theoretical and experimental values of Poole-Frenkel factor β in case of materials samples of relatively large thickness (~2 mm).

Computer modeling of surface potential decay

Potential distributions along the solid material surfaces experimentally obtained during the decay process reflected transverse or longitudinal transport of charges in/on the materials. The performed computational studies allowed for evaluating material properties (volume and surface conductivities as well as dielectric permittivities) at which their contributions to the dynamics of surface charges became most essential. Both the experiments and simulations revealed that bulk conduction is the most suitable mechanism for describing SPD on the studied HTV silicone rubbers. The results of the modeling agreed well with the measured characteristics if materials field-dependent conductivities and dielectric constants at 50 Hz were taken into account. It also indicated that volume conductivities obtained from standard method at elevated temperatures were overestimated. The performed parametric study has demonstrated also that surface conduction may influence the surface potential decay on highly resistive materials such as XLPE.

10. Future work

Possible suggestions for future studies can be as follows.

- The work related to electrical characterization and potential decay was performed on flat samples of polymeric materials of thicknesses larger than few hundreds of μm. Similar studies can be performed on thin films (in the range of μm) to investigate further possible effects of bulk space charges, which were found to be negligible for the dimensions of the presently studied insulation materials.
- In the conducted work, sandwich structures were prepared by putting material samples together taking advantages of the sticky nature of HTV silicone rubbers that, however, may not be recommended for deeper analysis due to possible defects (e.g. presence of air bubbles between the material layers). In this regard, employing proper techniques (similar to vulcanization, degassing, etc.) could improve the quality of samples preparation, especially, the contact between the materials.
- Further investigations of surface potential decay method for evaluating conductivities of highly resistive and hard insulating materials such as polyethylene. In connection to that, determination of frequency or range of frequencies at which the dielectric constants of the materials should be considered for estimating the magnitudes of conductivities from SPD characteristics (recall equation (2.6)) may provide better realization of such complementary tools.
- A more sophisticated model involving, in particular, a description of charge transport through the material (including multi-layered structures) may provide better understanding of the dynamics of surface potentials and the role of interfacial polarization.

REFERENCES

[1] G. Chen, M. Hao, Z. Xu, A. Vaughan, J. Cao and H. Wang, "Review of high voltage direct current cables", CSEE, J. Power Energy Systems, Vol. 1, No. 2, pp. 9-21, 2015.

[2] M. Tenzer, H. Koch and D. Imamovic, "Compact systems for high voltage direct current transmission", Proc. Int. ETG Congress, Bonn, Germany, Nov. 17-18, pp. 1-6, 2015.

[3] S. Kumara, "Electrical charges on polymeric insulator surfaces and their impact on withstand performance", PhD thesis, Chalmers University of Technology, Gothenburg, Sweden, 2012.

[4] Z. Fang, R. A. Fouracre and O. Farish, "Investigations of surface charging of DC insulator spacers", IEEE Conf. Elec. Insul. Diel. Phenomena, San Francisco, USA, pp. 149-152, 1996.

[5] D. K. Das-Gupta, "Surface charge decay on Insulating Films", IEEE Int. Symp. Elec. Insul., Boston, MA, USA, pp. 296-299, 1988.

[6] S. Okabe, "Phenomena and mechanism of electric charges on spacers in gas insulated switchgears", IEEE Trans. Diel. Elec. Insul., Vol. 14, No. 1, pp. 46-52, 2007.

[7] K. O. Papailiou and F. Schmuck "Silicone composite insulators", Springer-Verlag Berlin Heidelberg New York, 2013.

[8] R. Hackam, "Outdoor high voltage polymeric insulators", Proc. IEEE Int. Symp. Elec. Insul., Toyohashi, pp. 1-6, 1998.

[9] I. Ramirez, S. Jayaram, E. A. Cherney, M. Gauthier, and L. Simon, "Erosion resistance and mechanical properties of silicone nanocomposite insulation", IEEE, Trans. Diel. Elec. Insul., Vol. 16, No. 1, pp. 52-59, 2009.

[10] F. Su1, J. Zhidong, G. Haifeng, and G. Zhicheng, "Influence of fillers on silicone rubber for outdoor insulation", Annual Report IEEE Conf. Elec. Insul. Diel. Phenomena, Vancouver, BC, pp. 300-303, 2007.

[11] L. A. Dissado and I. C. Fothergill, "Electrical degradation and breakdown in polymers", Peregrinus Ltd, 1992.

[12] G. C. Montanari, "Bringing an insulation to failure: the role of space charge", IEEE Trans. Diel. Elec. Insul., Vol. 18, No. 2, pp. 339-364, 2011.

[13] Salama and M. Arief, "The performance of silicone rubber for HV insulators under natural tropical aging", IEEE Int. Conf. Solid, Diel., pp. 304-307, 2004.

[14] V. M. Moreno and R. S. Gorur, "Accelerated corona discharge performance of polymer compounds used in high voltage outdoor insulators", Annual Report IEEE Conf. Elec. Insul. Diel. Phenomena, pp. 731-734, 1999.

[15] S. Kumara, S. Alam, I. R. Houqe, Y. V. Serdyuk and S. M. Gubanski, "DC flashover characteristics of a cylindrical insulator model in presence of surface charges", IEEE Trans. Diel. Elec. Insul., Vol. 19, No. 3, pp. 1084-1090, 2012.

[16] F. Wang, Q. Zhang, Y. Qiu and E. Kuffel, "Insulator surface charge accumulation under DC voltage", Proc. IEEE Int. Symp. Elec. Insul., pp. 426 – 429, 2002.

[17] J. A. Giacometti, and O. N. Jr. Oliveira, "Corona charging of polymers", IEEE Trans. Elec. Insul., Vol. 27, No. 5, pp. 924-943, 1992.

[18] B. Lutz and J. Kindersberger, "Surface charge accumulation on cylindrical polymeric model insulators in air: simulation and measurement", IEEE Trans. Diel. Elec. Insul., Vol. 18, No. 6, pp. 240-248, 2011.

[19] K. Nakanishi, A. Yoshioka and Y. Shibuya, "Surface charging on epoxy spacer at DC stress in compressed SF6 gas", IEEE Trans. Power App. Sys., Vol. 102, pp. 3919-3927, 1983.

[20] C. W. Mangelsdorf and C. M. Cooke, "Static charge accumulated by epoxy post insulation stressed at high DC voltages", IEEE Conf. Elec. Insul. Diel. Phenomena, pp. 220-227, 1978.

[21] A. Kumar, D. Wu, R. Hartings and B. Engström, "Experience from first 800 kV UHVDC long-term test installation", Proc. 6th Int. Conf. Power Trans. Distr. Tech., Guangzhou, China, Nov. 10-12, 2007.

[22] F. Messerer, M. Finkel and W. Boeck, "Surface charge accumulation on HVDC – GIS – spacer", IEEE Int. Symp. Elec. Insul. , Boston, MA USA, April 7-10, 2002.

[23] T. Nitta and K. Nakanishi, "Charge accumulation on insulating spacers for HVDC GIS", IEEE Trans. Elec. Insul., Vol. 26, No. 3, pp. 418-427, 2002.

[24] P. Molinie, "Measuring and modeling transient insulator response to charging: the contribution of surface potential studies", IEEE Trans. Diel. Elec. Insul., Vol. 12, No. 5, pp. 939-950, 2005.

[25] P. Molinie, M. Goldman, and J. Gatellet, "Surface potential decay on corona-charged epoxy samples due to polarization processes", J. Appl. Phys., Vol. 28, pp. 1601-1610, 1995.

[26] E. Kuffel, W. S. Zaengl, and J. Kuffel, "High voltage engineering fundamentals", Pergamon Press, 1984.

[27] M. M. Shahin, "Nature of charge carriers in negative coronas", Appl. Opt. Suppl. Elec. Photogr., Vol. 82, pp. 106-110, 1969.

[28] M. M. Shahin, "Mass – spectrometric studies of corona discharges in air of atmospheric pressures", J. Chem. Phys., Vol. 43, pp. 2600-2605, 1966.

[29] R. Toomer, and T. J. Lewis, "Charge trapping in corona-charged polyethylene films", J. Phys. D: Appl. Phys., Vol. 13, No. 7, pp. 1343-1355, 1980.

[30] E. A. Baum, T. J. Lewis and R. Toomer, "Decay of electrical charge on polyethylene films", J. Phys. D: Appl. Phys., Vol. 10, No. 4, pp. 487-497, 1977.

[31] J. Kindersberger and C. Liderle, “Surface charge decay on insulators in air and sulfurhexafluorid – part II: measurements”, IEEE Trans. Diel. Elec. Insul., Vol. 15, No. 4, pp. 949-957, 2008.

[32] Y. Späck, S. Kumara and S. M. Gubanski, "Charge decay measurements on a polymeric insulation material under controlled humidity conditions”, Nordic Insul. Symp., Trondheim, Norway, pp. 149-152, 2013.

[33] Z. Xu, L. Zhang and G. Chen, “Decay of electric charge on corona charged polyethylene”, J. Phys. D: Appl. Phys., Vol. 40, pp. 7085-7089, 2007.

[34] S. Alam, Y. V. Serdyuk and S. M. Gubanski, “Potential decay on silicone rubber surfaces affected by bulk and surface conductivities”, IEEE Trans. Diel. Elec. Insul., Vol. 22, No. 2, pp. 970-978, 2015.

[35] J. Hillenbrand, T. Motz, G. M. Sessler, X. Zhang, N. Behrendt, C. S. Soglio, D. P. Erhard, V. Altstädt and H. W Schmidt, “The effect of additives on charge decay in electron-beam charged polypropylene films”, J. Appl. Phys., Vol. 42, pp. 1-8, 2009.

[36] A. Sylvestre, P. Rain and S. Rowe, “Silicone rubber subjected to combined temperature and humidity effects”, Annual Report IEEE Conf. Elec. Insul. Diel. Phenomena, pp. 355-358, 2002.

[37] G. Chen, J. Zhao and Y. Zhuang, "Numerical modeling of surface potential decay of corona charged polymeric material”, Proc. Int. Conf. Solid Diel., Potsdam, Germany, pp. 1-4, 2010.

[38] P. Molinie, “A review of mechanisms and models accounting for surface potential decay” IEEE Trans. Plasma Sci., Vol. 40, No. 2, pp. 167-176, Dec. 2012.

[39] G. Chen, “Anomalous phenomena in solid dielectrics under high electric fields”, IEEE 9th Int. Con. Prop. Appl. Diel. Mat., pp. 954-960, 2009.

[40] P. Molinie and P. Llovera, “Surface potential measurement: implementation and interpretation”, Proc. 8th Int. Conf. Diel. Mat. Meas. Appl., pp. 253-258, 2000.

[41] P. Llovera and P. Molinie, “New methodology for surface potential decay measurements: application to study charge injection dynamics on polyethylene films”, IEEE Trans. Diel. Elec. Insul., Vol. 11, No. 6, pp. 1049-1056, 2004.

[42] E. A. Baum, T. J. Lewis and R. Toomer, “The lateral spreading of charge on thin films of polyethylene terephthalate”, J. Phys. D: Appl. Phys., Vol. 11, pp. 963-977, 1978.

[43] A. Crisci, B. Gosse, J. P. Gosse and V. O. Duréault, “Surface potential decay due to surface conduction”, J. Appl. Phys., Vol. 4, pp. 107-116, 1998.

[44] J. Kindersberger and C. Liderle, “Surface charge decay on insulators in air and sulfurhexafluorid – part I: simulation”, IEEE Trans. Diel. Elec. Insul., Vol. 15, No. 4, pp. 941-948, 2008.

[45] T. J. M. Gaertner, T. Stoop, J. Tom, H. F. A. Verhaart and A. J. L. Verhage, “Decay of surface charges on insulators in SF6”, Proc. IEEE Int. Symp. Elec. Insul., Montreal, Canada, pp. 208-213, 1984.

[46] I. W. McAllister, “Decay of charge deposited on the wall of a gaseous void”, IEEE Trans. Elec. Insul., Vol. 27, No. 6, pp. 1202-1207, 1992.

[47] S. Alam, “Surface charge dynamics on polymeric insulating materials for high voltage applications”, Licentiate thesis, Chalmers University of Technology, Gothenburg, Sweden, 2014.

[48] S. Kumara, B. Ma, Y. V. Serdyuk and S. M. Gubanski, “Surface charge decay on HTV silicone rubber: effect of material treatment by corona discharges”, IEEE Trans. Diel. Elec. Insul., Vol. 19, N0. 6, pp. 2189-2195, 2012.

[49] Y. Liu, Z. An, Q. Yin, F. Zheng, Y. Zhang, “Rapid potential decay on surface fluorinated epoxy resin samples”, J. Appl. Phys., Vol. 113, pp. 164105-164105-8, 2013.

[50] P. Molinie, “Potential decay interpretation on insulating films: necessity of combining charge injection and slow volume polarization processes”, Proc. 7th Int. Conf. Diel. Mat. Meas. Appl., Bath, England, pp. 50-55, 1996.

[51] A. T. Hoang, Y. V. Serdyuk and S. M. Gubanski, “Mechanisms of surface potential decay on enamel wire coatings”, IEEE Trans. Diel. Elec. Insul., Vol. 22, N0. 6, pp. 3470-3480, 2015.

[52] G. Teyessedre and C. Laurent, “Charge transport modeling in insulating polymers: from molecular to macroscopic”, IEEE Trans. Diel. Elec. Insul., Vol. 12, No. 5, pp. 857-875, 2005.

[53] D. L. Chinoglia, G. F. Leal Ferreria, J. A. Giacometti and O. N. Jr. Oliveria, “Corona-triode characteristics: on effects possibly caused by the electronic component”, 7th Int. Symp. Electrets, pp. 255-260, 1991.

[54] T. Blythe and D. Bloor, “Electrical properties of polymers”, Cambridge University Press, 2005.

[55] H. Sjöstedt, “Electric charges on insulator surfaces and their influence on insulator performance”, Licentiate Thesis, Chalmers University of Technology, Göteborg, Sweden, ISSN 1652-8891, No. 34/2008, 2008.

[56] Dr. Maciej and A. Noras, “Non-contact surface charge/voltage measurements fieldmeter and voltmeter methods”, Trek Application Note, 2002.

[57] P. Llovera, P. Molinie, A. Soria, and A. Quijano, “Measurements of electrostatic potentials and electric fields in some industrial applications: Basic principles”, J. Electrostatics, Vol. 67, pp. 457–461, 2009.

[58] D. C. Faircloth and N. L. Allen, “High resolution measurement of surface charge densities on insulator surfaces”, IEEE Trans. Diel. Elec. Insul., Vol. 10, No. 2, pp. 285-290, 2003.

[59] W. S. Zaengl, **“**Applications of dielectric spectroscopy in time and frequency domain for HV power equipment”, IEEE Elec. Insul. Magazine, Vol.19, No. 6, pp. 9-22, 2003.

[60] R Lovellt, “Decaying and steady currents in an epoxy polymer at high electric fields” J. Phys. D: Appl. Phys., Vol. 7, pp. 1518-1530, 1974.

[61] A. K. Jonscher, “Dielectric relaxation in solids”, J. Phys. D: Appl. Phys., Vol. 32, pp. 57-70, 1999.

[62] V. Adamec and J. H. Calderwood, “The interpretation of potential decay on the surface of a charged dielectric specimen”, J. Phys. D: Appl. Phys., Vol. 20, pp. 803-804, 1987.

[63] M. Ieda, G. Sawa and S. Kato,“ A consideration of Poole-Frenkel effect on electric conduction in insulators”, J. Appl. Phys. , Vol. 42, pp. 3737-3740, 1971.

[64] M. Ieda, G. Sawa and I. Shinohara, “A decay process of surface electric charges across polyethylene film”, J. Appl. Phys., Vol. 6, pp.793-794, 1967.

[65] H. V. Berlepsch, “Interpretation of surface potential kinetics in HDPE by a trapping model”, J. Phys. D: Appl. Phys., Vol. 18, pp. 1155-1170, 1985.

[66] T. J. Sonnonstine and M.M. Perlman, "Surface potential decay in insulators with field dependent mobility and injection efficiency", J. Appl. Phys. Vol. 46, pp. 3975-3981, 1975.

[67] M. A. Lampert, “Simplified theory of space charge limited currents in an insulator with traps”, Phys. Rev. Vol. 103, No. 6, pp. 1848-1656, 1956.

[68] T. Breuer, U. Kerst, C. Biot, E. Langer, and H. Ruelke et al., “Conduction and material transport phenomena of degradation in electrically stressed ultra low-k dielectric before breakdown”, J. Appl. Phys. , Vol. 112, 124103, 2012.

[69] D. Min, M. Cho, A. R. Khan and S. Li, “Charge transport properties of dielectrics revealed by isothermal surface potential decay”, IEEE Trans. Diel. Elec. Insul., Vol. 19, No. 4, pp. 1465-1473, 2012.

[70] D. Min, M. Cho, A. R. Khan and S. Li, “Surface and volume charge transport properties of polyimide revealed by surface potential decay with genetic algorithm”, IEEE Trans. Diel. Elec. Insul., Vol. 19, No. 2, pp. 600-608, 2012.

[71] C. C. Reddy, “Conduction and space charges in polymeric dielectrics and nanocomposites”, IEEE Int. Conf. Indust. Info. Sys., Chennai, India, pp. 1-4, 2012.

[72] IEC 62631-3-1 Dielectric and resistive properties of solid insulating materials - Part 3-1: Determination of resistive properties (DC methods) - Volume resistance and volume resistivity - General method, IEC, 2016.

[73] ASTM D257-14 Standard test methods for dc resistance or conductance of insulating materials, ASTM International, West Conshohocken, PA, 2014.

[74] I. A. Tsekmes, “Electrical characterization of polymeric DC mini-cables by means of space charge & conduction current measurements”, PhD thesis, Delft University of Technology, Delft, Netherlands, 2012.

[75] S. Yamanaka, T. Fukuda, G. Sawa, M. Ieda, M. Ito, and T. Seguchi, “Effect of filler concentration on electrical conductivity and ultralow-frequency dielectric properties”, IEEE, Trans. Diel. Elec. Insul., Vol. 2, No. 1, pp. 54-61, 1995.

[76] A. Rakowska and K. Hajdrowski, “Influence of different test conditions on volume resistivity of polymeric insulated cables and polyethylene samples”, Proc. 8th Int. Conf. Diel. Mat. Meas. Appl., Edinburgh, pp. 281-284, 2000.

[77] C. O. Olsson, "Modelling of thermal behavior of polymer insulation at high electric dc field", 5th European Thermal-Sciences, Conf., The Netherlands, 2008.

[78] G. R. G. Raju and M.A. Sussi, "Factors influencing conduction currents in Teflon", Proc. IEEE, Int. Conf. Cond. Breakdown, Solid, Diel., Vasteras, Sweden, pp. 249-252, 1998.

[79] Y. Zhu, K.S. Suh and H. Xie, "Interfacial effect on electrical conductivity in filled polymer composite", Proc. 5th Int. Conf. Prop. Appl. Diel. Mat., Seoul, Korea, pp. 918-921, 1997.

[80] J. Viertel, L. petersson, A. Friberg, G. Dominguez and C. Törnkvist, "Electrode influence on dc conductivity measurements of low density polyethylene", IEEE. Int. Conf. Solid, Diel., Bologna, pp. 1048-1051, 2013.

[81] J. K. Nelson, "Dielectric polymer nanocomposites", Springer 2010.

[82] B. Lutz and J. Kindersberger, "Determination of volume resistivity of polymeric insulators by surface charge decay", Proc. Int. Symp. High Voltage Engg., Johannesburg, pp. 28-33, 2009.

[83] G. G. Raju, "Dielectrics in electrical fields", Dekker, Inc. 2003.

[84] J. L. Auge, C. Laurent, D. Fabiani and G.C. Montanari, "Investigating dc polyethylene threshold by space charge current and electroluminescence measurements", IEEE Trans. Diel. Elec. Insul., Vol. 7, No. 6, pp. 797-803, 2000.

[85] S. Diaham and M-L Locatelli, "Dielectric properties of polyamide-imide", J. Phys. D: Appl. Phys., Vol. 46, pp. 1-8, 2013.

[86] S. J. Mumby, G. E. Johnson and E. W. Anderson, "Dielectric properties of some PTFE-reinforced thermosetting resin composites", Proc. 19th Elec. Electronics, Insul. Conf., Chicago, pp. 263-267, 1989.

[87] W. S. Zaengl, "Dielectric spectroscopy in time and frequency domain for HV power equipment, part 1: theoretical considerations", IEEE Elec. Insul. Magazine, Vol.19, No. 5, pp. 5-19, 2003.

[88] V. D. Houhanessian and W. S. Zaengl, "Time domain measurements of dielectric response in oil-paper insulation systems", IEEE Int. Symp. Elec. Insul., Vol. 1, pp. 47-52, 1996.

[89] B. Oyegoke, P. Hyvonen, M. Aro and N. Gao, "Applications of dielectric response measurement on power cable systems", IEEE Trans. Diel. Elec. Insul., Vol. 10, No. 5, pp. 862-873, 2003.

[90] C. Yuan, C. Xie, L. Li, X. Xu, S. M. Gubanski and Z. He, "Dielectric response characterization of in-service aged sheds of (U) HVDC silicone rubber composite insulators", IEEE Trans. Diel. Elec. Insul., Vol. 23, No. 3, pp. 1418-1426, 2016.

[91] D. Yujian, L. Weiming, S. Zhiyi, L. Qingfeng, G. Chen, and S. Zhaoying, "Switching impulse voltage flashover characteristics of air gaps in ±800kV UHVDC transmission tower and altitude correction", CIGRE, 2012.

[92] Y. P. Raizer, “Gas discharge physics”, Springer-Verlag Berlin Heidelberg New York, 1991.

[93] U. Hõrrak, “Air ion mobility spectrum at a rural area”, PhD thesis, University of Tartu, Tartu, Estonia, 2001.

[94] S. Pancheshnyi, “Role of electronegative gas admixtures in streamer start, propagation and branching phenomena”, Plasma Sources Sci. Tech., Vol. 14, pp. 645–653, 2005.

[95] M. A. Abdul-Hussain and K. J. Cormick, “Charge storage on insulation surfaces in air under unidirectional impulse conditions”, Proc. Phys. Sci. Meas. Instrumentation Management Education, Vol. 134, No. 9, pp. 731-740, 1987.

[96] S. Kumara, I. R. Hoque, S. Alam, Y. V. Serdyuk and S. M. Gubanski, “Surface charges on cylindrical polymeric insulators”, IEEE Trans. Diel. Elec. Insul., Vol. 19, No. 3, pp. 1076-1083, 2012.

[97] H. C. Kärner and M. leda, “Technical aspects of interfacial phenomena in solid insulating systems”, Proc. 3rd Int. Conf. Prop. Appl. Diel. Mat., Tokyo, pp. 592-597, 1991.

[98] A. Sihvola, “Electromagnetic mixing formulas and applications”, The institution of electrical engineers 1999.

[99] F. Rogti and M. Ferhat, “Maxwell-Wagner polarization and interfacial charge at the multilayers of thermoplastic polymers”, J. Electrostatics., Vol. 72, pp. 91–97, 2014.

[100] W. Choo, G. Chen and S. G. Swingler, “Temperature gradient effect on the conductivity of an XLPE insulated polymeric power cable”, IEEE. Int. Conf. Solid, Diel., Potsdam, Germany, pp. 1-4, 2010.

[101] Y. Gao, B. X. Du, F. Y. Van, K. Hou, Z. Y. Liu and J. D. Chai, “Effects of charging temperature and charging time on surface potential decay of PTFE film with back electrode ungrounded”, 14th Int. Symp. Electrets, Montpellier, pp. 105-106, 2011.

[102] Z. Ziari, H. Mallem and S. Sahli, “Influence of the temperature on the surface potential decay of polymer films charged negatively by corona discharge under light radiation”, Proc. Mediterranean, Microwave, Symp., Marrakech, pp. 1-4, 2014.

[103] D. Fabiani, G. C. Montanari, R. Bodega, P. H. F. Morshuis, C. Laurent, and L. A. Dissado, “The effect of temperature gradient on space charge and electric field distribution of HVDC cable models”, Proc. Int. Symp. Elec. Insul. Mat., Niigata, Japan, pp. 93-96, 2014.

[104] W. Choo and G. Chen, “Electric field determination in dc polymeric power cable in the presence of space charge and temperature gradient under dc conditions”, Int. Conf. Conditions Monitoring and Diagnosis, Beijing, China, pp. 321-324, 2008.

[105] T. Mizutani, “High-voltage dc insulation and space charge”, Proc. 6th Int. Conf. Prop. Appl. Diel. Mat., Xi'an, China, pp. 18-23, 2000.

[106] W. W. Shen, H. B. Mu, G. J. Zhang, J. B. Deng, and D. M. Tu, “Identification of electron and hole trap based on isothermal surface potential decay model”, J. Appl. Phys. , Vol. 113, 083760, 2013.

[107] W. Shen, G. Wang, Y. Niu, J. Wang, L. Zhang, Y. Zhang and G. Zhang "The energy distribution of traps in polymers based on isothermal surface potential decay measurement", Int. Conf. High Voltage Engg. Appl., Shanghai, China, September 17-20, 2012.

[108] T. C. Zhou, G. Chen, R. J. Liao, and Z. Xu, "Charge trapping and detrapping in polymeric materials: trapping parameters", J. Appl. Phys., Vol. 110, 043724, 2011.

[109] S. Kumara, Y.V. Serdyuk and S.M. Gubanski, "Surface charge decay on polymeric materials under different neutralization modes in air", IEEE, Trans. Diel. Elec. Insul., Vol. 18, No. 5, 2011.

[110] D. K. Das-Gupta, "Conduction mechanisms and high-field effects in synthetic polymers", IEEE Trans. Diel. Elec. Insul., Vol. 4, No. 2, pp. 149-156, 1997.

[111] Anh. T. Hoang, "Electrical characterization of partial discharge resistant enamel insulation", Licentiate thesis, Chalmers University of Technology, Gothenburg, Sweden, 2014.

[112] U. H. Nguyen, A. Sylvestre, P. Gonon and S. Rowe, "Dielectric properties analysis of silicone rubber", IEEE Int. Conf. Solid, Diel., pp. 103-106, 2004.

[113] H. Hillborg, ABB, Västerås, Sweden, private communication.